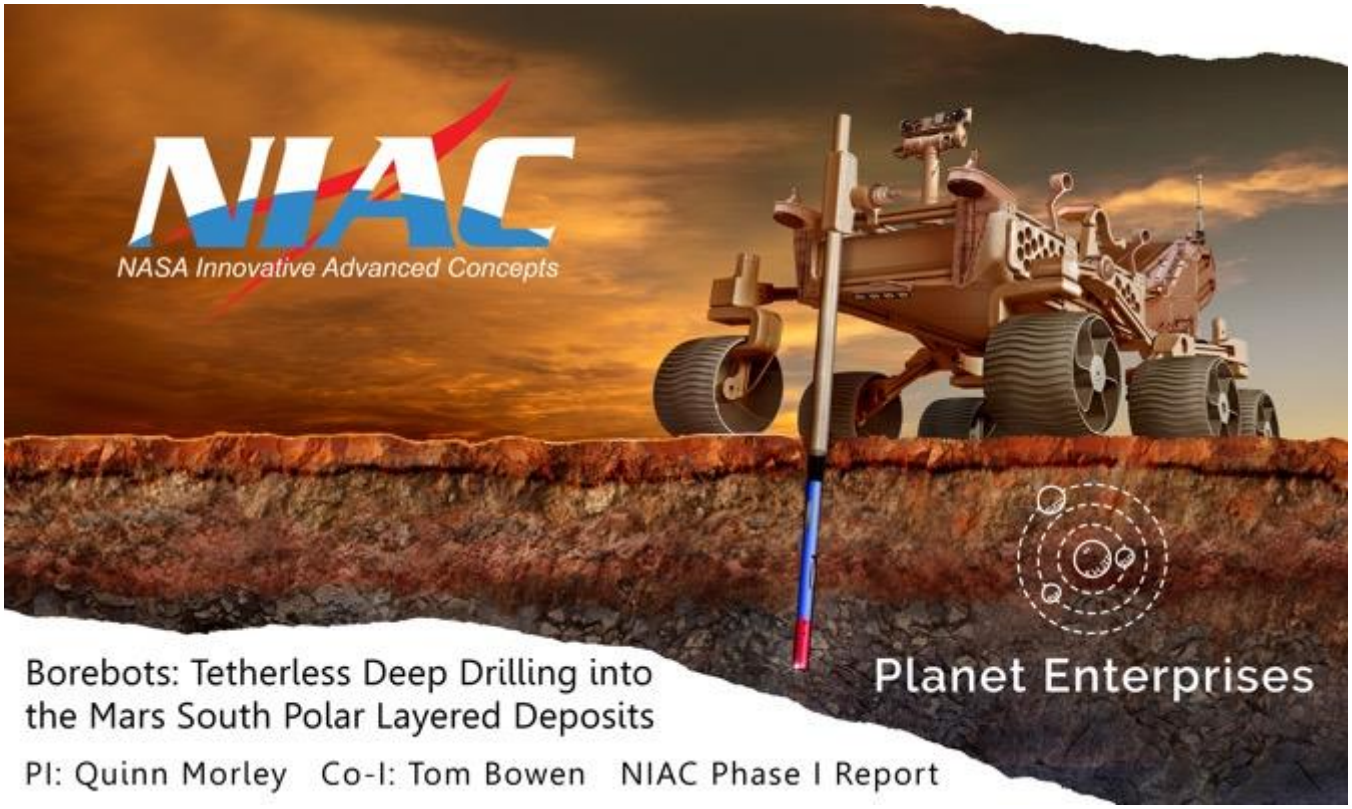
NIAC
NASA Innovative Advanced Concepts
Borebots: Tetherless Deep Drilling into
the Mars South Polar Layered Deposits
PI: Quinn Morley Co-I: Tom Bowen NIAC Phase I Report
Planet Enterprises

Borebots: Tetherless Deep Drilling into the Mars South Polar Layered Deposits

Final Report for:

Autonomous Robotic Demonstrator for Deep Drilling (ARD3)

2021 NIAC Phase I Study

PI: Quinn Morley **Co-I: Tom Bowen**

Planet Enterprises

webinquiries@planet.enterprises

https://borebots.fyi/

This work was funded by NASA grant no. 80NSSC21K0690.

Abstract

A method is presented for performing deep ice drilling on Mars with an electromechanical drill that has no physical link to the surface. Whereas cable-suspended electromechanical drills have a tether to the lander and a system for raising and lowering the drill, this system instead utilizes self-driving robots called borebots as the downhole assemblage. This investigation has found several key advantages to the borebots system, mainly a reduction in single-point-of-failure items like the winch and cable. Instead, several borebots can be used in a sequential mode of operation which evenly distributes mechanical wear and affords time to recharge borebots between trips. This offers the ability to start additional boreholes at new drill sites when desired, or after a catastrophic loss of downhole equipment. Disadvantages include depth limits due to power storage mass/volume requirements, which can be further limited by inefficiencies in the borebot drivetrain; and the potential for cumulative wear of the borehole wall which could result in a negative outcome in soft or unconsolidated substrates.

Contents

Foreword

We owe many thanks to members of the scientific and engineering community that were able to keep an open mind when faced with such an innovative and ambitious technology concept. Among these are the drilling legend Dr. Kris Zacny of Honeybee Robotics, Dr. Chris Dreyer of Colorado School of Mines, Dr. Mike Malaska of the Jet Propulsion Laboratory, Dr. Peter Buhler of the Planetary Science Institute, and Dr. Than Putzig also of the Planetary Science Institute. Laura Forczyk, M.S. of Astralytical was instrumental in both the development of the winning Phase I proposal and this manuscript. Most of all, we would like to thank the NASA Space Technology Mission Directorate (STMD) for the opportunity to perform this work. The NASA Innovative Advanced Concepts (NIAC) program is so inspiring, and we are honored to be a part of it. It is our wish that other undergraduates and non-traditional proposers are inspired to follow in our footsteps and take that first leap toward making their ideas a reality.

This investigative team has a passionate, unfettered interest in the exploration of this mission concept and the key enabling technologies that may one day make it possible. A best effort was made to evaluate, explore, examine, innovate, and document in an objective fashion, without bias; however, biases may be present. For this reason, each investigator has provided a value statement. If bias is present in this work, may it be attributed to these values and not come as a surprise.

Quinn's Value Statement

I believe in the philosophy of open hardware, and the romance and hope inspired by the opening space frontier. I believe that a culture of innovation and discovery is the antidote to most of the problems faced by America today. In recent years I have become inspired by the prescient work on leadership, organizations, and innovation by Dr. W. Edwards Deming. I try to apply Deming's teachings in my role as a leader and innovator as much as possible. The search for knowledge is the main driver in my life. It has inspired me to investigate the exploration of the south pole of Mars, and to search for a way to access the possible subglacial liquid water under the polar cap. I tend to favor the subglacial lake hypothesis.

Tom's Value Statement

Serving my community and humanity more broadly has always been important to me. The excitement I have for engineering challenges is in direct proportion to how I see them benefiting our shared efforts to survive and thrive in the difficult future we have made for ourselves. I am passionate about the role of public funding in stretching our collective understanding of what is possible. From my many years working with Department of Defense contracts, I feel a strong obligation towards responsible use of public moneys. While I favor our current architecture, I continue to critically assess other paths to 50 meters. I have no particular beliefs about the polar deposits, and continue to work towards a robust and adaptable vehicle for the broad range of conditions expected.

A Primer on the South Polar Layered Deposits

The South Polar Layered Deposits (SPLD) is an ancient ice cap, comprised mainly of water ice and dust. It was laid down over millions of years as successive layers of ice and dust, in both annual cycles and obliquity cycles. The thickness of individual layers isn't known to any certainty, but both thin layers and thick layers are visible in images taken from orbit. Generally, the SPLD is water ice with 10% to 15% dust content. This "bulk density" varies by location. For example, some areas may be almost pure water ice, and some may contain up to 25% dust on average (Li, 2012; Arthern, 2000). The way the dust content in the ice varies from layer to layer is unknown, but it is thought that layers can range from <1% dust to 50% dust. The multiple types of layering may represent the complex way the annual, precession, and obliquity cycles interact (Smith, 2020, section 1.2).

During rare and unique conditions in an obliquity cycle, large quantities of CO_2 ice can be trapped by a water ice layer that gets deposited on top of the frozen CO_2, which can be seen in the "Reflectance-Free Zone" (RFZ) shown in Figure 1 (Phillips, 2011). However, there is no evidence for large quantities of buried CO_2 ice near the area being considered in this study (Putzig, 2011). Generally, water ice is deposited slowly enough that CO_2 capturing like this is rare. Said another way, CO_2 can escape from under thin layers of water ice (this is called cryptic terrain, and can happen annually), but not thick layers. It is only trapped permanently when buried under a thick, nonporous layer at a sufficiently fast rate (Manning, 2019). The possibility of encountering CO_2 ice layers is discussed in more detail in the South Polar Layered Deposits section of the Technical Discussion chapter.

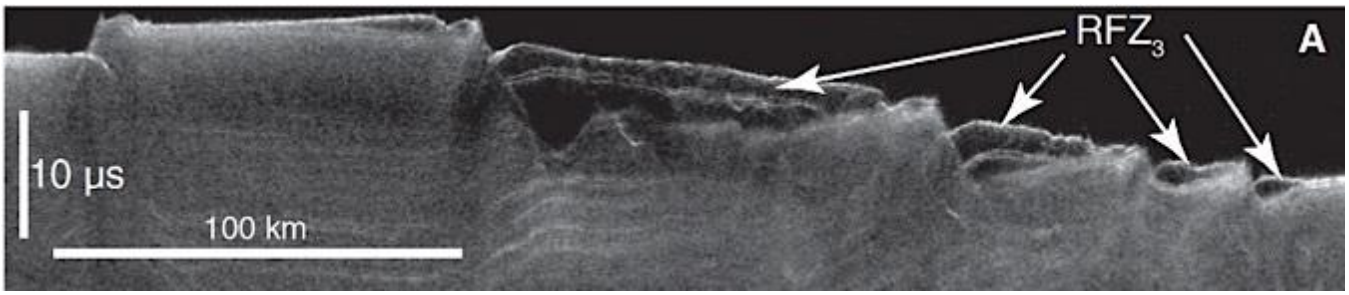

Figure 1, a SHARAD radargram showing RFZ_3 (Phillips, 2011, Fig. 1A).

When water ice forms on the surface of the cap (either as snow, or frost) it appears to densify differently than snow does on Earth; however, we have to extrapolate this from what we can see and sense from orbit. It is believed that vapor exchange with the thin and cold atmosphere helps the old snow (firn) become very dense after it is buried by only a few meters of additional snow/frost (Arthern, 2000). On Earth, this can take hundreds of meters of depth to occur and is driven by compaction due to gravity. The exact densification process at the poles is not known. This is also discussed in more detail in the South Polar Layered Deposits section of the Technical Discussion chapter. The important takeaway here is that there doesn't appear to be a top "firn" layer in the SPLD (Clifford, 2000; Smith, 2020; Vasavada, 2000). This is good news for those who wish to drill into the formation. It is also worth noting that the age of an ice layer at a certain depth is much older on Mars when compared to the same depth on Earth. This means that ice on Mars densifies much sooner if you are measuring depth, but much slower if you are measuring time.

The SPLD seems to be in a state of very slow decay, either from drainage winds called katabatic winds – which also occur on Earth – slowly eroding the surface, or from the ice vaporizing (called sublimation), leaving behind a layer of dust that gets cemented by ice in following seasons. It is likely that a combination of both processes occurs. For these reasons, it is expected that a lander would touch down on a thin layer of loose dust, under which would be ice-cemented dust that would be hard like rock. This kind of a layer is called a "sublimation lag layer" (Byrne, 2009). We don't know the specifics of this layer, although it may be up to 100 meters thick. We have reason to believe that it is at least 30 meters and less than 45 meters, but this is simply an early hypothesis to explain a "fog" effect seen in radar returns from the SHARAD Ground Penetrating Radar (GPR) instrument of the Mars Reconnaissance Orbiter (Whitten & Campbell, 2018; section 4.2, para. 2). Ground-based GPR is already flight-proven (the Perseverance rover is fitted with a GPR instrument called RIMFAX, see Farley et al., 2020); so, we should be able to estimate the lag layer thickness much more accurately after touching down.

In 2018 the planetary science community was shocked by the announced detection of what could be a liquid water lake under the SPLD, in an area centered on 81° South, 193° East (Fig. 2 & 3). This area is now commonly referred to as the "high-reflectance area," and is about 1.5 kilometers under the ice (Orosei, 2018a, 2018b). The team of Italian researchers used data collected by the MARSIS instrument on the European Space Agency (ESA) Mars Express orbiter, and presented a very convincing and thorough case for their determination. However, due to the extraordinary nature of the claim, the issue remains hotly contested (Sori & Bramson, 2019; Lauro, 2019; Lalich, 2021). It appears as though the most likely alternative hypothesis is some kind of hydrated sediment layer under the SPLD, like frozen clay or mud (Bierson, 2021; Smith, 2021). For more on the this, see the South Polar Layered Deposits section of the Technical Discussion chapter.

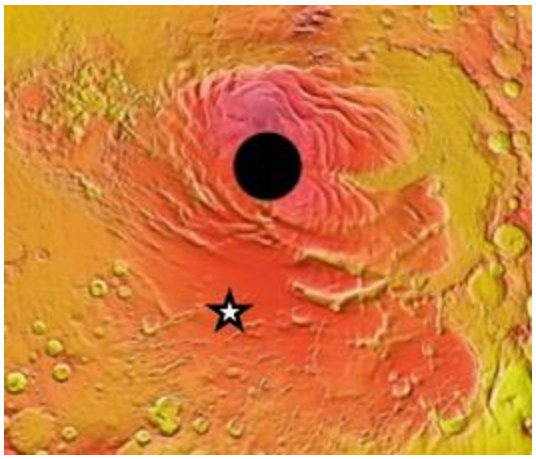

Figure 2. View of the SPLD with elevation relief. The High-Reflectance Area (HRA) from Orosei, (2018) at 81°S, 193°E indicated with a star. NASA/JPL/University of Arizona (uahirise.org).

Although the poles are very different, we anticipate that a mission to the North Polar Layered Deposits (NPLD) would pose the same challenges and level-of-difficulty as the SPLD. Challenges explored in the Technical Discussion chapter may apply more to one pole or another; however, overall feasibility of deep drilling in a Martian polar environment is shared between the two geographic locations. For this reason, SPLD and NPLD deep drilling missions are treated as interchangeable in this report unless a specific notable difference exists.

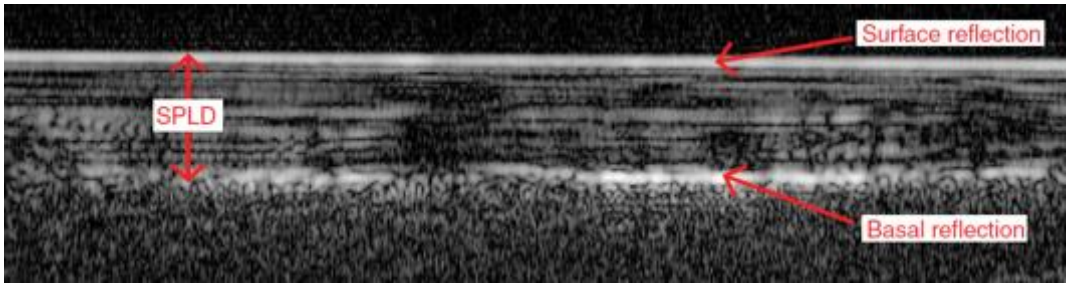

Figure 3, a MARSIS radargram showing the High-Reflectance Area at the base of the SPLD. From Orosei, et al. 2018 (Figure 2A, p. 3).

Mission Concept & Architecture Overview

Mission concept

The mission concept centers around deep drilling into the SPLD, and extracting ice cores. As a primary mission goal, it was decided that 50 meters is the most prudent numerical target and that it should be achievable in 90 days. However, to lend a more logical basis to the selection of the primary goal, we can say the depth should be enough to make it through the sublimation lag layer (plus any transition layers) and into the bulk of the formation itself. Once an ice core is retrieved from below the lag layer, the primary mission will be successful. Unfortunately, today we do not know the thickness of this lag layer (this is discussed in further detail in the South Polar Layered Deposits section of the Technical Discussion chapter), but it is likely to be somewhere between 30 and 45 meters thick. Although coincidental, this reasoning supports the primary target depth of 50 meters in this mission context. Regarding the length of the mission, in order to mitigate the risk from unexpected challenges slowing the drilling operation (which are likely), the landing should be timed such that a full Martian southern summer is available to complete the primary mission. If planned for mid-spring to mid-autumn, this could equate to roughly one Earth year, staving off the risk associated with the long and unforgiving polar winter affecting the primary mission.

The science return from this primary mission goal would be virtually unrivaled in Mars exploration, if successful. Just centimeters below the surface there may be frozen life, alive or dead (McKay & Stoker, 1989, p. 16-17). This offers a plausible astrobiology context for the primary mission goal. Deeper layers may hold a record of life-bearing layers that existed in the past. Astrobiology aside, merely drilling into the SPLD and visually imaging the borehole would dramatically change our knowledge of the climate and geophysical history of Mars on a time scale of millions of years. Going beyond simple imaging, the addition of downhole science instruments and surface sample processing (life detection, precision gas analysis, etc.) could create a potentially robust science return, enabling decades of discoveries that would indisputably change our understanding of Mars.

The extended mission goal is to drill through the entirety of the formation, using a triaged approach to science activities and sample processing. As depth increases, the secrets of Mars' obliquity and climate cycles will be revealed. Ice conductivity & density data can help scientists better understand orbital remote sensing data, allowing them to predict what lies ahead for the drilling operation as we begin to understand the stratigraphy better. If landing near 81° South, 193° East, the basal unit may contain a liquid water lake or frozen hydrated sediments at a depth of 1.5 kilometers, as previously discussed. In a follow-on study examining the high-reflectance area, Lauro et al. hypothesized that a form of ancient super-cooled brine may be present under the ice, stable for millions of years, which could contain oxygen. Lauro et. al concluded:

> "The water bodies at the base of the SPLD therefore represent areas of potential astrobiology interest and planetary protection concern, and future missions to Mars should target this region to acquire experimental data in relation to the basal hydrologic system its chemistry, and traces of astrobiological activity" (2021).

The basal unit and surmounting ice have also witnessed eras of the Martian past, and are certain to contain records of these periods in the ice. In 2005, Smith and McKay recommended drilling in this region, concluding:

> "At depths of ~1000 m, the effect of the obliquity cycle is dampened and permafrost at this depth would be unaltered over geological time. Biological material, rather than a mineralized fossil, is needed if we are to determine if Martian life represents a second independent genesis. Deep drilling on robotic or human missions could be focused on obtaining this material in ways that do not contaminate the Martian subsurface…" (p. 6).

On the other side of the pole, an ancient formation called the Dorsa Argentea Formation (DAF) covers a much larger area, rivaling or exceeding the age of deposits discussed by Smith and McKay (Head & Pratt, 2001). However, it appears that the DAF extends under the SPLD (Whitten et al., 2020, section 4). The DAF and the area studied by Smith and McKay may both be remnants of an older ice cap, which is simply in varying states of decay. If this is the case, the younger SPLD materials may be protecting material that witnessed the climate events of 3.5 billion years ago. Only deep drilling can reveal the truth.

The extended mission goal is likely to take 5-10 years, with a duration less than 3-4 years being unlikely. Therefore, two or more Martian polar winters are expected. It is impossible to consider this mission low-risk; however, each meter descended is extremely valuable (for the reasons outlined above), therefore, the rewards increase in proportion to the risk in the extended mission phase.

An auxiliary extended mission goal would be to drill additional boreholes at locations identified during an exploration phase, which could occur during the first weeks after landing. Exploration by the rover, by scout helicopter(s), or by intense orbital imaging could identify these locations of interest. The first drill site would occur at the most promising location; however, if the drilling operation is forced to abandon the borehole, a new borehole could be started at an additional location nearby instead of attempting to salvage the depth attained at the first drill site. It is the goal of this investigative team to give mission planners and scientists the utmost flexibility while contemplating these decisions. Therefore, the drilling architecture outlined in the following section of this report provides several redundant operating modes, and represents a robust capability that could start several new boreholes throughout the mission (even after a catastrophic loss of downhole equipment); or could enable branching of the borehole above a failure location by using advanced autonomous drilling techniques so drilling can continue. In all cases the challenges associated with the Martian polar environment are kept in mind. Deep drilling in to the SPLD is used as the mission context whenever possible in this report, in order to provide a consistent and fair analysis.

Figure 4: Borebots concept artwork, showing a borebot being deployed from a tube on a rover. Jim Vaughan Illustration.

Borebots Deep Drilling Architecture

Self-driving drilling robots that are approximately one meter in length (borebots) perform deep drilling activities autonomously from a large rover, very close in capability to the Mars 2020 / Perseverance Rover (as described in Farley et al., 2020), shown in our concept art (Figure 4). Ideally, the NASA Jet Propulsion Laboratory (JPL) would be able to produce a twin of Perseverance that would require only slight modification to accommodate the borebots architecture. Notable modifications include the addition of a three Degree of Freedom (DoF) deployment tube mechanism opposite the existing robot arm (shown in Figure 5), and the replacement of the MOXIE technology demonstration instrument with a science payload. Other requirements include adding borebot servicing capabilities (cleaning, charging, assembling, etc.), and a reduction in turret science payload to make room for a capable tube-grasping end effector. Further recommendations regarding the rover can be found in the Technical Discussions chapter. This section will focus on the workflow of the core concept. The rover and drill heads shall be treated as strawmen here, with Perseverance used as an example. The system can work with any sufficiently-equipped lander or mobility platform, and with a variety of drill head designs.

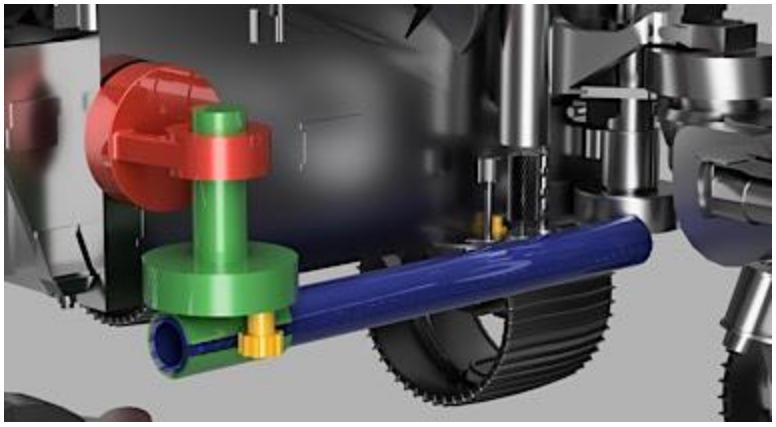

Figure 5: A deployment tube (colored) with 3 Degrees of Freedom.

When a suitable location is found to begin the drilling operation, the initial drilling sequence starts with the movement of the deployment tube into the drilling position (Figure 6). Ideally, a borebot is flown to Mars pre-assembled and loaded in the deployment tube. This allows for drilling several meters and taking dozens of ice cores even if the robot arm were to fail catastrophically upon deployment. The pre-loaded borebot

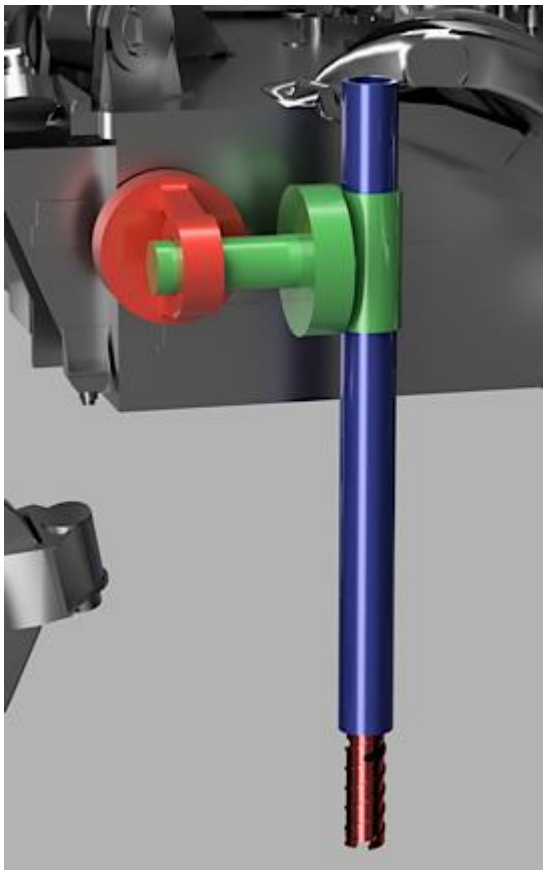

Figure 6: Deployment tube in drilling position.

drives down the tube and begins the automated drilling procedure, taking a ~40 mm by 150 mm core. While the automated drilling process is being carried out by the first borebot, a second drill head is retrieved from a storage location and loaded into the assembly station (Figure 7), and a second borebot is retrieved from storage and mated to it. This second borebot is now standing by for deployment (waiting for its turn). When the first borebot completes its drilling cycle, it drives up the deployment tube and waits for the tube to move to the re-coring station (Figure 8). It is worth noting that borebots can either be pre-assembled, or assembled via an automated workflow *in-situ*. Spacecraft mass, volume, and budget considerations (along with the desired drilling depth) are the primary driver in this decision.

The automated re-coring process is carried out next. Either the borebot can provide the rotation for re-coring, or the re-coring station on the rover can have a motor built-in. The re-coring station uses the same drill bits and sample tubes that Perseverance uses for rock coring (Moeller et al., 2021). During re-coring, the chips and dust that are created are blown into a pneumatic sample handling system, which can route the samples to instruments or dump them overboard if not needed (this pneumatic collection is similar to the system used on the Dragonfly hexacopter, see Zacny et al., 2019a). Since these chips come from the center of the ice core, they are much purer than the chips created by the borebot when originally taking the core. After re-coring, the drill bit and sample tube are moved from the re-coring station to the Adaptive Caching Assembly (ACA) bit carousel; see Figure 10 (Novak et al., 2019). The drill bit will be swapped for a new or sanitized one, and will be fitted with a new or sanitized sample tube. For more on this process, see the Rover Sample Handling section of the Technical Discussion chapter.

The deployment tube moves back to the drilling position, allowing the borebot to drive *up* the tube to offer itself to the robot arm. This allows the robot arm to remove it from the tube and move it to the cleaning station (shown next to the assembly station in Figure 8). Here, remaining debris are removed. Once placed in the cleaning station, the next borebot (that has been waiting on standby) is moved to the deployment tube by the robot arm, and the cycle begins again. Battery charging can be accomplished during a borebots stay in either the cleaning station or the assembly station.

Figure 7: Assembly station mockup integrated into the mounting bracket for Perseverance's 5-DoF robot arm.

Notably, the order of operations for the re-coring process will change during the extended mission (depth greater than 50 meters) phase: the first borebot (when surfacing, after drilling) would instead be placed in a staging area (likely the cleaning station, next to the assembly station) while the next borebot is deployed via the tube. Then, the first borebot (that still needs re-coring) could be placed back in the deployment tube so re-coring can occur while the longer driving/drilling cycle inherent to deep drilling is occurring down the hole.

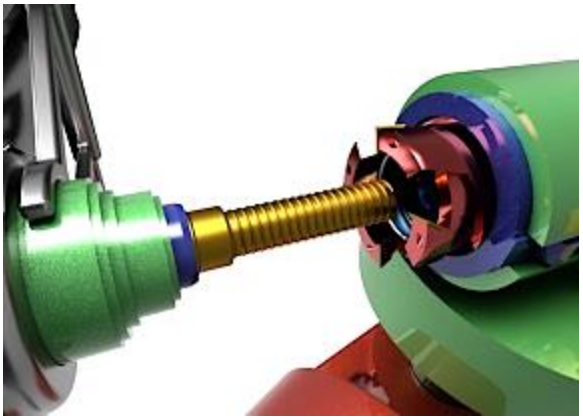

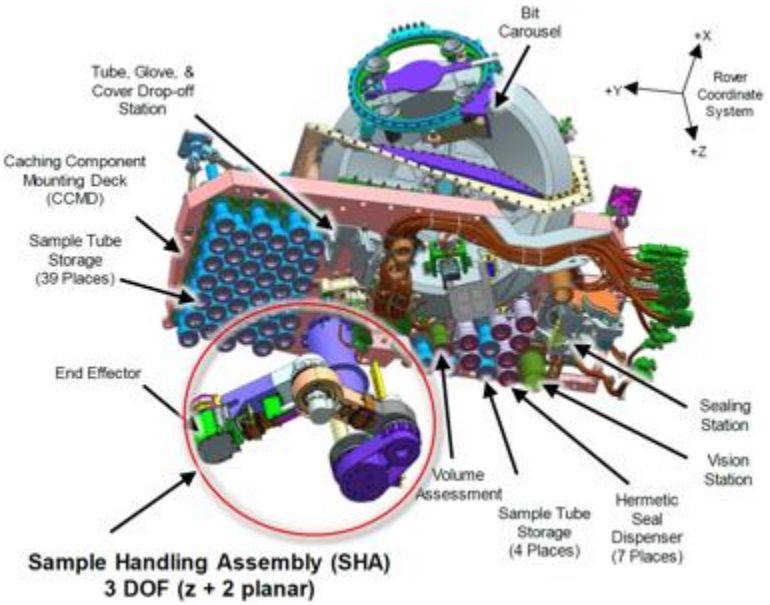

Figure 8, 9, & 10 (top to bottom): Deployment tube offering a borebot to the re-coring station, re-coring close-up showing ACA drill bit, and an overview of the Perseverance ACA from Novak et al. (2019, fig. 3).

This compact and simultaneous mode of autonomous operation would be impractical with any other drilling architecture. To provide flexibility to mission planners, the cleaning station must be capable of cleaning the drill head completely (even if re-coring is skipped), and it should be tied-in to the pneumatic sample handling system. This way, if a core is only desired every few meters, time and wear-and-tear could be saved by skipping re-coring. Samples (chips / debris from the drill head cleaning process) can be routed to instruments pneumatically if desired. This topic is presented here to illustrate the flexibility afforded by the architecture; for more on this, see the Rover Sample Handling & Science Instruments section of the Technical Discussions chapter.

The drilling, re-coring, cleaning, and staging cycle continues for as long as is necessary. 12 borebots can be brought to offer a measure of redundancy, and to spread out the component wear-and-tear among a greater number of robots. Having the option to distribute the drilling workload is the key advantage to the borebots deep drilling architecture, and as we will see in the next chapter, is easily adapted to other mission classes.

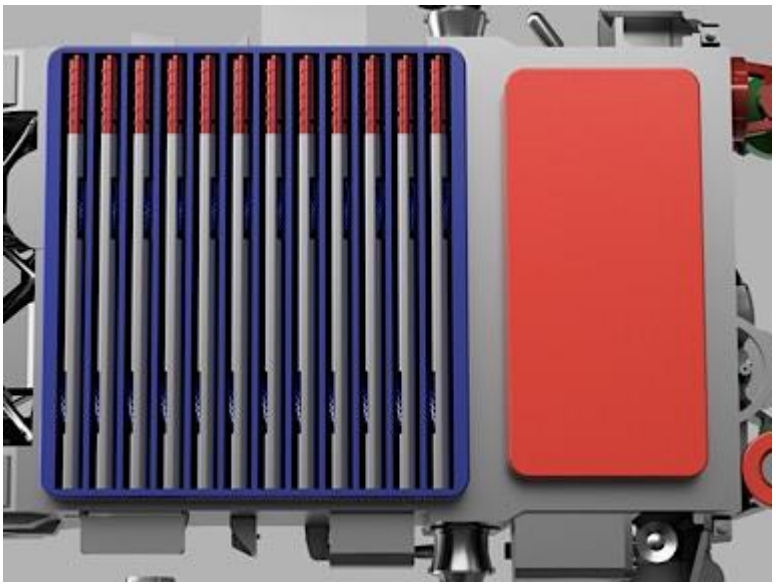

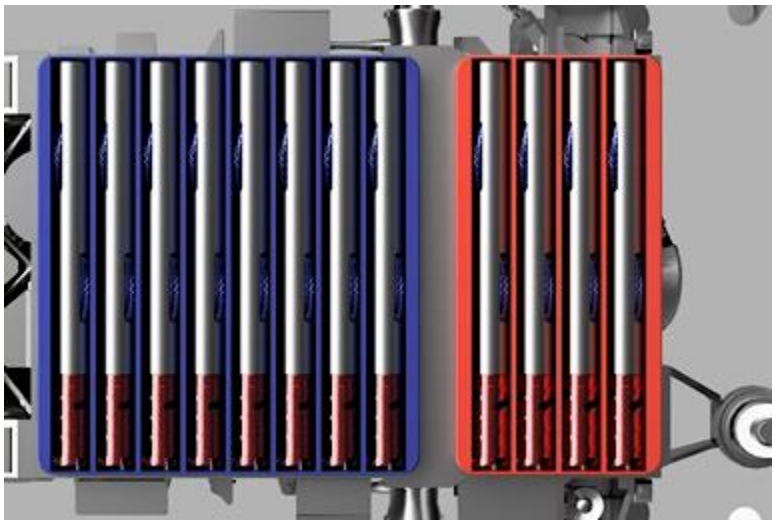

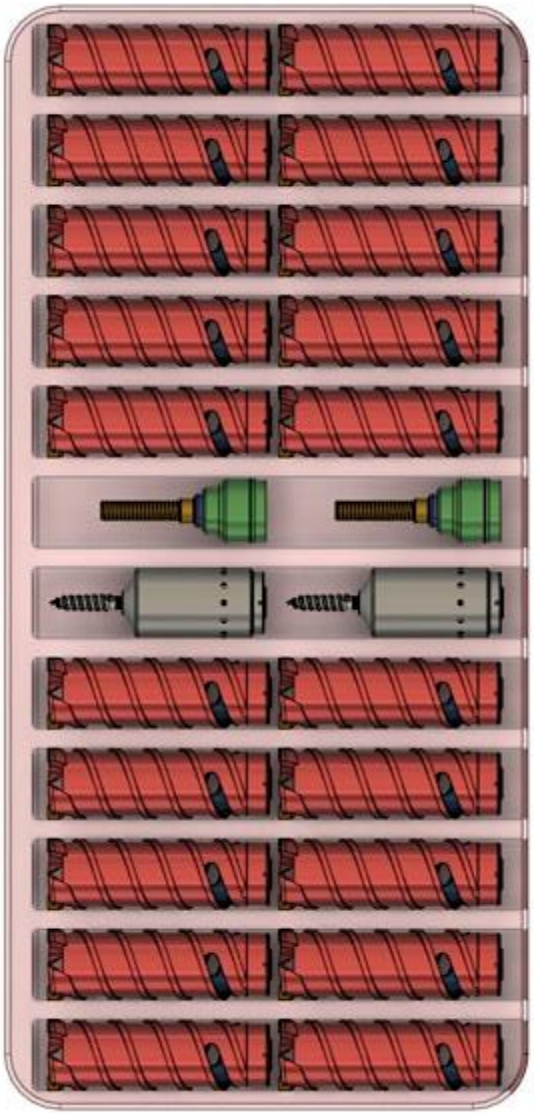

Figure 11 (top left): 64 mm x 1.1 m borebots stored in the trunk (blue), with the frunk area shown in red (ref. Figure 12).
Figure 12 (right): Cut view showing extra 64-mm end effector storage in frunk unit (which can be jettisoned or hinged).
Figure 13 (above): 108 mm x 1.1 m borebots stowed. The lg. borebot size is desirable, but difficult to store and manipulate.
Figure 14 (below right): Side view of a Mars-2020-style rover, showing the storage areas located below the rover body.

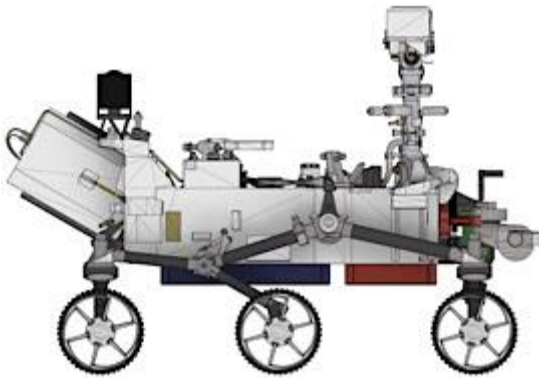

Storing borebots on a rover similar to Perseverance is actually simple, the problem is replacing borebots in storage when not in use. “Trunk” and “frunk” storage areas can be located below the rover body. The trunk (blue in Figures 11, 13, and 14) occupies the same space as the Mars Helicopter (Balaram, 2021, fig. 2), although it is expanded in width, and has less of an effect on ground clearance. Borebots could be retrieved from this location by dropping them on the ground and driving backwards to pick them up. A shuttle system for moving borebots between the storage location and the front of the rover may also be a good option. The “frunk” (red in Figures 11 - 14) could attach to the cover plate of the SHA, which is normally jettisoned shortly after landing. A hinge and actuator could be used, which would enable protection of the SHA from CO_2 buildup during polar winter, and add a storage location with easy forward access.

Alternate Borebot Architectures

A 2003 report by The Committee on Planetary and Lunar Exploration discusses the challenge of learning about the past climate of Mars, emphasizing the importance of returning samples to Earth:

> "Learning about the past climate of Mars is another important objective of Mars science, and returned samples offer the best way to understand an important product of past climates. Ultimately it may be possible to return ice cores from the martian poles that directly address the planet's climate history…" (National Academies, 2003, p. 84).

Just pages later they recommended "on the order of 10" sample return missions during the Mars Sample Return (MSR) campaign, hopefully featuring deep drilling to reach below the radiation-afflicted surface to search for clues about past life and climate. This is clearly reminiscent of the "cheaper, faster, better" days of JPL, but was unlikely to be plausible in the "post-reassessment" era, following the tragic loss of the Mars Climate Orbiter (MCO) and Mars Polar Lander (MPL), (pp. 101-102). Little did they know that the "2011 sample return mission" they spoke of would in fact land during 2021 at a cost of $2.5 billion (The Planetary Society, n.d.).

The thought of ten Perseverance rovers being deployed to the most science-rich parts of Mars is tantalizing, and in 2022 we must try not to laugh at the political and financial impossibility of such an undertaking. On the other hand, we must not stop pressing forward with deep drilling technology development when told that Flagship missions are too expensive to pursue. In the span of twenty years, ten missions may have become impossible, but we refuse to believe the number has dropped to "one-and-done." Even if human colonization of Mars is successful as the century presses on, robotic exploration and MSR have their place. In that context, it could be argued that polar science is one of the most logical places for robotic science missions to target.

Although this investigative team doesn't believe in the practicality of ten missions nor the impossibility of "one more Mars flagship," we see many other possible versions of the borebots architecture, and all of them are cheaper. Our work so far has really shown us the advantages of using a Perseverance-twin; it appears to be the lowest-risk option with the longest potential mission life. However, the alternate architectures outlined in this chapter all feature ways to mitigate the risks intrinsic to smaller and cheaper missions. Redundancy and flexibility are something all borebot architectures have in common, and these alternate architectures are thusly robust and capable.

Small Static Lander

The success of the Phoenix and InSight landers have shown that static lander missions can have a significant science return at low to medium cost (Lockheed Martin, n.d.). Using a build-to-print lander could allow this class of deep drilling mission to compete in the NASA Discovery Program. This makes a mission more likely to get selected; however, it does trade financial risk for higher mission risk. The Heat Flow and Physical Properties Package (HP^3) on InSight shows us that drilling on-the-cheap is not easy, and that the risk intrinsic to these low-cost missions is very real. The mole probe, which is the centerpiece of the HP^3 instrument, failed to penetrate into the martian regolith properly, and is stuck just centimeters below the surface (Jet Propulsion Laboratory, 2021). We believe the borebots architecture can provide

a more resilient capability, and that a static lander could make significant progress drilling into the Polar Layered Deposits (PLD). This could allow both PLDs to be explored at less than half the cost of a single large rover deep drilling mission.

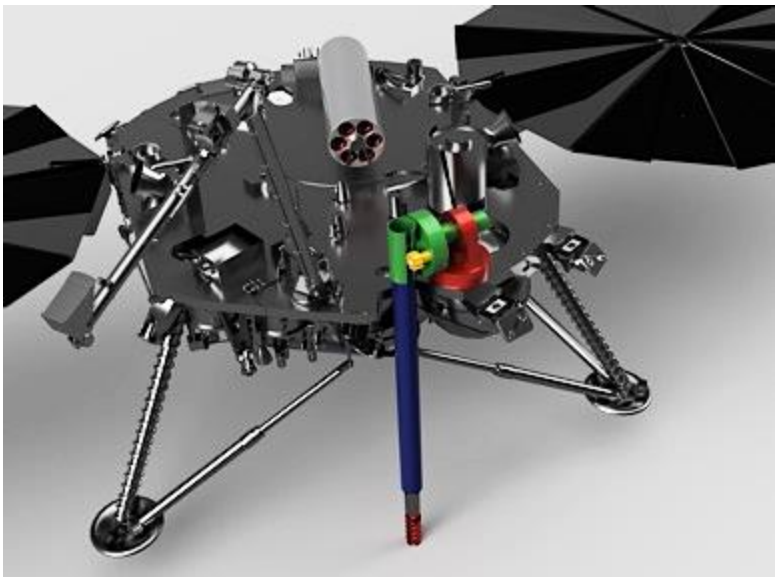

Figure 15: sketch of a static lander with a three DoF deployment tube.

The downside of this architecture is that drilling all the way to the basal unit is highly unlikely, due to the reduced capabilities of a static lander combined with the shorter lifetime when using solar power (although, the MPL may have been capable of surviving winter; see Clifford et al., 2000, section 3.3). Relocating for an auxiliary extended mission is also impossible, however, a second borehole may be possible (at an angle).

In this lower-cost context, a specific ice core analysis suite does not seem cost effective, and instead very small samples from ice cores (like the dust from the cleaning process) could be routed to instruments like TEGA and MECA from the Phoenix Lander (Smith, 2005). For more on science instruments, see the Technical Discussions chapter. With this type of mission, the motivation for core retrieval is lower energy consumption during drilling and the easier removal of material from the hole (and the drill head). It can be difficult to remove chips and dust from full-faced drills, so the coring strategy developed for the large rover architecture still has advantages here. It is worth noting, however, that a full-faced drill head could be attached to a borebot (the drill head used in this chapter is a strawman; any small/light drill head could be used). The example static lander in this section is based on the MPL / Phoenix / InSight platform, since the Phoenix science payload is very capable and could be re-flown in its entirety, saving additional money by using build-to-print instruments. Few modifications to the lander will be required. Efforts should focus on modernization and miniaturization of support systems to increase usable payload volume and overall power capacity.

To integrate the borebots capability into the lander, a three-degree-of-freedom deployment tube is added adjacent to the robot arm as shown in Figure 15. The tube is pre-loaded with a fully assembled borebot, and provisions to recharge the borebot in the deployment tube itself should be provided (i.e., side-mounted contacts). A cleaning station can be added under the deck of the lander (Figure 18), and plumbed into the pneumatic sample handling system as discussed previously (Zacny et al., 2019a). This first borebot will operate by itself for as long as possible, taking many cores and dumping the excavated material out under the lander (directly under the cleaning station). The entire volume of material removed from the hole will be about a quarter of a cubic meter at the completion of the primary mission. Considering this, the robot arm may be best used as a “cleaning assistant” to move material away from the borehole, and can also occasionally position itself under the cleaning station to capture a specific portion of a sample. The arm could also be fitted with a special scoop to take a piece of an ice core out of the drill head part-way through the cleaning process.

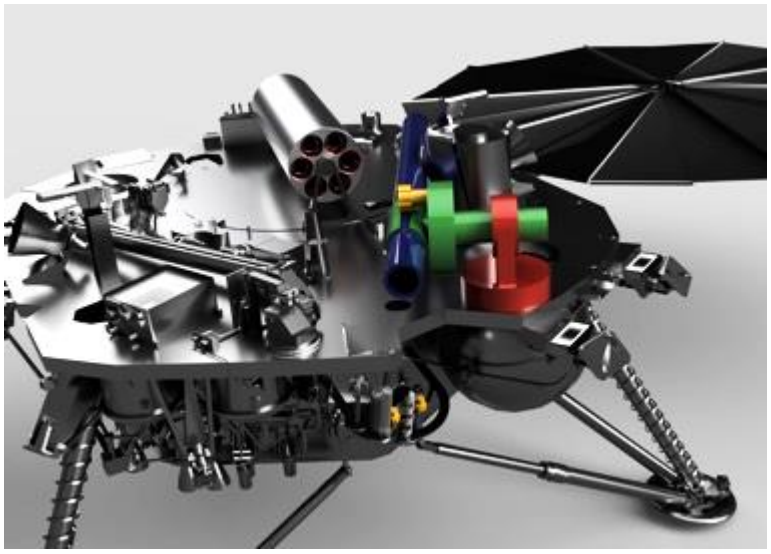

Figure 16 & 17: stowed configuration of deployment tube. Carousel containing six spare borebots is shown. Deck space is still availa for downhole science instruments or deck-mounted instruments.

Spare borebots (up to six spares, in addition to the one pre-loaded in the deployment tube) can be included, and could be stored next to the deployment tube on the rover deck. One option for this is a revolver-style borebot container is shown in (Figure 16 - 18). A second container (not pictured) could house downhole science instruments, or the space on the deck could be used for other science instruments (such as a weather station). The pre-loaded borebot would either be placed on the deck or discarded on the surface when it has exceeded its useful life (using the robot arm to push it out of the way). If the borebot being replaced is completely dead, the spare borebot being loaded could be used to push its deceased companion out of the tube. It may be wise to provide an electrical path between the tube and borebot for the purposes of firing pyros within a dead borebot, in order to sever the mechanical links in the drivetrain (this may be necessary for the spare borebot to push a dead borebot out of the tube). The same connections as the charging circuit could be used, but the pyro circuit could be sensitive to a sustained voltage or current spike.

Figure 18: strawman cleaning station shown under the lander deck.

Small Rover

A Mars Exploration Rover (MER)-class mission could provide a low-cost mission profile that could mitigate some of the risks of the static lander mission by being mobile. Using build-to-print components, it may be possible to fit a mission of this class into a Discovery Program budget. To integrate the borebots system into an MER-class rover, it may be best to forego the mast entirely and install a two-DoF deployment tube in its place. If the MER science strategy is followed, the robot arm will be responsible for the majority of the science duties (NASA MER, n.d.). Lessons learned from Perseverance's turret instruments could be applied here, in miniature form. The arm could examine chips and fines from the cleaning process before scooping them out of the way. A cleaning system similar to the previous section is envisioned, which makes fitting a robot arm a challenge due to the limited room for stowage (Figure 19 & 20; robot arm not shown). In order to offer drilling redundancy, the deployment tube could be a "double-barrel" design. This mission class shares the short life and lower power availability with the static lander concept.

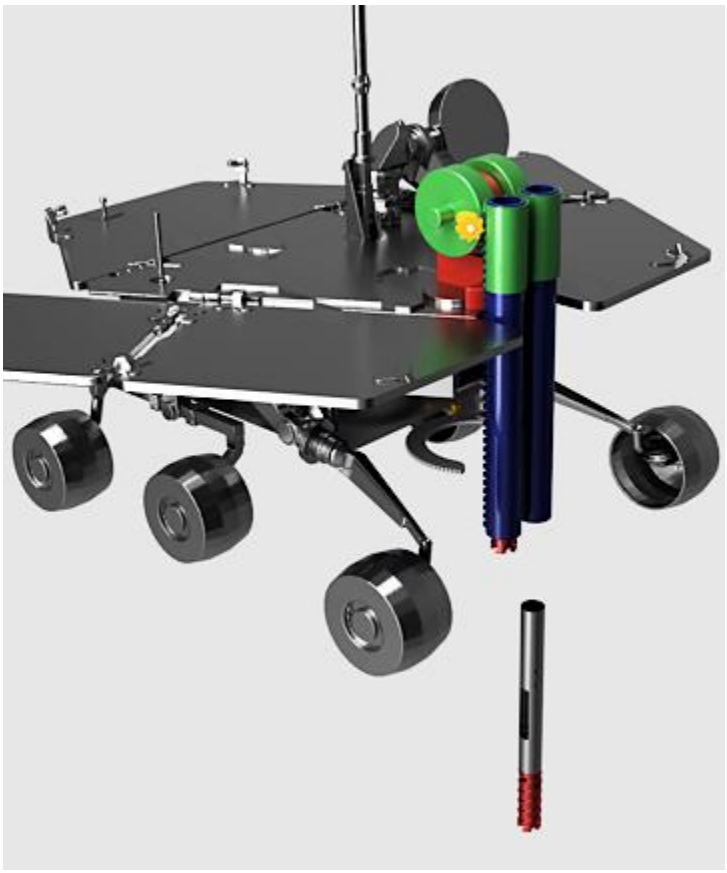

Figure 19 (above): MER-class small rover with a 2-DoF double-barrel deployment tube, shown during a drilling operation. Figure 20 (below): Stowed configuration of double-barrel deployment tube. Stowed cleaning station can also be seen.

To make up for the decreased science payload intrinsic to small rover missions, a downhole instrument suite may be the best way to increase science return. Perhaps the second deployment tube could be used to deploy a borebot fitted with downhole science instruments selected from amongst the options discussed in the Downhole Instruments section of the Technical Discussions chapter. The rover could maneuver the main deployment tube over the hole for drilling operations, and maneuver the second deployment tube over the hole to deploy the science borebot. This complex mode of operation would increase up-front costs, but

offer an increased science return without substantial changes to existing rover designs. Another option may be a simplified microscopic imaging module (UV/optical) that can be built into the borebots themselves. Future work on integration could choose to retain or omit the robot arm for this mission class. Stowing the front wheels, cleaning station, and robot arm in the available space will be a challenge.

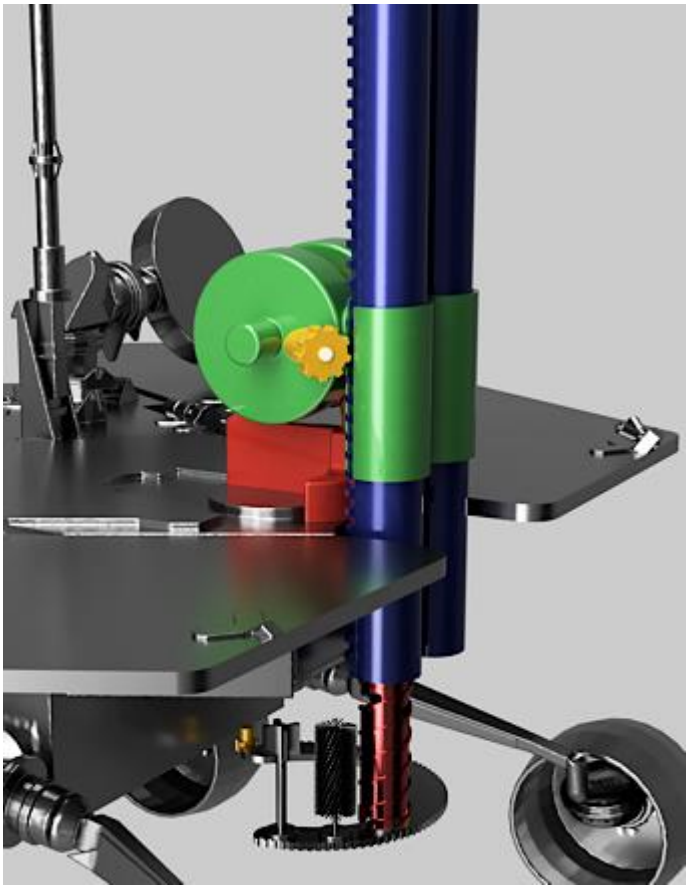

Figure 21: MER-class rover using a strawman cleaning station. Note that the front wheels, cleaning station, robot arm, and a camera module all would need to occupy this space during flight.

To mitigate the risk from the external science payload options, a SuperCam-esque instrument (Maurice et al., 2021) could be permanently affixed adjacent to the cleaning station (under the rover deck). This may not be compatible with the presence of the robot arm, but may be more useful in practice. It could feature a very limited 2 DoF range of motion, in order to analyze dust and chunks of ice core from a distance. The main challenge of an MER-class mission then becomes a game of miniaturization and integration. Can we fit two deployment tubes in the mast volume? Can we add enough science to the small and weak robot arm? Can we add a significant remote science payload (SuperCam) to mitigate risk if the external science payloads fail or have a low return? Do we have to remove the robot arm to make room for the cleaning station? These challenges are substantial. The advantage of mobility will need to be weighed against these risks during future work. Having the ability to abandon a drilling site (and even a borebot), and begin operations at a new location makes this system much more flexible. The limiting factors here would be the available rover power and borebot longevity (including the drilling head). Because of these limits, extended missions in this mission class should focus on additional boreholes, not greater depth, in order to maximize science return within the limited power and component lifespans.

One interesting note on an auxiliary extended mission profile: it was recommended by a previous decadal mission concept study to use small rovers to perform spectrometry work on excavated material in polar regions (Calvin, 2010, p. 21 para. 5). There may also be a benefit to drilling several shallow holes while traversing down a slope (Clifford et al., 2013, section 3.1). If the external science payloads fail, the rover could focus on mobility and near-surface sampling. It is likely that the deployment tubes could be used to dig trenches during this kind of a mission, even if (or after) all of the borebots have died. The MER rovers also used their wheels to dig trenches at times (NASA, 2008). If a suitable SuperCam-esque instrument can be integrated into the front of the rover (or mounted to the outside of the deployment tubes), this would be a very substantial auxiliary extended mission goal, and one that isn't available to a static lander. This mission phase could continue until polar winter seals the rover's fate.

Small Rover + Static Lander Combo

This concept combines the first two alternate architectures into a packaged New Frontiers mission, on a single launch vehicle. A defining feature of the static lander in this case is the inclusion of a multi-mission Radioisotope Thermoelectric Generator (MMRTG), which can enable over-wintering. The static lander would be well-equipped with scientific instruments, de-scoping only what is required to physically fit the MMRTG. Sample handling can be primarily pneumatic (from the cleaning station), with the option to have the rover use the cleaning station on the lander in order to offer samples to the pneumatic system. A strategy could be developed that would enable the small rover to "dock" next to the static lander, and connect a power umbilical to keep the small rover alive through winter. This concept may be able to achieve basal unit access if enough borebots can be brought along. This architecture is presented as a second potential way to reach the basal unit during extended operations, at less than half the cost of a flagship large rover mission.

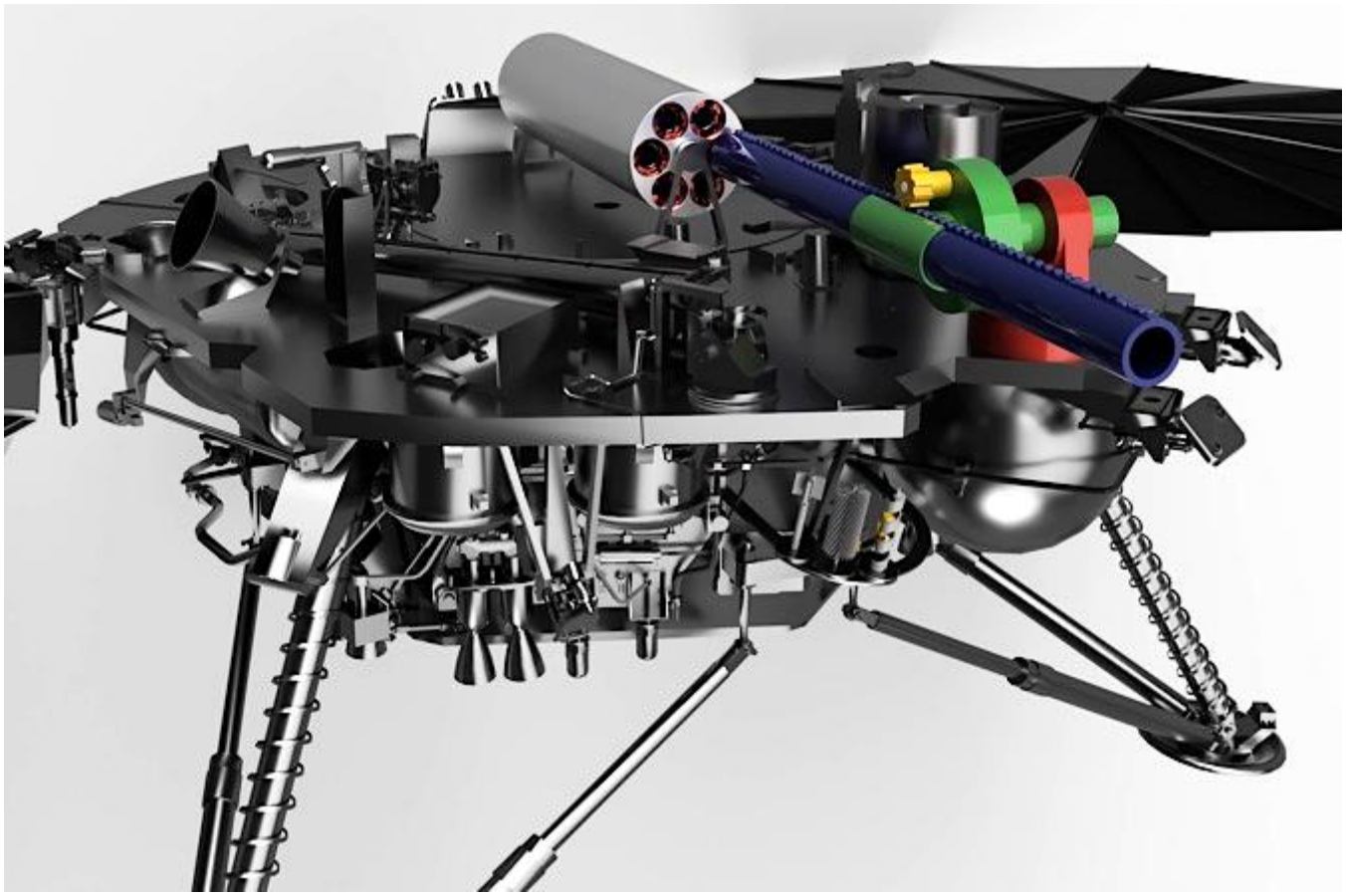

Figure 22: The deployment tube of a static lander in position to receive a borebot from storage. Note that a similar, smaller dispenser could be stored directly to the left of the one shown, which could hold three or four downhole science instruments pre-installed on borebots. A weather station or other instrumentation could be added elsewhere on the deck.

Commercial-off-the-Shelf Robots

Figure 23: Boston Dynamics Spot robots exploring a cave using a team-based approach. Photo Credit: Nasa/BRAILLE Team, (Sleater, n.d.).

NASA has been looking at ways to explore caves with Commercial-off-the-Shelf (COTS) robots, as exemplified by the NASA Biologic and Resource Analog Investigations in Low Light Environments (BRAILLE) project, shown in Figure 23 (Sleater, n.d.). The end goal here is to enable the exploration of lava tubes on our Moon and Mars using these systems. This work could be leveraged and applied to a Borebots context. The existing team-based approach to cave exploration could be augmented for use in polar science, limited to a single summer season. By adding additional robotic team members designed to perform drilling activities, an extremely low-budget deep drilling architecture emerges.

Figure 24 shows a sketch with three possible Boston Dynamics Spot robot configurations that could be added to the existing team dynamic in order to perform deep drilling work (Spot 3D model credit to Great, n.d.). A roll-out solar array could be fitted with charging docks for the Spot robots, perhaps with drill cleaning stations between the charging docks. With a $75,000 list price, Spot robots offer the lowest-cost way to explore the polar regions for a single season. It may be wise to send two or three missions of this type to a region prior to landing a more expensive and capable lander. The best of the scouted sites could be selected for follow-up work, and would already be mapped in 3D.

Figure 24: Boston Dynamics Spot robots in a borebots context sketch.

Technical Discussion

Borebots

On Earth, deep drilling requires a massive infrastructure (most of it at the surface) and relies heavily on manpower and fuel-burning generators. There is always some physical link with the surface, either a tether or steel drill pipes (Bar-Cohen & Zacny, 2009, pp. 320-328). One of the leading deep drilling systems designed for use on Mars is shown in Figure 25 at the right. Known as Auto-Gopher 2, it belongs to the "Planetary Deep Drill" family of drills developed by Honeybee Robotics, with part of the funding coming from the Planetary Society (Davis, 2018). Along with its cousin WATSON (Eshelman et al., 2019; Malaska et al., 2020), these drills represent the state of the art for 100-meter-class extraterrestrial deep drills. The high degree of miniaturization and automation mean far less surface infrastructure than most systems designed for use on Earth. However, the current versions of these drills rely on towers over three meters tall, large winches, generators for power, and human intervention to remove cuttings or cores from the drill head. For more on the topic of wireline (cable-suspended) drill systems, see the Borebots vs. Competing Deep Drilling Architectures section in the Feasibility Assessment chapter of this report.

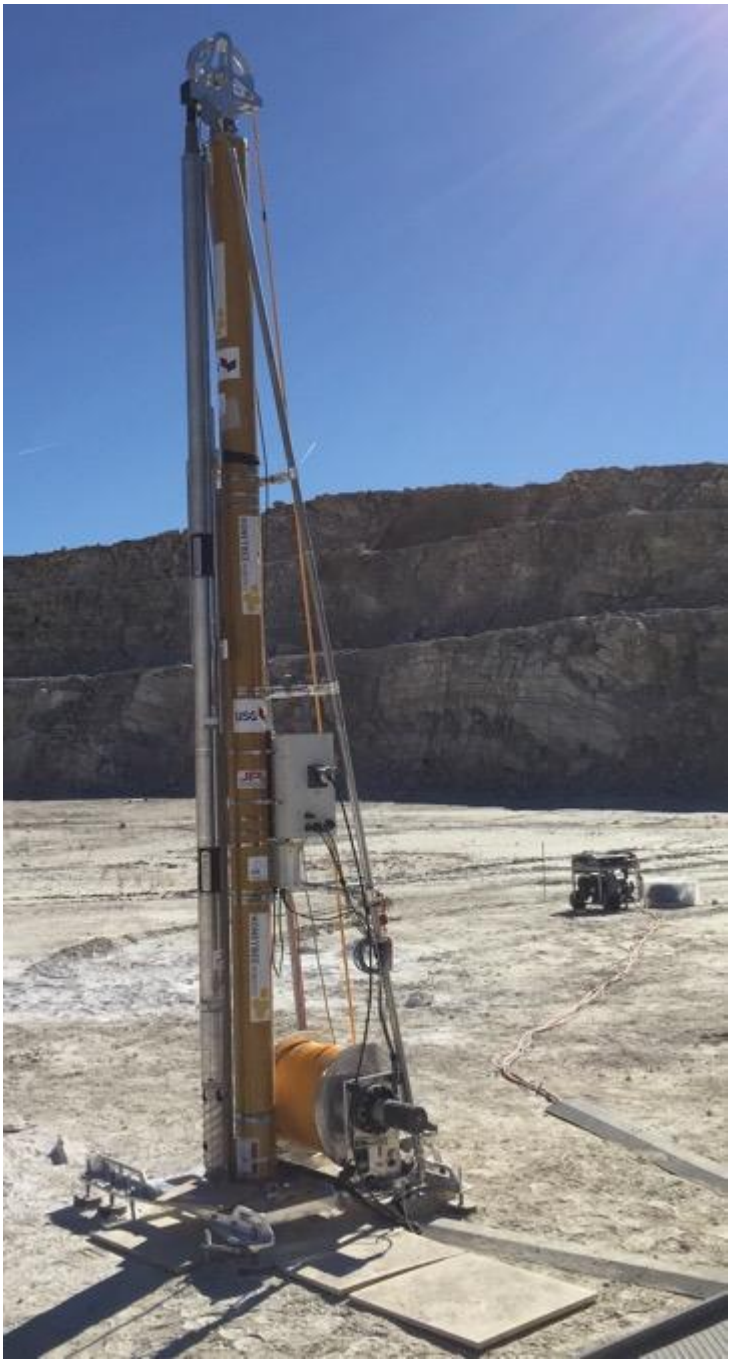

Figure 25: Auto-Gopher 2 deep drill during testing at the Fish Creek gypsum deposit in California (Davis, 2018). The drill and rig are both over 3 m tall. A generator can be seen in the background.

At the heart of the borebot concept is the idea to replace the tether with some kind of driving apparatus. A large spool of cable (the tether) can be seen at the base of the drill rig in Figure 25, which is an absolutely critical component of a wireline drilling system – a failure of the winch or tether is a failure of the mission. These components are so large and heavy that it may be impossible to carry a spare. Struggling with the ramifications of this problem is what kindled the desire for a self-driving system with a high level of redundancy (multiple units and spare parts). Thus, the borebots concept was born.

A suitable drive system was first hacked together in 2018 (Figure 27; video: https://git.io/JBbJ1), during night and weekend fabrication and experiment sessions by the PI. The first functioning mockup drive system was envisioned to be "squish-fit" into the borehole, maintaining pressure against the borehole wall by using the Hooke's law behavior of the flexible components. To accentuate this effect, the drivetrain was staggered, so the tank tracks could act like rubber bands, and would spend most of their time under tension. Tension increases as the components pushed against each other. Herringbone gears were used to provide intrinsic stability and self-centering of the gear and pulley system. This allows for the addition of "idler" gears that can free-float inside the tracks, providing more "squish" to evenly distribute the traction forces on the borehole wall. The gear geometry was based on a design by Emmett Lalish and was published on Thingiverse.com to respect the open-source license (Lalish, 2013; Morley, 2019). The potential for one of the idlers to become misaligned and shift towards one of the other gears does exist. Therefore, floating idlers may not be in future designs; however, it remains a convenient layout for testing. A borehole size of 64 mm was chosen, as it matches the original Planetary Deep Drill diameter and represents the practical lower size limit for a robust mechanical system of this type.

Figure 26 (left): A borebot is shown in its natural habitat, and with two pairs of tracks. As shown, the borebot has just finished the deployment sequence by driving out of the tube and to the bottom of the borehole to being drilling.
Figure 27 (center): Mark 1 drive system mockup with floating idler gears to intensify pressure at borehole interface.
Figure 28 (right): Schematic of the drive system, with gears shown doubling as "tank tracks." Idlers omitted.

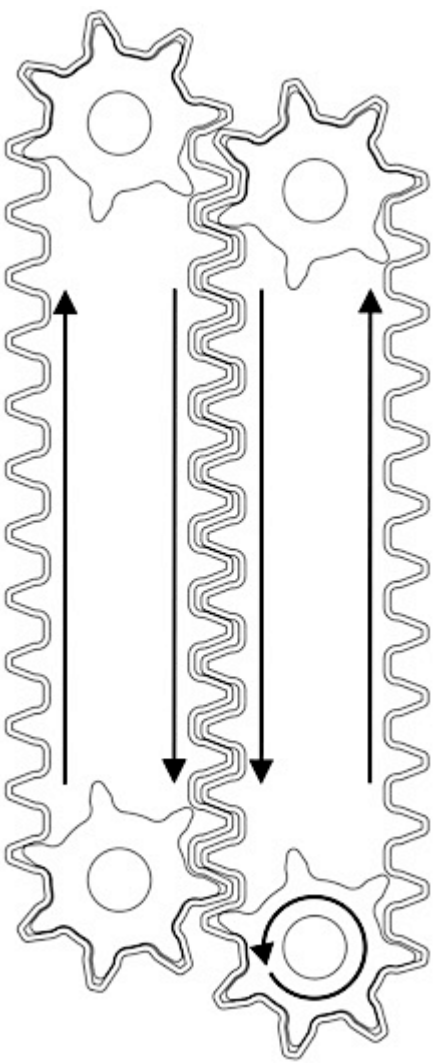

A consequence of the squish-fit design is the "linking" of the tracks, meaning that drive power only needs to be applied to one track, and the power is transmitted to the other track as through a pair of gears (Figure 28). This has advantages with respect to miniaturization and robustness, but also has disadvantages. Some positives of the linked system are that only one motor is required for each pair of tracks, more space is available for each mechanical component (because they nest into each other), small bits of ice and rock can pass through the middle of the system, and the presence of a "mechanical fuse" (the tracks can skip past each other and then resume normal operation; this can also be thought of as a safety clutch). The disadvantages of the linked system are a lack of independent track control, lack of pressure control (normal force against the borehole is controlled by the Hooke's law behavior of components and is not adjustable on the fly), and greater mechanical energy waste due to friction. The force against the borehole is also kept relatively high due to the "preload" tension in the system, which is a prerequisite to enjoying the benefits. It may be possible to mitigate some of these disadvantages by creating a sliding mechanism for one of the tracks, to adjust the stagger distance and therefore the pressure on other components (preload tension) and the borehole. The "Mark 3" prototypes have been developed without the staggered approach, although early work shows that the self-tensioning effect from the staggered components is missing, and belt tension becomes a critical design factor (and one that may need to be controlled in order to guarantee trouble-free operation over the life of the mission).

In order to continue the discussion about the flexible gear drivetrain, it is important to understand the method via which the 3D printed gears were made. In the prototype stage, the inventor has a high degree of control over the compliance of the printed components using a few simple techniques. In more advanced design stages, analytical methods can be used to define an internal structure that strictly controls the way the gears deform when compressed. This can enable finite-element simulation of component performance, and offer strict configuration control which can allow for physical testing and statistical analysis. Using an analytical approach to achieving the correct pressure on the borehole wall (via the control over the component properties) may also allow for the selection of existing materials that have less-specific fabrication requirements, decreasing cost and possibly increasing component reliability due to a more isotropic material response.

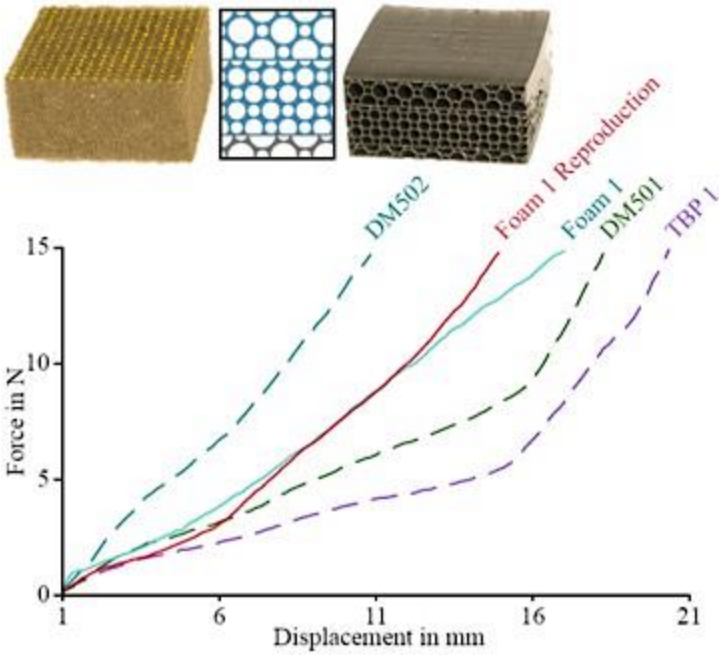

Figure 29: Figure 10 from Bickel et al., 2010. DM502, DM501, and TBP 1 are 3D printing materials that are being stacked to reproduce foam 1. Designers have complete control of the cell geometry. The slicer creates toolpaths for a 100% solid part, creating a machine program capable of producing the cell structure geometry in a physical part exactly as it was input.

In the context of additive manufacturing (3D printing), the design of materials with a specific deformation behavior is discussed thoroughly in Bickel et al. (2010), with an example shown in Figure 29. Continuing this line of thinking, Schumacher et al. present

a technique for controlling the elastic behavior of a material as a function of location within the component volume (2015), see Figure 30. A class of materials called “metamaterial machines” was discussed by Ion et al., and an application was released that allows the general public to design machines composed only of their shear-cell design elements, which is then able to be printed as one complete unit (2016). An example metamaterial mechanism can be seen in Figure 32, and a screenshot from the user-interface of the application can be seen in Figure 31. These works represent methods that can be applied carefully during the design phase to achieve a predictable result.

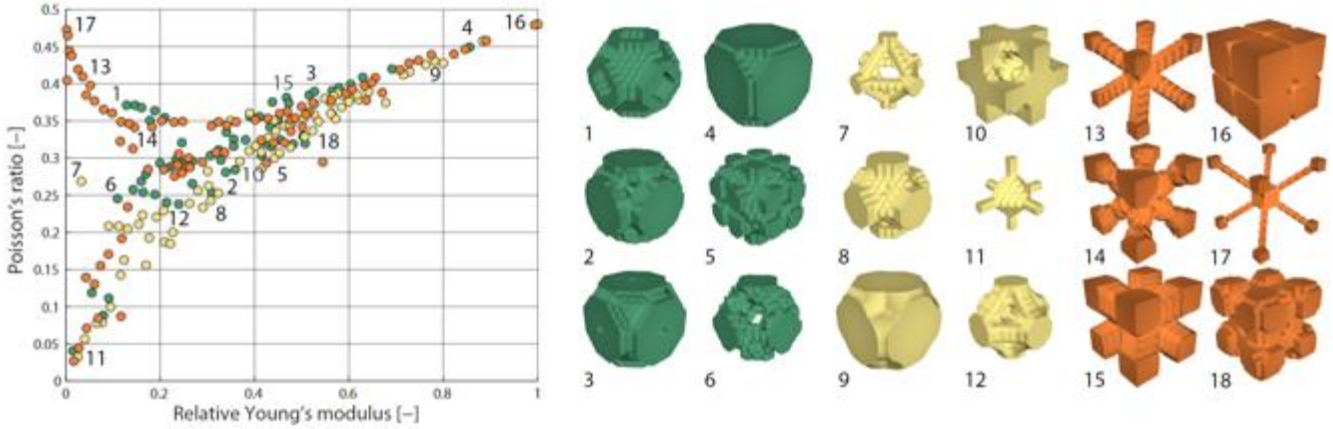

Figure 30: Each color is a “family” of unit cells; 6 examples of each family are shown. The 3D unit cells build on the work of Bickel et al., allowing control of elasticity as a fn. of location, not just compressibility (Schumacher et al., 2015, figure 13).

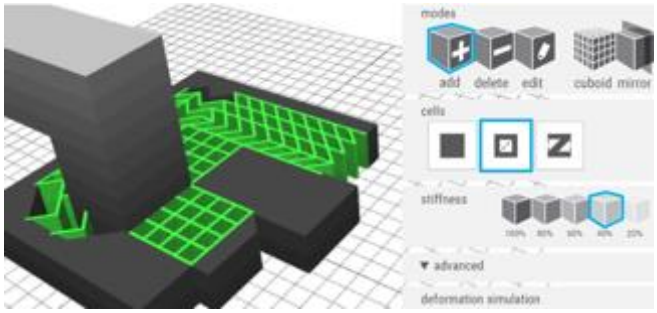

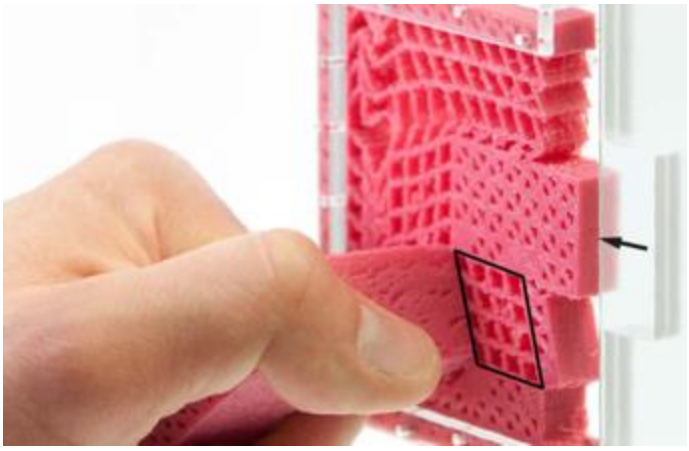

Figure 31 (above): Screenshot from the editor, available at https://jfrohnhofen.github.io/metamaterial-mechanisms/
Figure 32 (right): A metamaterial mechanism door handle. Figures from Ion et al., 2016, Fig. 1C and 1B, respectively.

During the prototype phase, instead of the employing the above methods with their up-front design commitments, a family of techniques known as “slicing tricks” was used to generate geometry that could then be printed and tested. A “slicer” is an automatic Computer-Aided Manufacturing (CAM) software tool that creates lines of code representing discrete vertical increments of a part (or “slices”), which are compiled into a machine program and subsequently used to create a physical part via 3D printing. Since each gear is relatively small (and therefore, prints quickly), an iterative approach was used until the elasticity of the gear was acceptable. Although slicing tricks exist as a form of tribal knowledge within the 3D printing community, it is difficult to find literary references for these techniques. Generally, the idea is to leverage a shortcoming of the technology *to the advantage of the designer or operator*. The first example of effectively using slicer settings to affect the elasticity of a printed object may have been the “Recreus Sneakers” line of DIY footwear, released by the inventor of one of the first widely available flexible filaments, Filaflex (Garcia, 2013, 2014). However, a mention of using property modifiers

to force the slicer software to achieve a variable elasticity was mentioned by Dr. Adrian Bowyer, the creator of the first Replicating Rapid Prototyper (RepRap) 3D printer, in a 2011 forum post (Hodgson, 2012, Pg. 1766). Both approaches leverage the fact that 3D printed parts are often fabricated with a "sparse infill" pattern, designed to produce a structure that can quickly take up space during fabrication. Infill plays a minor structural role in most applications, primarily resisting buckling loads, but occasionally supporting high compression loads (Hermann, 2018; Sanladerer & Hermann, 2019). The largest advantage of sparse infill is that it supports the horizontal layers that will be printed later, which makes the fabrication process smoother and of a higher quality.

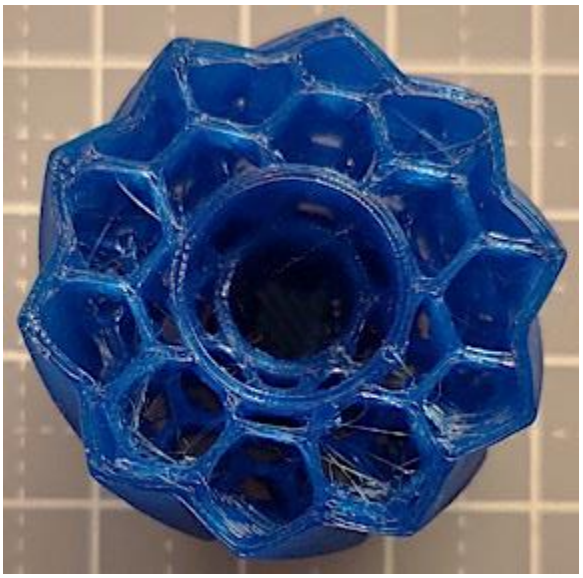

Figure 33: honeycomb fill with no top/bottom layers.

When considered in the context of flexible materials, the overall part density (and thus, the infill) controls the bulk elasticity of the flexible component to a high degree. One other technique (which likely predates any online discussion or published literature) is to "turn off" the top and bottom solid layers for the part, allowing the infill pattern to have a greater degree of control of elasticity (this can be seen in Figure 33). These techniques were employed by the Principal Investigator to give the prototype gears less elasticity and more resiliency in the center of the gear, and more elasticity towards the sides. This allows the gear to conform to the radius of the borehole while creating less wasted energy. If a rock is ingested into the track system, the sides of the gear can flex with less force, but contain pockets for the bearings (limiting total deformation); while the center section is more resilient, but containing no bearings, offers slightly more available deflection to pass objects through. Moving the bearings from the gears to the Borebot housing may allow for the easier passing of stones; however, when the bearings are placed in the gears, the prototypes are much easier to assemble.

The parameters for slicing the gears used in the Mark 3 drivetrain can be seen in Table 1, while Figure 34 & 35 show the result. NinjaTek Cheetah Shore 95A filament was used in all cases. These gears can be printed individually, or in multiples printed simultaneously with the belts (ring gears). The resulting elastic properties of the gear allow it to conform to the borehole (here, a 64 mm ID acrylic tube) as seen in Figure 36, while Figure 37 shows the same for the gear with a belt installed. The gears and belts pictured were generated with 60° pressure angles, which seems to allow for smoother operation. All

Table 1 - Gear Print Settings - PrusaSlicer 2.3.1	
External perimeters extrusion width	0.50 mm
Perimeters extrusion width	0.60 mm
Infill extrusion width	0.50 mm
Layer height	0.2 mm
Nozzle diameter	0.4 mm
Number of perimeters	2
Number of bottom solid layers	0
Number of top solid layers	0
Infill density	14%
Infill density modifier (middle 11 mm)	20%
Infill/perimeter overlap	30%
Infill pattern	honeycomb
Speed (all print moves)	30 mm/s
Accelerations (all print moves)	250 mm/s^2

previous prototypes were created with 45° pressure angles, which exhibited a pronounced "clicking" motion as the rolling resistance oscillated with the passing of the gear teeth. Elasticity affects this clicking behavior, but not as much as the pressure angle and the overall pressure in the system. Greater pressure angles may lower rolling resistance further, and both pressure angle and elastic properties are good parameters for optimization (at a 90-degree pressure angle, the gear belt turns into a standard flat belt).

One problem with optimizing the pressure angle parameter (in the context of stuffing belts and gears into a tube), when the pressure angle is changed, so must be the diameter of every component. This is compounded by each pressure angle / elasticity combination "meshing" (and flexing in response to meshing) in different and subtle ways. For these reasons, the iterative design approach will need to be continued and the diameters that work best will need to be tabulated. This will allow analyses as described earlier in this section to generate geometries which yield the desired elastic properties, but that rely on the tabulated diameters from the iterative design process. From there, more iterations may be required to balance rolling resistance and the force against the borehole wall. The prototype phase of drivetrain development should be continued until the Weight on Bit (WOB) requirements are finalized to mitigate the potential for late-stage redesign of the drive system, by evolving both the drilling requirements and drive system at the same time (WOB is discussed in detail in the Drilling Technical Discussion section).

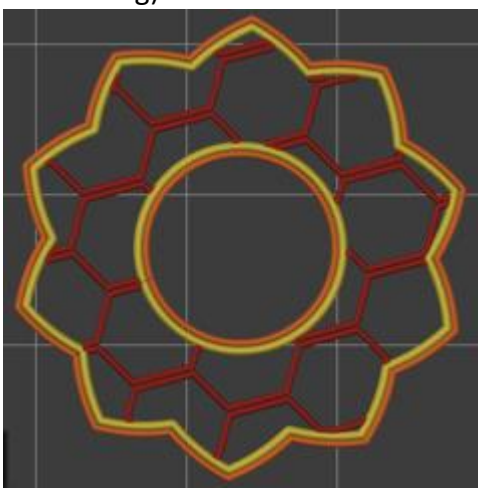

Figure 34: 14% honeycomb infill

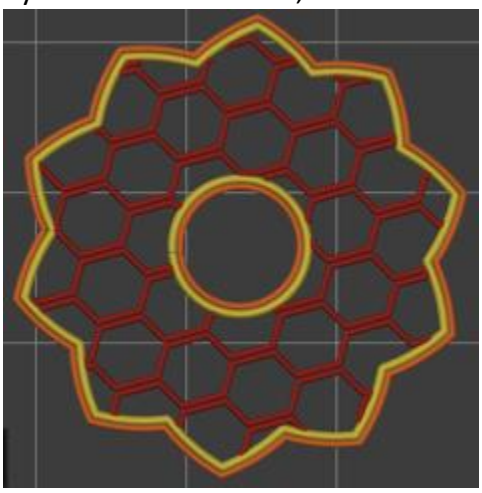

Figure 35: 20% honeycomb infill

Alternatively, components generated with ideal elastic properties could be modified by only a scale factor to compensate for late-stage WOB requirement changes. Another option may be to build-in some form of adjustment for the track system, so the gears can be forced against the wall to increase pressure on the fly (this is discussed in more detail later in this section). This could also be part of a steering mechanism, but could add its own cost and complexity.

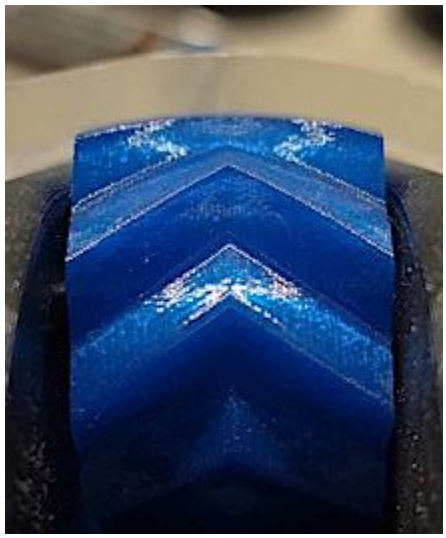

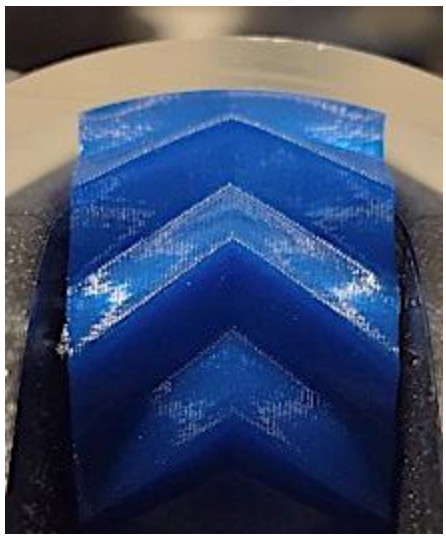

Figure 36 (left): Gear deforming to match the contour of the bore.
Figure 37 (right): Gear with a belt installed, both conforming to the bore contour.

Although these tricks are difficult to describe and get an intuitive understanding for, they can be done in practice in a matter of seconds. As briefly mentioned earlier, the first prototype drivetrains (hereafter called Mark 1 and Mark 2) were in fact made entirely from a publicly shared, customizable 3D model called the Gear Bearing (Figure 38) by Thingiverse user Emmett Lalish (2013). Careful readers may have noticed the hexagonal hole in the gears shown in Figure 27. These gears are multiples of the sun gear generated by the Gear Bearing customizable model. The Mark 2 drivetrain replaced the hexagonal hole with round holes in a post-processing step, and eventually moved the bearings to counterbores, in what could best be described as the Mark 2B.

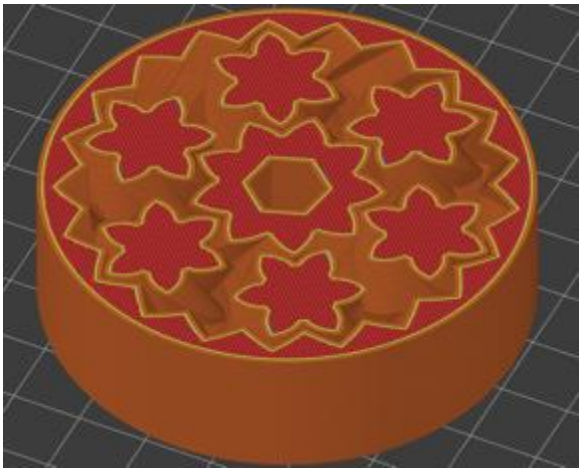

Figure 38: The Gear Bearing sliced normally, as the designer intended. Note the hex hole in the sun gear. The design code for this model was customized to generate the Mark 1 & 2 drivetrain components.

As if this process didn't seem mystical enough to the uninitiated already, the gear-belts for the Mark 1 and Mark 2 prototypes *are the ring gears from the Gear Bearing customizable model*, printed with a slicing trick. The print settings used are the same as in Table 1, except the infill percentage was set to zero. The main motivator behind the Mark 3 drivetrain was to generate our own geometry in a CAD program in order to give us more design control, while still employing slicing tricks to create the final elastic properties of the part. The Mark 3 gear belts come from a ring gear CAD model that we created, but only the inside surface of the ring gear was modeled – the outside surface is a result of the slicing trick (Figure 39 and 40).

More traditional belt-drive components may produce a resilient enough drive system (Figures 41 - 43), while putting less of a demand on the borehole wall by eliminating the "clicking" motion caused by some of the more aggressive gear teeth. In both the gear-drive and belt-drive varieties, directional drilling may be achieved by deflecting one end of one track(s) out to provide an axial deflection in the borehole. We are moving the architecture forward using both gear drive and belt drive systems.

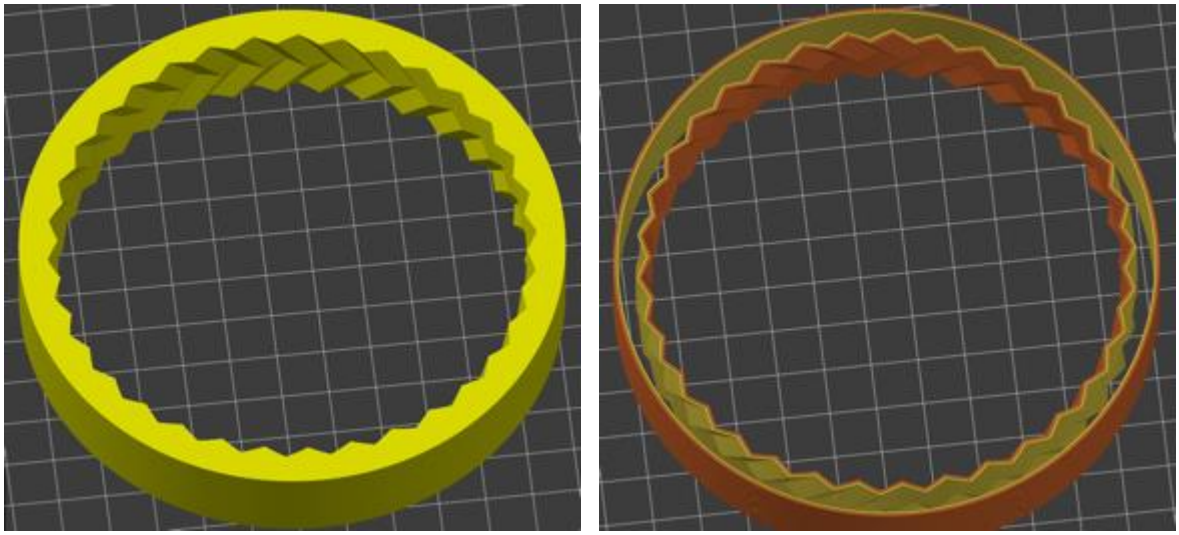

Figure 39 (left): Mark 3 ring gear model loaded into the slicing program, PrusaSlicer.
Figure 40 (right): Sliced Mark 3 ring gear, showing the creation of the exterior belt surface.

The largest challenge faced by the borebots architecture is power consumption. Therefore, the system must be designed to balance mechanical, thermal, electronic, and power storage considerations in order to guarantee the level of performance required to reach the target depth. This is discussed in depth in the Power and Components section of this chapter. Testing will be required to determine which drive system methodology is preferable. Energy efficiency is the primary motivator in this selection, but system robustness should be weighed in the decision as well. Testing strategies should focus on iterative design of bench-testable prototypes, only integrating the best versions into functional prototypes.

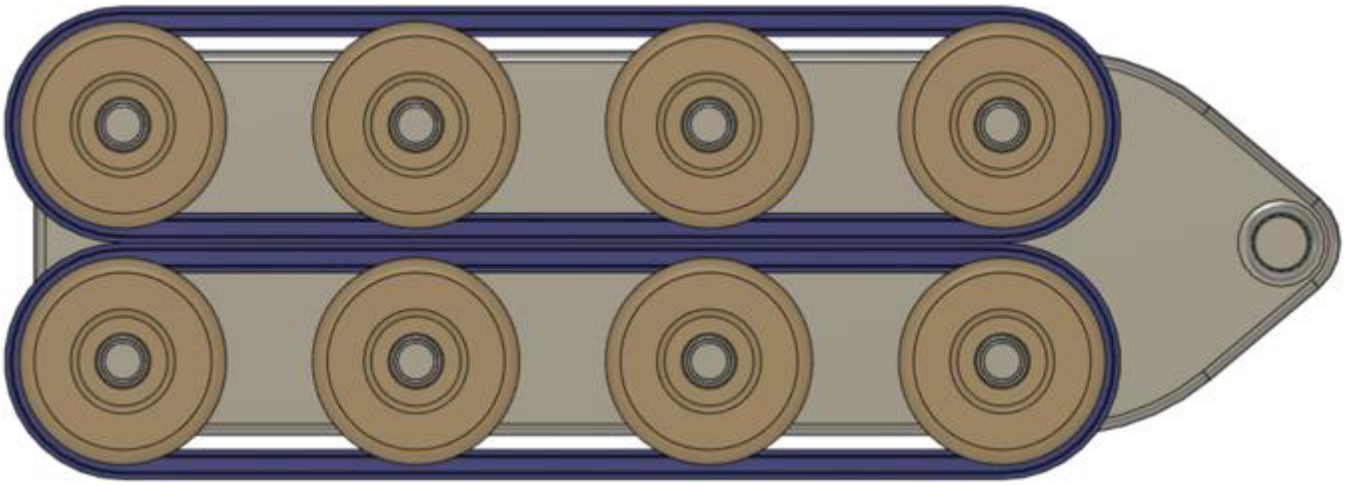

Figure 41 (top) & 42 (bottom): Mark 3 gear-belt drivetrain prototype module, and a flat-belt, flanged-pulley mockup.

For the flat belt drivetrain (Figures 42 & 43), there are three options worth considering, which are shown side-by-side in Figures 44 - 46. The first two types both rely on crowned pulleys, and the third uses flat pulleys with a flange. Crowned pulleys are commonly seen on belt sanders today, and used to be common in lineshaft machine shops (Matthews, 2005). Flanged pulleys are frequently used in robotics; however, the flange would normally interfere with the bore in this case.

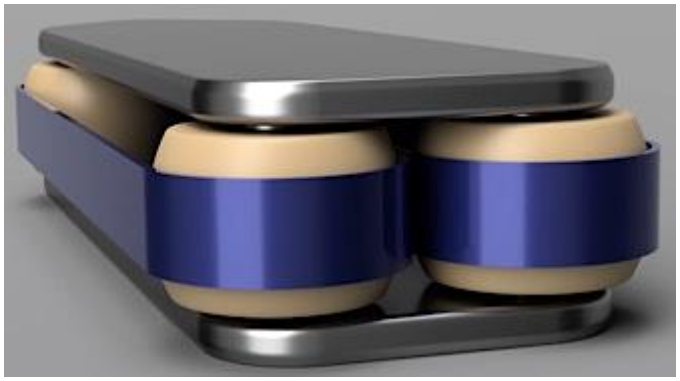

Figure 43: Mockup prototype module of a flat-belt drivetrain. The crowned shape of the pulleys provides a centering force when the belt is deflected off the centerline of the pulley.

The parameter space for this type of flat belt drivetrain is actually complex, with the rolling resistance, centering force, size requirements and power transmission all playing a role. A standard flanged pulley would come in last place on nearly all marks if off-the-shelf components were used: the risk of high friction when the belt goes off-center and crowds the flange, no centering force beyond the constraint of having a flange, the larger diameter required for the flange causing interference with the borehole, and the impracticality of having the belt transfer the drive power from one track to the other via the center belt-to-belt contact region as with the other options (and with the gear belt options). However, if the belt is made extremely thick it can overcome these challenges using a conventional (but uncommon) type of flanged pulley.

Figure 44, 45, & 46: Mark 3 flat-belt drivetrain mockups; crowned pulleys left and center, with a flanged pulley at right.

The crowned pulleys don't really need much more of an explanation: either they will prove themselves useful during testing, or they won't. The flanged pulley, however, has a much more uphill battle, and the new type of thick belt still needs to be fully described and prototyped.

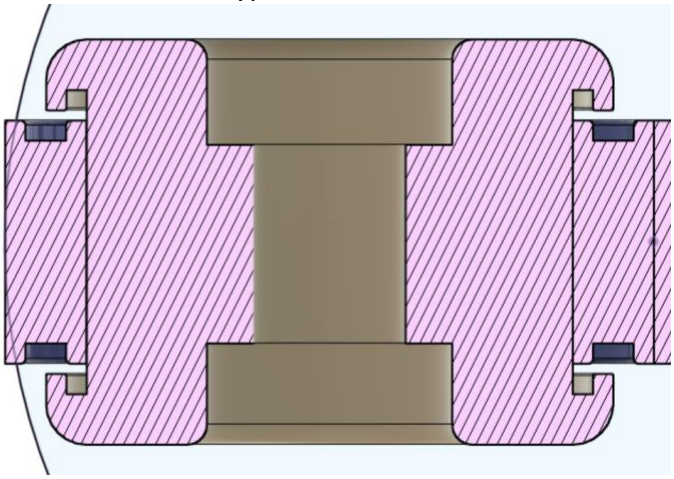

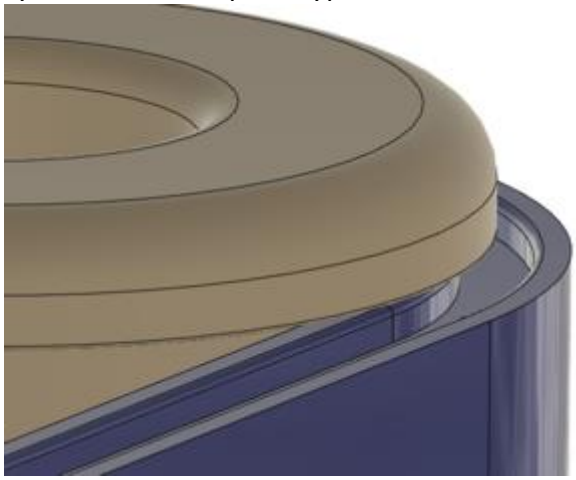

Figure 47 (above left): Cross-section view of the crowned pulley and thick belt option, designed to minimize crowding of the flange as recommended in Matthews, 2005.

Figure 48 (above right), 49 (left): Mockup flat-belt drivetrain prototype module using flanged pulleys and a thick belt. Belt thickness is the easiest parameter to adjust, with pulley spacing and pulley diameter as secondary and tertiary parameters.

There are several options for powering the borebots drivetrain. However, we will be focusing on a simplified chain-drive version for the next (first truly "self-propelled") borebot prototype. The original Mark 1 prototype used a rubber belt and an integral pulley, added to one of the gears with a Boolean operation (Figure 50). This can also be seen in the video linked to earlier (https://git.io/JBbJ1) and in Figure 27 (the black gear). This configuration proved cumbersome and unreliable for testing. Although a rubber belt may be the ultimate solution, using #25 chain can allow for a lower-profile component stackup and more reliable interface for prototyping work (Figure 51). Other notable drive options include a "direct" gear-drive that acts on the outer surface of the gear-belt, and a worm drive configuration in which the worm gear would be placed between the two gear-belts. The power modeling that is currently in work – and the lessons learned from the chain-drive prototypes – will help to focus our efforts, and define a range of motor power requirements.

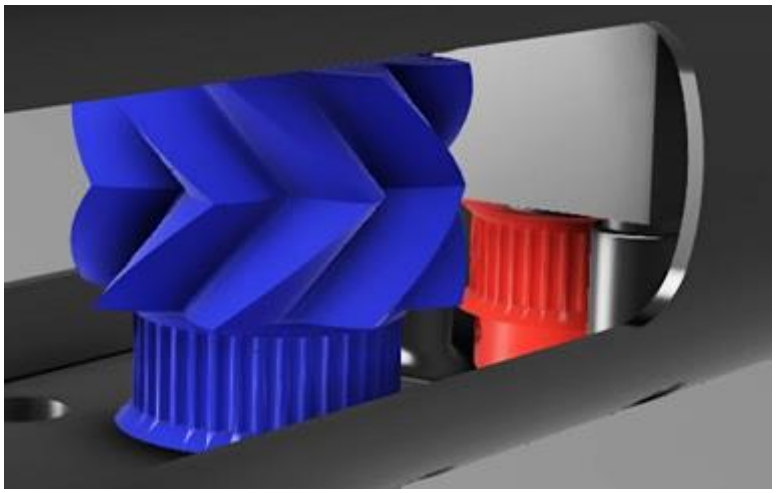

Figure 50: Mk 1 components in their approximate locations. The blue gear and pulley are a single piece, and are powered by the red pulley. The belt connecting them is omitted for clarity. See also: Fig. 13.

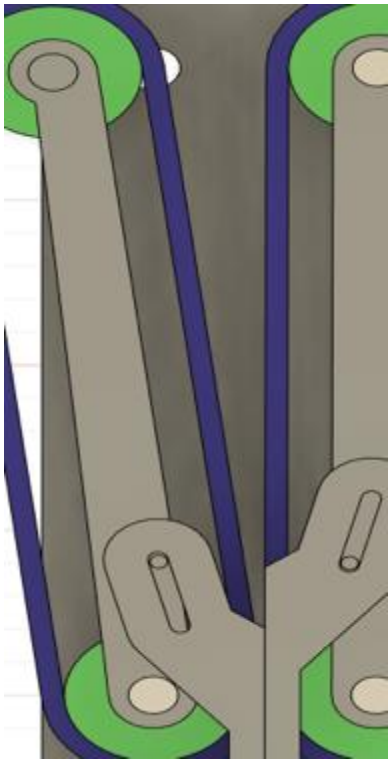

Figure 52: An early sketch of a variable pressure drive, with enough deflection to "steer."

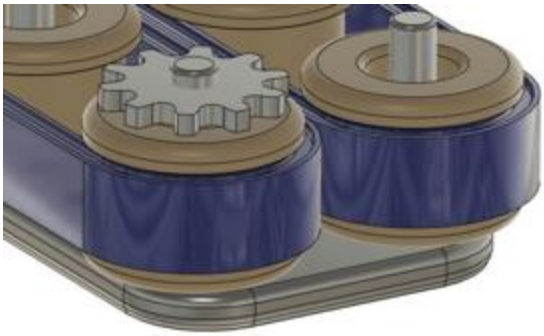

Figure 51: Sketch of a sprocket for chain drive

The borebot will be responsible for providing the Weight on Bit (WOB) needed by the drill, the effective pressure against the borehole wall (either by design or by active control, see Figure 52), and will also need to provide attitude corrections to maintain the straightness of the borehole. While WOB and pressure have been touched on previously, the concept of "steering" adjustments makes the situation more complicated, and further makes the case for mechanical control of track pressures. It does appear that having a variable-pressure drive can increase drivetrain efficiencies overall (and still provide good traction for WOB demands during drilling), so this consideration alone may make it the more desirable choice. However, the available steering angle is limited to around one degree, so the usefulness is limited to maintaining vertical.

If true directional drilling is desired, we believe that linking two borebots together with a flexible articulated joint is the only way to provide a truly robust directional drilling capability. This will allow for the drilling of branch bores, as shown in Figure 53, and may allow for drilling around a stuck borebot.

When a branch borehole is desired, the articulated joint can be retrieved from storage and mated to the front of a borebot. The companion borebot (the one with the drill attached), can be deployed into the borehole, and the joining of the articulated joint and the drilling borebot can take place downhole. The unit can be removed from the hole, cleaned, and recharged as a whole (by the same process discussed previously). For the duration of branch bore operations, coupled articulated units will have to be used. This halves the number of available units, and doubles the wear that each borebot will have to endure. For this reason, if branching is considered for purposes of going around an obstruction (stuck borebot or other obstruction), abandoning the borehole and starting a new one should be considered.

If creating a branch borehole simply to take an "extra" core at a certain depth in the stratigraphy, it is likely that normal operations can be resumed afterwards (although this may only be feasible if the borebots have two or more pairs of tracks). It can be seen in Figure 53 that a single-track-pair borebot would have a difficult time climbing past the intersection with the branch. However, if the clocking of the borebot can be controlled (which is not currently planned or envisioned), a single-track-pair borebot could have adequate traction through the intersection area if the tracks were oriented 90 degrees to the plane of the intersection. Said another way, in Figure 53, the track pairs that can be seen facing the camera are always engaged with the borehole, and the track pairs lying in the plane of the intersection can lose traction due to the excavated area of the intersection. If a single borebot attempts to navigate the main borehole after the creation of the intersection, the tracks must be aligned to have traction the entire time. If clocking control is not available, multiple tracks can mitigate this challenge, but may not eliminate it.

The challenges of developing an articulating joint, stowing it on the spacecraft, and installing it *in-situ* are considerable; and are likely to be a significant burden on mission development activities and mission operations. However, branch bore operations with wireline drills are likely an even more significant burden. This study doesn't attempt to speak for wireline drill system designers, but in the borebots context, we recommend against the incorporation of a branch bore capability into an PLD deep drilling mission. A borebots mission with sufficient component lifetimes to enable a 1500-m-deep bore would be able to drill roughly nine 500-m-deep boreholes instead. Therefore, abandoning the borehole and starting another borehole is highly desirable when weighed against heroic measures to salvage a borehole that is obstructed, etc. Multiple boreholes could even be drilled simultaneously. The borebots architecture makes all of these options more feasible and less risky, and arguably makes the goals interchangeable after landing.

Figure 53: Branch bore drilling using an articulated joint.

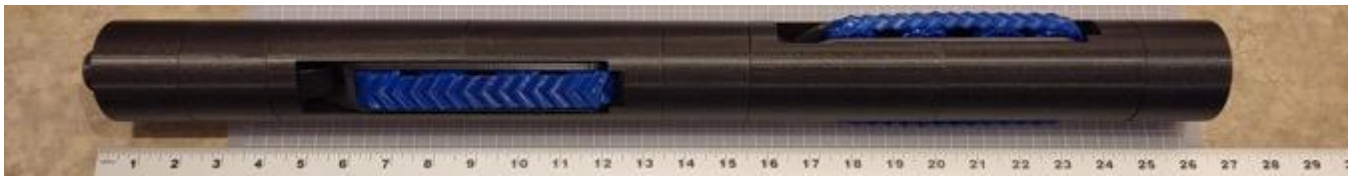

Figure 54 (above): Modular drag-test prototype. Scale shown reads in inches.

Figure 55 (right): Drag test prototype in a 64-mm diameter, two-meter-long acrylic tube.

The prototyped components discussed earlier in this section were integrated into "modules" (Figure 41) that could be tested alone or integrated into a larger modular mockup unit (Figure 54). The larger unit helps to keep tracks aligned with the bore properly, reducing the tendency of the belts to go off-center. Recall that the Mark 3 drivetrain is highly sensitive to belt tension, which was not the case in the earlier staggered self-tensioning versions. An additional consequence of the lack of self-tensioning is that the floating idlers tend to get misaligned. For this reason, floating idlers will be discontinued in favor of fixed idlers in future iterations. With idlers properly aligned, a 20 N force is required to move individual units during "drag tests," while the larger mockup unit often required 50 N to keep the movement going at a constant speed, and often experienced the misaligned idler issue, or belt deflection due to the sensitivity to tension. These forces are prohibitively high. Mark 2 prototypes required a consistent 25 N of force and experienced little noticeable variation, except for "flat spots" when the unit had been sitting for extended periods of time. With idlers removed, the larger prototype unit with two Mark 3 drivetrains could be moved with less force than a single Mark 2 drivetrain (around 20 N).

We believe that a force of 20 N is consistently achievable for initial TRL 3 prototypes, and hope that future iterations can bring this down to 10 N for the gear-belt and below 5 N for the flat-belt versions of the drivetrain (if the flat belt versions can be proven reliable). This means we expect an order-of-magnitude reduction in "drivetrain friction force" from where it is today, which is a very bold claim. However, the early status of the prototypes and the nature of the challenges that we are experiencing do indicate that these problems can be solved, and the friction forces reduced. If the higher forces persist it will reduce achievable depth by around 500 m, increasing the number of required battery packs to seven or eight, which would make the 64 mm borebots too long to be feasible for basal unit access in our SPLD deep drilling mission context. Larger diameter borebots would be better suited to this type of drive system force, but they may be able to optimize the drive system to a greater extent due to the reduced challenge of miniaturization.

Overall, the drivetrain challenges remaining are significant, which is why we are increasing our focus on the drivetrain itself, and increasing our commitment to iterative design and testing of drivetrains. Note: generally, we refer to the track system as the drivetrain. However, when other drivetrain components are being discussed (as in the Power and Components section), the phrase "track system" will be used to add clarity. In this section, the drivetrain *is* the track system, as upstream components have been only tangentially referenced.

The question of "what do you do when a borebot gets stuck?" really is a significant one, and is the most common question that we get. Drilling failures are likely in any extraterrestrial deep drilling mission. As an alternative to using branch boring to avoid a stuck borebot, the best way to mitigate this is to use one or more borebots as "tugs" in order to extricate their stuck companion. A procedure for extrication was developed and is outlined below. Note that if the batteries have simply died, it may be possible to charge one borebot from another (like a jump-start). A modular jump-start pack could also be made that could fit in the core volume of the drill head itself, so a jump start functionality could be provided without removing the drill head from a borebot. Regarding borebot communication, the range is expected to be extremely limited. If a borebot doesn't show up at the surface when it is expected, another borebot will have to act as a relay station to drive down, collect troubleshooting data, and come back up to transfer the data to the rover. If this process were to fail, it would indicate a dead borebot.

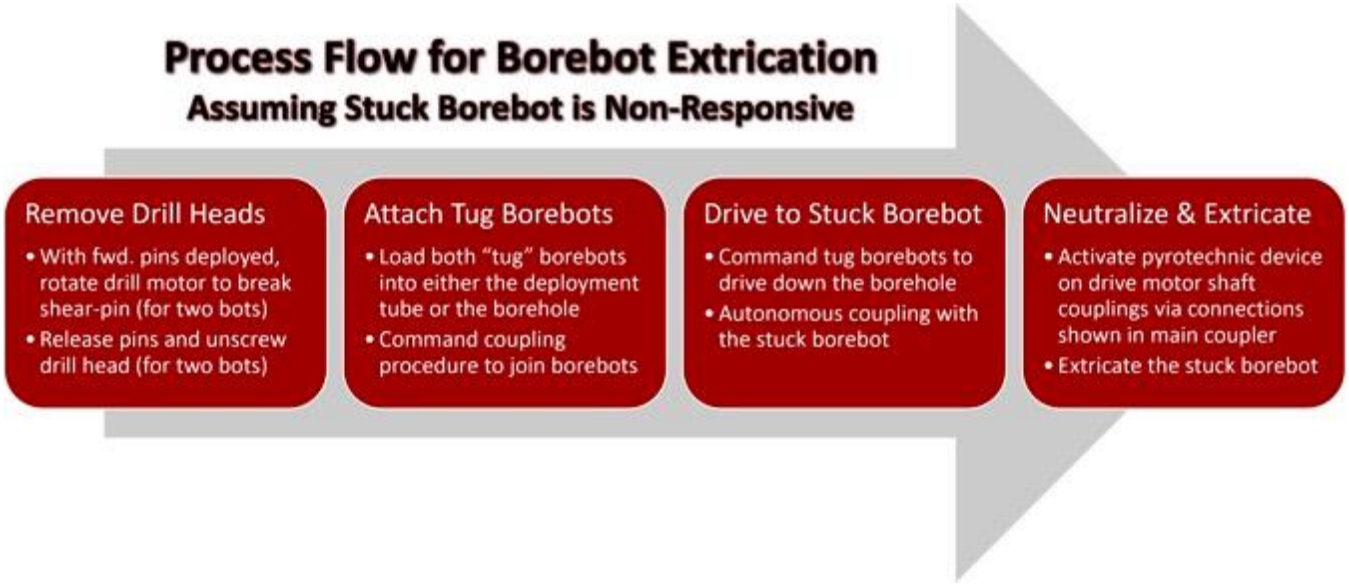

Figure 56: Process flow for borebot extrication, assuming the stuck borebot is non-responsive. Ref. Figures 55 & 56.

If recovery efforts are unsuccessful, the borehole should be abandoned, and a new drill site selected (as discussed previously). Most competing architectures would not be able to start a second (or third) borehole with a loss of downhole equipment, so we view this as an advantage to the borebots architecture, not a disadvantage. The flexible nature of a borebot itself is a strong argument for having an assembly capability on the spacecraft. As is shown with this extrication strategy, a unique solution to a problem can be developed using only the natural functionality of the borebot. Every attempt should be made to anticipate this type of unique solution ahead of time, so small design decisions that could allow for greater flexibility can be incorporated into the hardware. If, after considering this, an assembly capability on the spacecraft is still undesirable, it may be prudent to bring as many borebots as possible.

The most logical way to couple borebots to end effectors (or other borebots) is with a threaded union (Figures 57 & 58), so the drill motor can be used to couple / decouple the attachment. For units pre-assembled on Earth, a shear pin can be pressed into the threaded union to act as a mechanical fuse. Units assembled *in-situ* may have to rely on a pre-determined torque value, or a shear-pin installation device can be included in the assembly station. The shear pin should be designed to fail at a torque level below the maximum of the drill motor, so a borebot can lock the drill head from rotating (via pin pullers, discussed in the next paragraph), and break the shear-pins. The attachment can then be unscrewed.

Figure 57 shows not only the main coupler (threaded boss at center), but also two large pins and two small electrical contacts. The electrical contact pins can provide both a charging current (low amperage) and a pyro detonation current (momentary high amperage). Figure 58 shows the copper slip ring to make a solid electrical connection with the electrical contact pins. The larger deployable pins, however, can have many uses. Space is extremely limited in this area, but motor gearheads are commonly a slightly smaller diameter than the motor itself, creating an annular volume for the integration of pin puller mechanisms (Figure 62 – 65).

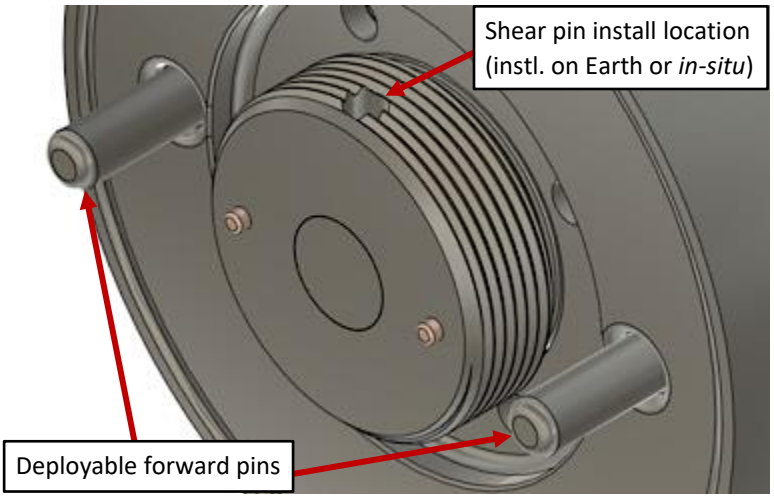

Figure 57 (above): Coupler on fwd. end of a borebot. Note electrical contacts. Fwd. pins are in the deployed position. See also: Figure 60.

Figure 58 (below): Receptacle on aft end of a borebot.

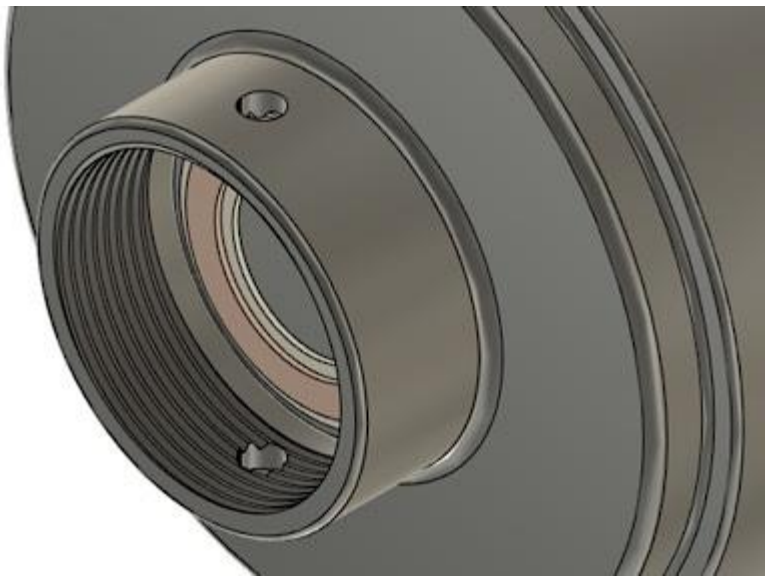

Two options for pin pullers in this small volume were developed during Phase I, the first being the bimetal pin puller concept shown in Figure 65. After sketching this concept out, enough annular volume remained to allow for a more advanced mechanism. The second option was then developed, which is the annular solenoid. The annular solenoid should be a more robust device that can be proven before it is integrated into a borebot.

The mechanisms described here are merely examples that were developed to demonstrate the feasibility of small annular pin pullers in this context. The main driver for this is the need to actuate the iris. However, the deployable pins ("Forward Pins") can also be used to break shear pins prior to removing a drill head, and can be used to actuate the water sampler penetration probe release mechanism (See the Sampling Subglacial Liquid section). They may offer other advantages when used with other end effectors. For example, six types of mechanical input could be provided by using the pins as part of a mechanical computer (fwd. no pins, fwd. 1 pin, rev. 2 pins, etc.). This could provide mechanical power to sub-sampling devices, science instruments, etc.

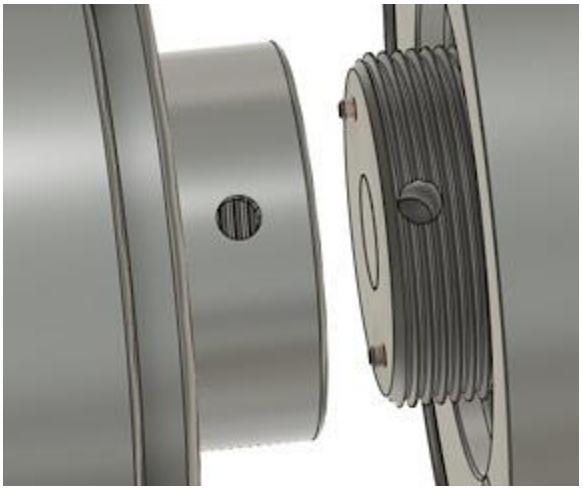

Figure 59: Two borebots being coupled.

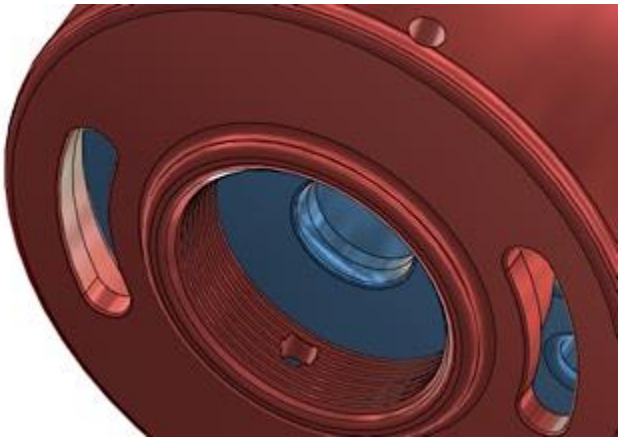

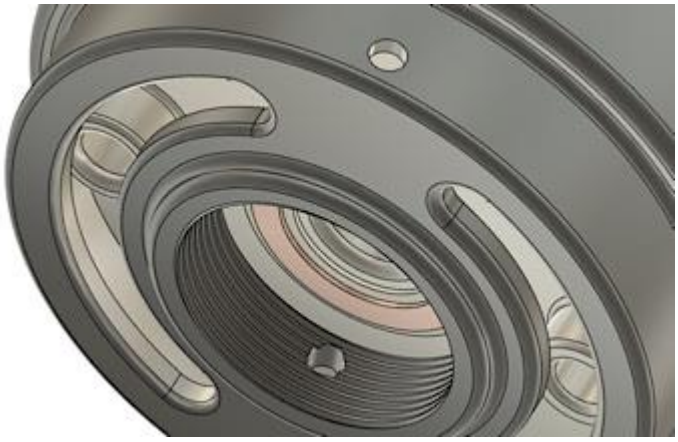

Figure 60 (left): Aft end of a drill head with receptacles for the threaded coupler and forward pins.
Figure 61: Aft end of a water sampling device, with a copper slip ring and greater range of motion for forward pin rotation.

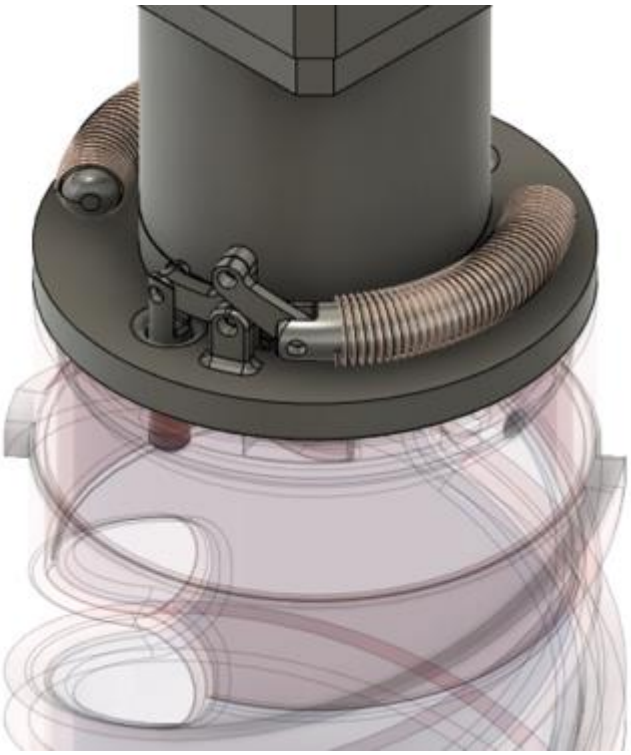

Figure 62, 63 & 64 (left, below, and below left): Pin pullers for the forward pins are required to be annular in nature, and can fit around the gearhead of the drill motor. One possible configuration is an annular solenoid laid out as shown.

Figure 65 (bottom right): Another option, using annular bimetals as pin pullers. Other options exist.

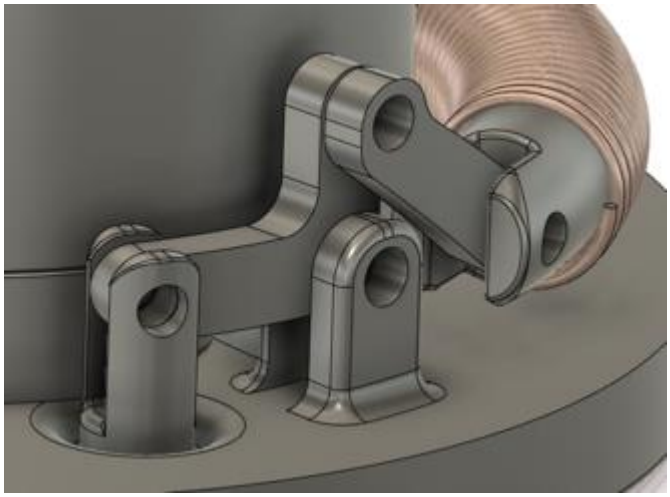

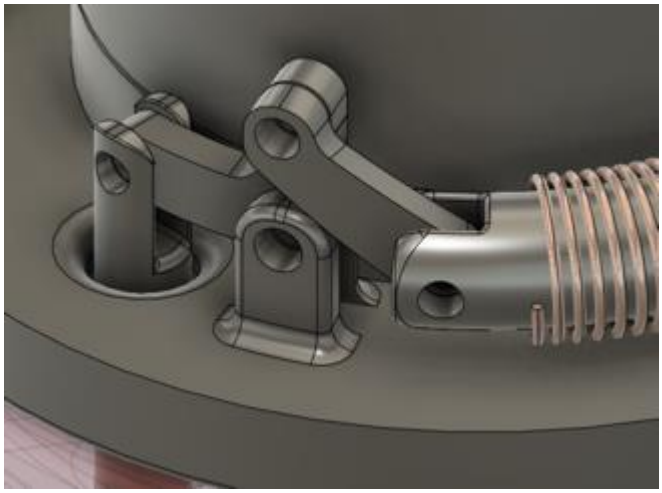

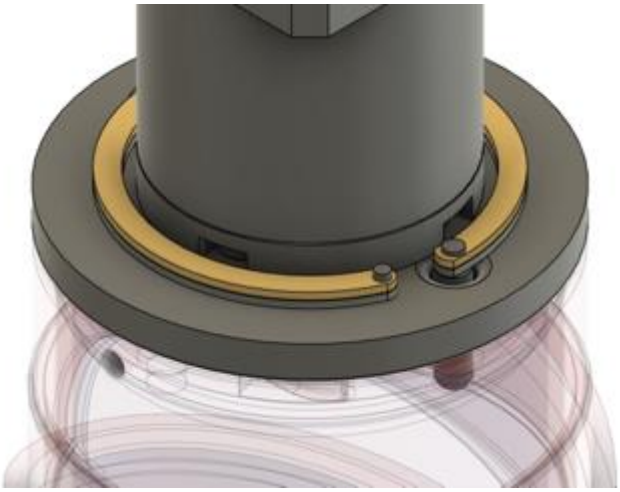

Drilling

Generally speaking, any drilling head can be used with the borebots system if the drill head in question can be made to match the diameter of the borebot (which itself can be modified). The size of the borebot could be increased to match a drill head if it had advantages over other options. The size of the borebot was chosen to represent a practical lower diameter limit and to align with existing drill heads in the NASA technology pipeline (like the Planetary Deep Drill mentioned previously; see Zacny et al., 2016). That said, there are unique limitations to the borebot system that merit the design of a unique family of drill heads specifically tailored for integration into the borebots architecture. The two main limitations are the Weight on Bit (WOB) available to the drill head (as the drivetrain must supply nearly all of the WOB experienced by the drill), and drilling efficiency. If drilling efficiency suffers, the drilling process will have to be cut short in order to leave enough power available for the return trip.

The design of drill heads for the borebots architecture is a secondary consideration for this project, and is mainly undertaken to provide a jumping-off point for mission planners. The modification of existing drill heads can be undertaken to reduce WOB requirements while keeping drilling efficiency reasonable. The authors do not claim to be drilling experts; however, we note that conventional drilling wisdom (Talalay, 2014) does not fully align with the most optimal cutting geometries as described in Ueda & Kalafut (1989). This misalignment may be due to the "luxury" of high WOB, combined with the power availability inherent with heavy tethered (read: surface powered) systems. This is the logical basis for the development of an annular drill head with a 30-degree-rake angle for use with the borebots system. We then bifurcate this drill head into two versions, one with a thicker annulus and one with a thinner annulus. The thicker annulus allows room for a unique core breaking and retention mechanism, while the version with the thinner annulus uses a more traditional "core dog" retention device.

The drill head with simple core dogs is shown in Figure 66. The core dog retention devices were based on Figure 68, but rotated 90° (Talalay, 2014, fig. 25). The location of the core dogs is shown in detail in Figure 67. It should be noted that this is just one option for core retention; this configuration is simple and robust, but difficult to manufacture. With a diameter of 64 mm and a core diameter of 45 mm, breaking the core usually isn't the hard part – holding on to it is. To mitigate the challenges of retaining the core (especially when the composition is uncertain), a spherical iris cutting and retention mechanism was investigated (Figure 69, closed position; Figure 70, open position). The device can be seen with the outer (red) part of the drill hidden in Figure 71 and 72. Two animations of the iris closing action are available; they can be downloaded from https://git.io/JsKah and https://git.io/JsPov.

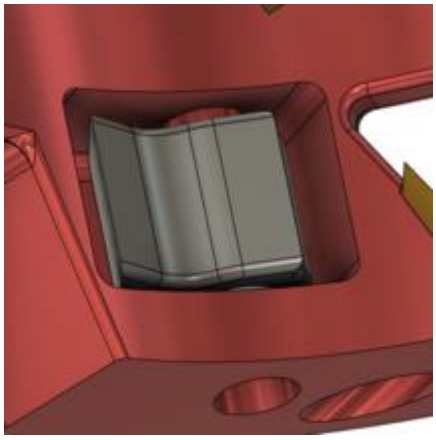

Figure 66 (left) and 67 (right): Drill head with "core dogs," 45 mm core.

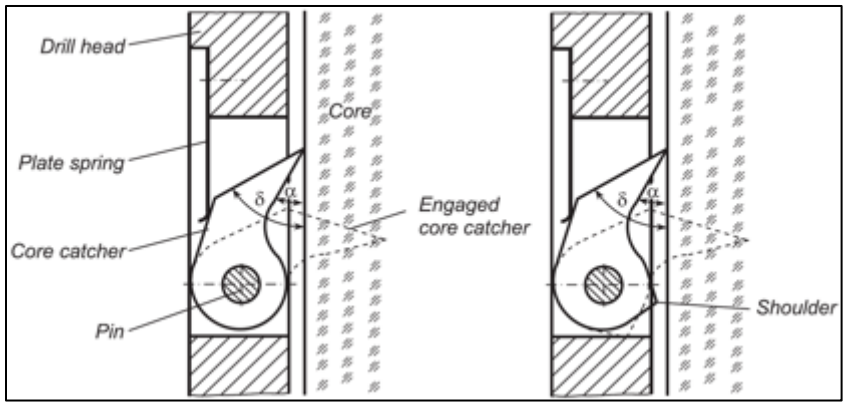

Figure 68 (left): core dogs diagram from Talalay, 2014 (fig. 25, p. 51).

Figure 69 (bottom left): iris core retention mechanism in the closed position. Titanium-Nitride-coated (gold colored) Carbide tips can be seen on the iris blades at the center.

Figure 70 (bottom right): iris core retention mechanism in open position. The mechanism reduces the core diameter to 40 mm.

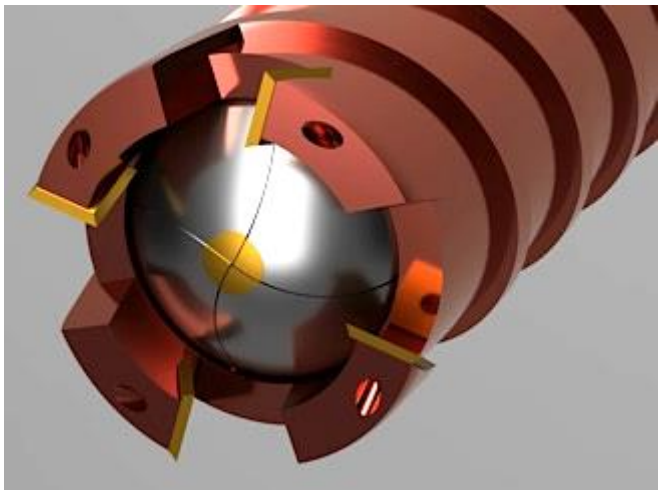

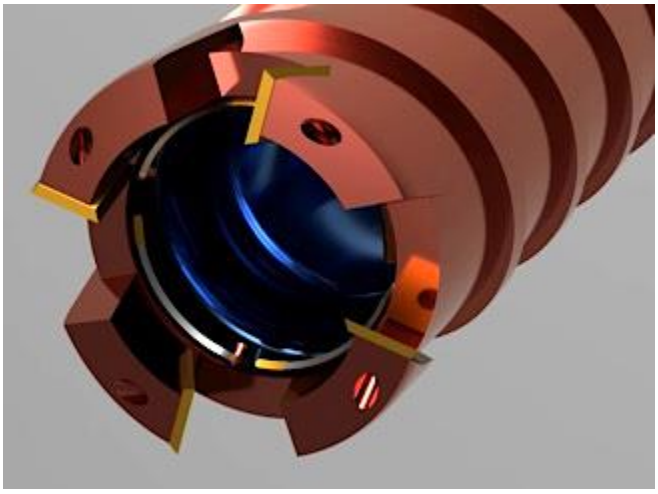

To accommodate the iris mechanism, the effective core diameter drops to 40 mm. Actuation of the iris is provided by the inner barrel (shown in blue), which can be locked to the borebot body via deployable pins (Figure 57) in the front of the borebot. This allows the drill motor to rotate the outer barrel (red) while the blue barrel remains fixed, providing the motion necessary to close the iris. The iris mechanism is based on a "print in place" preassembled iris box (Lalish, 2016; Kerr, 2016), and was published on Thingiverse.com to respect the open-source license (Morley, 2021).

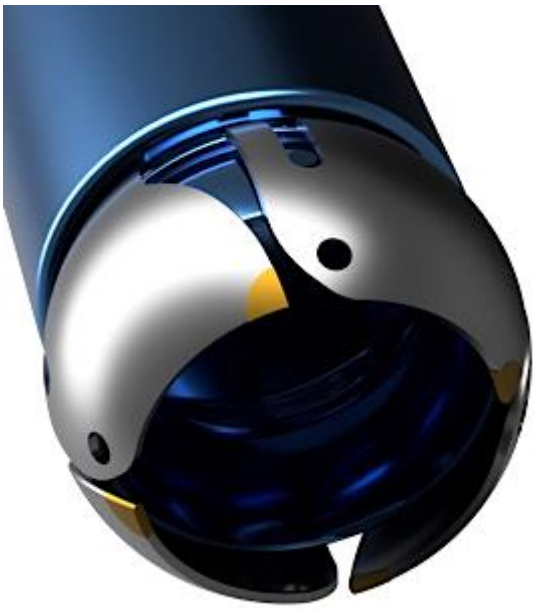

Figure 71 (left) and 72 (right): iris mechanism with red outer portion of drill hidden. Iris blades pivot around hole at fwd. end.

There are several advantages to this kind of a core breaker and retainer. For one, it can retain unconsolidated material or severely broken cores, while only reducing the overall core diameter by 5 mm. It is also possible to use the iris to incrementally cut solid cores, turning the core-breaking step into a machining procedure instead of a fracture procedure. This can reduce the required torque to initiate a break, which helps make a borebot with only a single pair of tracks more feasible. The incremental core-breaking process would require the installation of a ratchet in the aft end of the drill head, and there is room adequate for such a device. It is possible to reset the ratchet (after the iris is closed) using a few methodologies, the simplest being the operation of an electric solenoid via the electrical connection integrated into the borebot main coupler. Another method may be to only deploy a single pin puller (instead of the pair of pin pullers at once), thereby offering an analog mechanical input that can reset the ratchet when the drill motor is rotated with only a single pin puller deployed. Another method could allow for the ratchet to lock with slight counter-rotation, but to disengage with half-turn counter-rotation. Other methods are possible, these are offered as robust examples that fit the available space. Future prototypes are likely to feature ratchets that require a manual reset, to facilitate testing.

The presence of the inner barrel (and control over it) can help prevent chips and fines from packing in both the throat of the drill head and the hole at the top of the flutes (all cuttings are to be routed to the central chamber of the drill head, where room is available aft of the core for cuttings storage). This may potentially have a benefit even without the iris core retention, as smaller and more frequently-spaced holes can be added along the flutes to route material into the center chamber of the drill head, and these holes would match up with corresponding holes in the blue inner barrel. When the inner barrel is rotated, it could operate like a cheese-grader, bringing the cuttings into the central chamber (it may be desirable to add punched "scoops" to the inner barrel to accentuate this effect). This "cheese-grader" functionality has nothing specifically to do with borebots, it is simply a benefit to having an actuatable inner barrel. It will not be explored further, although the iris drill head will benefit by having the inner barrel available to keep the cuttings hole clear (video animation at https://git.io/JXkI8).

The WOB available to / required by the drill is still unconstrained (although Ueda & Kalafut, 1989 is encouraging). Due to lower gravity on Mars, it is wise to design the system such that 100% of the required WOB comes from the drivetrain. The borebot mass (on the order of 10 kg) may not be sufficient. WOB is a parameter for optimization, as the requirement at the drill head drives the normal force required of the drivetrain against the borehole wall. If, for example, $1000\ N$ of WOB is required, and a 0.25 coefficient of friction is used, the following normal force would be required from each track pair:

$$f_{friction} = \mu F_{normal}$$

$$f_{friction}/\mu = F_{normal}$$

$$F_{normal} = 1000\ N/0.25 = \mathbf{250\ N}$$

Practically, this would equate to a preload (when the tracks are squeezed to conform to the borehole diameter) such that the resulting normal force (from the Hooke's law behavior of the track/gear material) is $250\ N$ total, or $125\ N$ per individual track. This may be a good reason to use a variable-pressure track system, as such a normal force may not be required during driving, and could increase the friction in the drive system. This would then become an optimization parameter and could be leveraged with the approach discussed in Joshi (2021).

Power and Components

The Mars helicopter technology demonstrator Ingenuity has shown that relatively low-cost Commercial Off-The-Shelf (COTS) hardware can survive (and thrive) in Martian conditions. The thermal management used on Ingenuity is the best example we have for polar operations during the summer (Cappucci & Moulton, 2018). The borebots architecture potentially has a few advantages over Ingenuity, but some of them may come at a cost. For one, we have the opportunity to store borebots back in their flight-stowage location where they can enjoy an amenable thermal environment and a power link to the rover. This complicates the storage functionality, so it should be considered a last resort. It is true that the harshest conditions a borebot is likely to face are at the surface, so it is an option that should be kept in mind. Battery charging is possible when loaded in either the assembly station or the cleaning station, but there is no protection from the temperature at either location. Heaters inside the borebot can likely compensate for this. Another advantage is the time spent inside the ice (believe it or not). The ice can protect the electronics from solar and cosmic radiation, and provide a much more predictable thermal environment. It is estimated that the base of the ice sheet has a temperature between 180-200 K (Buhler, 2021; Sori & Bramson, 2019), which is approximately equal to the design criteria used for Ingenuity (Balaram, 2021; 2018). For more on the environmental conditions expected, see the South Polar Layered Deposits section of this chapter.

The body of a borebot has an inside diameter of between 54 mm and 58 mm, which (generally speaking) can fit batteries in groups of five in that space. The battery that we are looking at in-depth is the tried-and-true 18650 lithium-ion cell (Darcy & Scharf, 2015; Walker, 2017). Two groups of five batteries appears to be the minimum logical energy storage option for a borebot. However, we have the option to add up to five groups of five batteries before storage of borebots on a rover becomes challenging. The fewer batteries contained in each borebot, the more borebots total can be brought in a given spacecraft. Preliminary power modeling shows that there does not appear to be a penalty for increasing the energy storage capability in borebots. The available spacecraft storage, manipulation capability, and recharging ability are the primary reasons to limit the number of cells per borebot. The amount of heat needed to keep the batteries above zero Celsius (the lower practical limit for most chemistries) is watt-order, and is still poorly constrained. A sketch can be seen in Figure 73 which shows two groups of five cells, separated by a 1-watt radioisotope thermal generator (RTG) to help keep the batteries warm. To unlock SPLD basal unit access, it will take between six and twelve five-cell battery packs. Adequate storage is therefore challenging. Each five-cell pack has a nominal capacity of 2,200 mAh and a nominal voltage of 18 V.

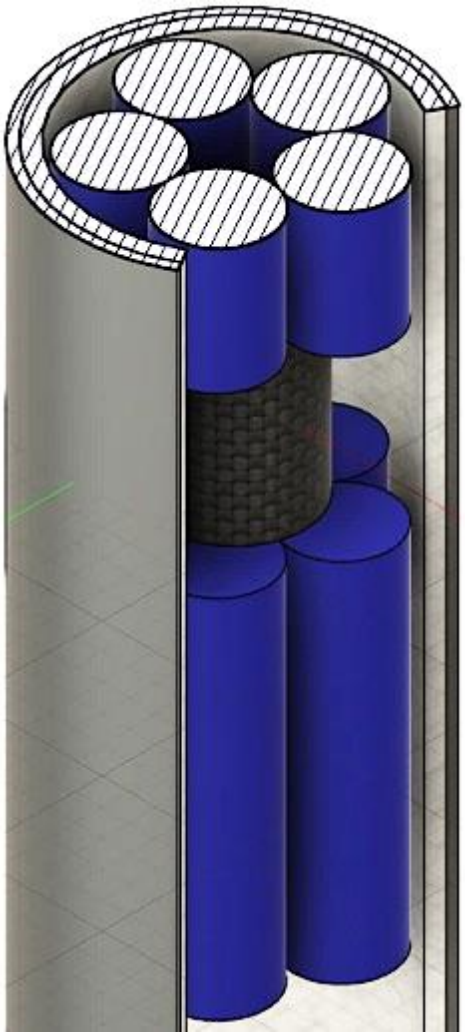

Figure 73: Ten 18650 Li-Ion cells and a 1-watt RTG to keep them warm.

Depth (m)	Number of Trips	Drive Time per Trip (min)	Cumulative Distance (m)	Trips per Bot
1	7	1	8.40	1
10	67	2	683.4	6
50	333	4	16,683	28
100	667	8	66,833	56
200	1,333	14	266,733	112
500	3,333	34	1,667,000	278
1,000	6,667	68	6,668,000	556
1,500	10,000	101	15,000,000	834

Table 2: Logistics of drilling a 1500 m borehole with 12 borebots. 150 mm core length, drilling time neglected.

The logistics of deep drilling with multiple borebots can boggle the mind when considered at scale. However, the concept does appear to stand up to rigorous analysis. Prototype bench testing is required in order to dial-in some of our unknowns and better constrain the parameter space. Optimization of the borebots system will be complicated but rewarding, as the plot below shows (Figure 74). The system is sensitive to very small changes, notably: friction in the drivetrain, hotel loads from onboard electronics during the drive, drive speed (which makes hotel loads higher-impact on longer drives), and available onboard power. Our power model has shown that the drivetrain power draw is expected to be the same order as the drilling power draw. Thus, the values can be set equivalent to simplify some of the parameters in order to find the theoretical depth limitations of a borebot system.

Figure 74 (below): Power model plot with two-to-seven packs of five 18650 cells each. Assumptions: driving and drilling consume 30 W each, with a 20-W electronics hotel load (50-W total draw), core length of 150 mm, 37.5 min. drilling time.

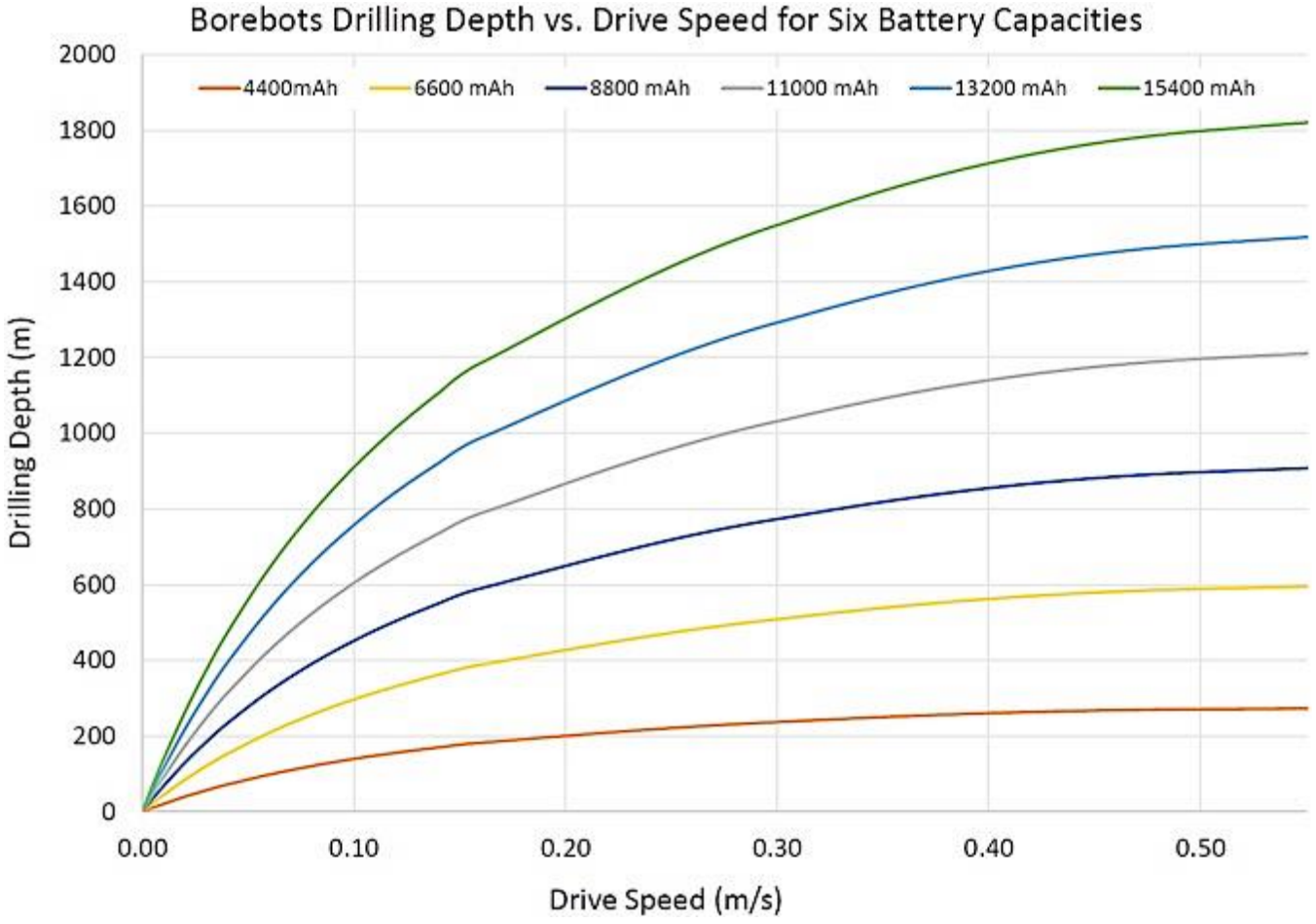

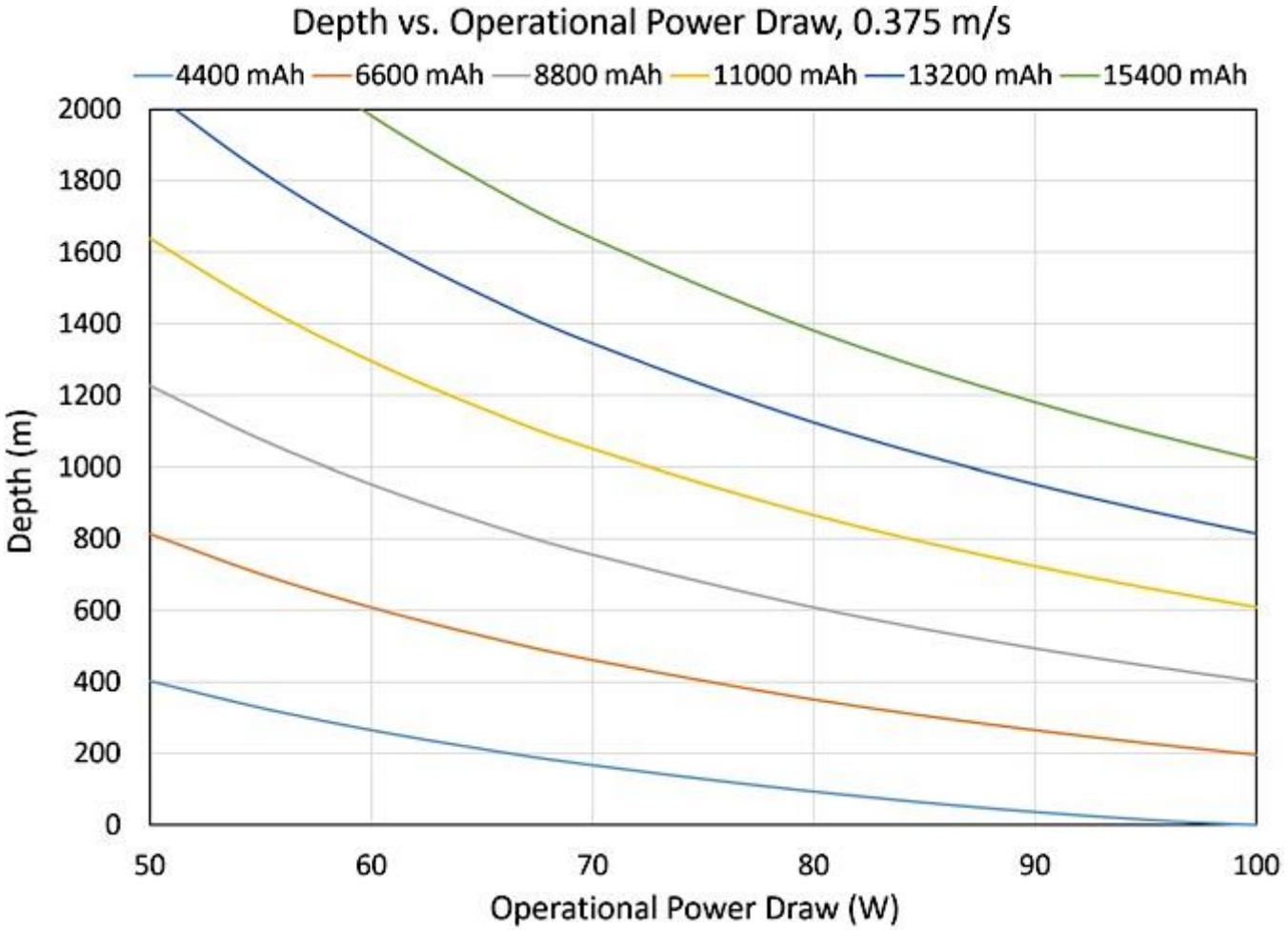

Figure 75 (above): Simplified power model; shows effect of high power draw on depth for 0.375 m/s travel speed.
Figure 76 & 77 (below): The same plot as Figure 75, with a drive speed of 0.25 m/s (left) and 0.50 m/s (right).

The equation used for drive power in the simplified power model is: drive power = (gravity · borebot mass · velocity) / (system efficiency) + friction · velocity. Depth in meters as a function of power is then: depth = velocity · [battery cap in Joules / (power draw) – drilling time] / 2. Assumptions: 20-watt hotel loads, core length of 0.15 m, fixed bot mass of 10 kg, 12 borebots, 37.5 minutes of drilling time per core, 18 V battery packs, minimum state of charge (SoC): 25%.

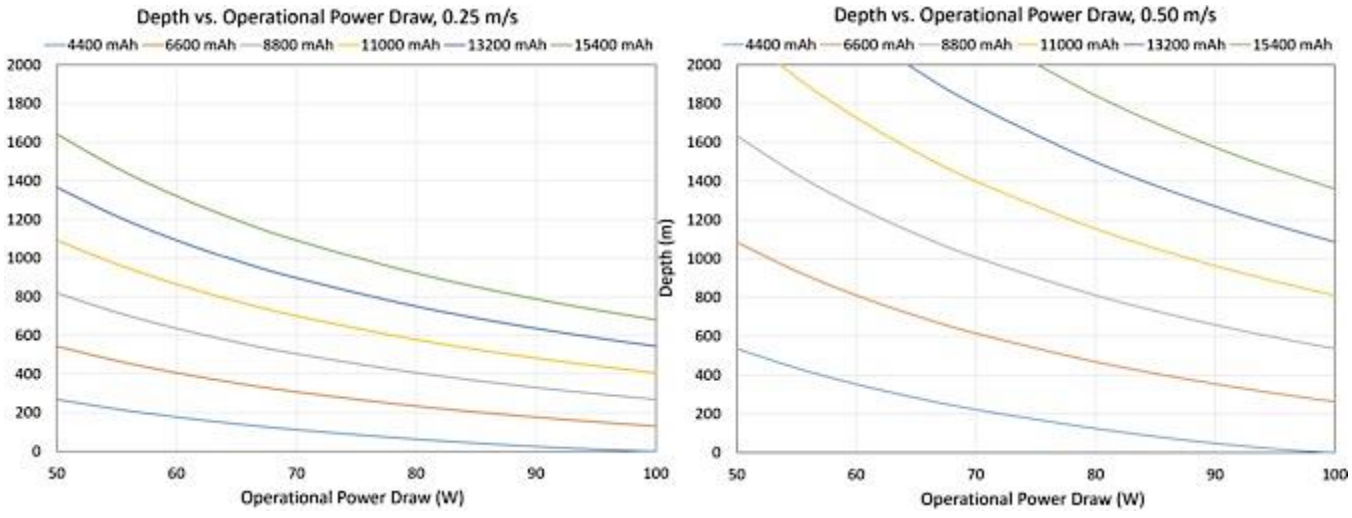

It can be seen in Figures 74 – 77 that battery storage requirements start to get prohibitive as depth increases. However, at drive speeds approaching 0.5 m/s, and with an efficient drivetrain, depths of greater than 2 km may be possible with as few as 20 of the 18650 cells. With the extended mission goal set at 1500 m, the real-world minimum required energy storage is 30 cells. The immediately obvious problem now is that the diameter of 64 mm used during the course of this work makes the storage of sufficient batteries a challenge. Approximately half a meter of borebot length would be devoted strictly to battery storage. This would make stowage and manipulation by the robot arm very challenging.

Increasing the borebot diameter to around 108 mm would allow for groups of 15 cells instead of five (Figure 78). The reason for the evaluation of 108 mm as "the next size up" is because it is the borehole diameter than the WATSON instrument was designed for (Eshelman, 2019; Malaska, 2020). See the Borebot Instruments / Downhole Science section for more about WATSON. As opposed to attempting to miniaturize the WATSON instrument, if the borebot diameter is increased to match, the battery storage problem is mitigated for missions targeting greater depths. Figure 78 shows that sixteen cells can fit (if one cell is placed in the center), or 15 cells with a centerline pass-thru capability for heaters, heat tubes, wiring, etc. In this configuration, two packs of 15 cells are much more reasonable than six packs of five. The larger diameter also helps prevent the borebot from becoming prohibitively long during integration activities (Bar-Cohen, 2009; Zacny, 2021). During Phase I, we didn't engage in any prototyping activities for larger-diameter borebots. However, the challenges of miniaturization are a significant struggle at the 64 mm size, and the larger diameter should offer improvements in both the mechanical design and assembly areas (in addition to greater science instrument compatibility and more favorable power storage). These are compelling reasons to look at sizes 108 mm and larger, especially in mission contexts involving larger landers and greater depth targets.

For potential ocean worlds missions (Europa, Enceladus, Titan, etc.), sub-surface ocean access may be possible (Figure 80 & 81), but an enormous amount of power storage would need to be available, so sizes approaching 300 mm may be worth considering. Significant uncertainty remains for depths greater than a few km, represented by the growing shaded area in Figures 80 & 81.

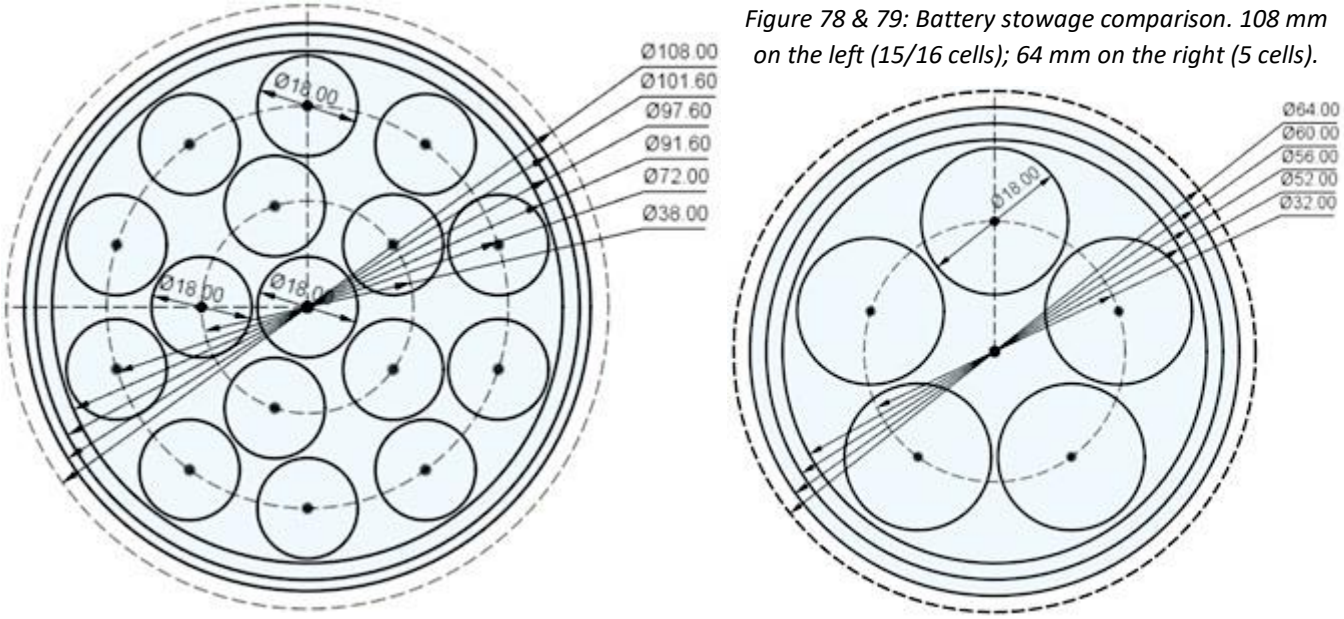

Figure 78 & 79: Battery stowage comparison. 108 mm on the left (15/16 cells); 64 mm on the right (5 cells).

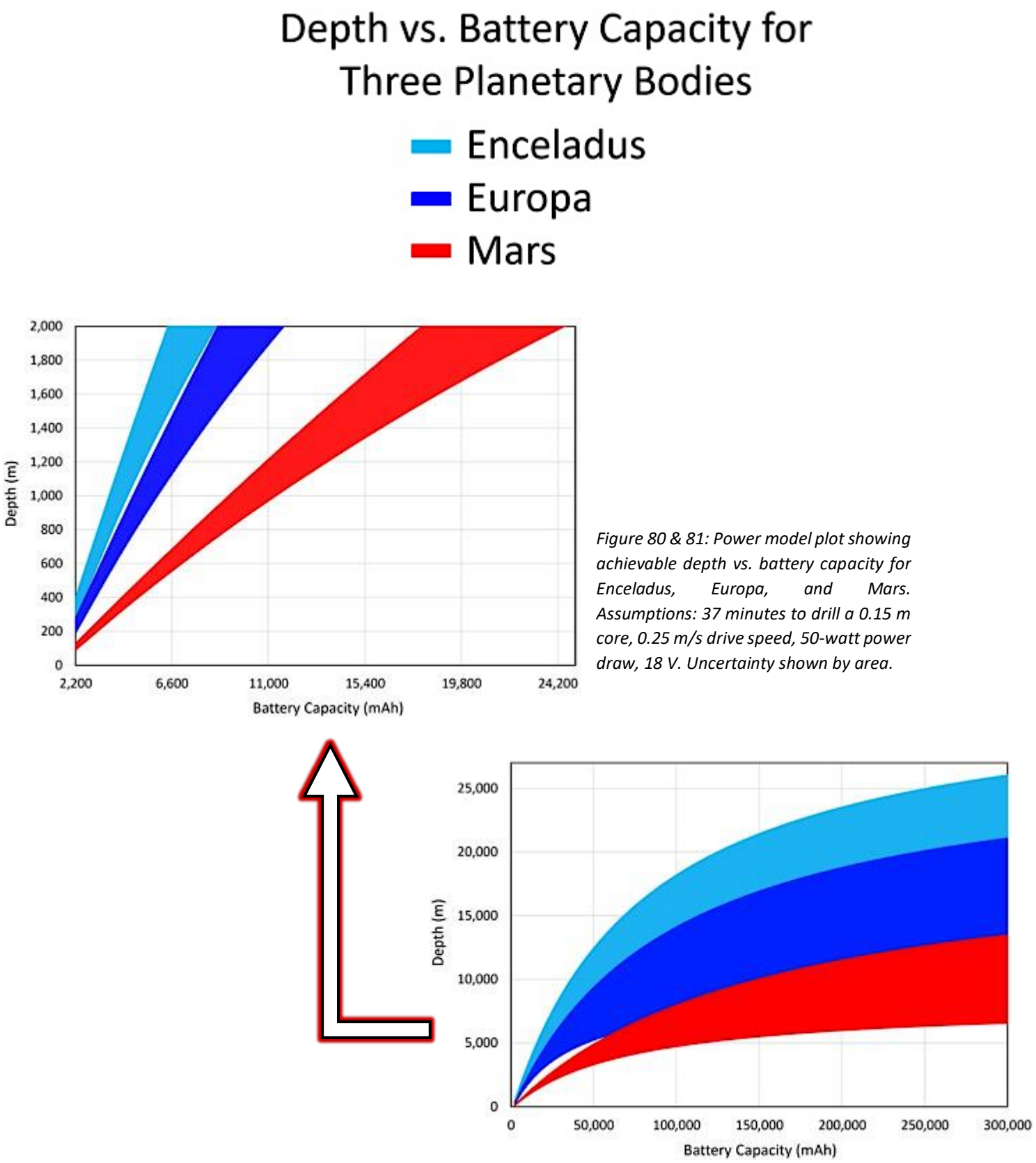

Figure 80 & 81: Power model plot showing achievable depth vs. battery capacity for Enceladus, Europa, and Mars. Assumptions: 37 minutes to drill a 0.15 m core, 0.25 m/s drive speed, 50-watt power draw, 18 V. Uncertainty shown by area.

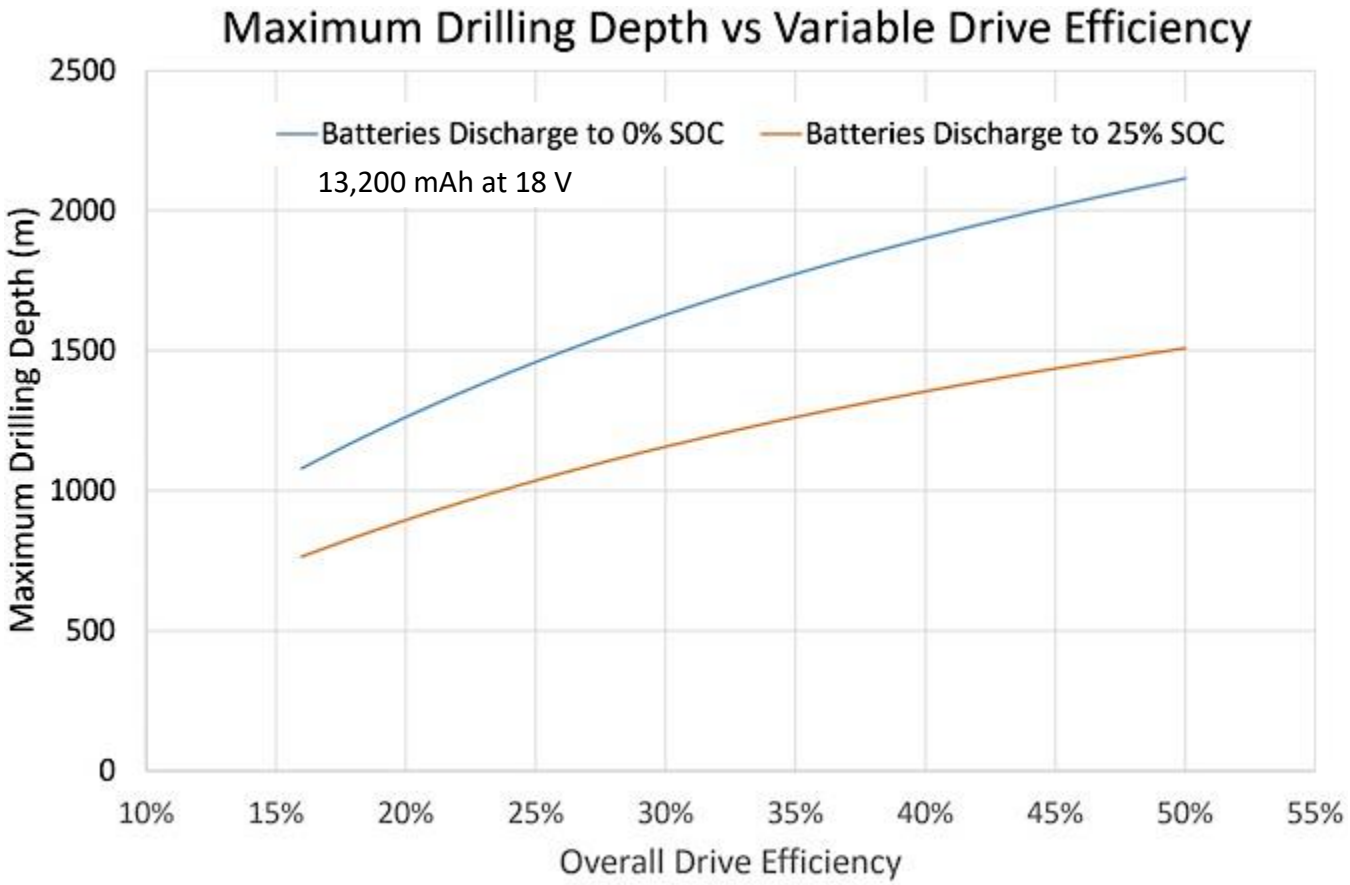

Figure 82: Borebots system sensitivity to overall drivetrain efficiency, 0.25 m/s. Six battery packs (13,200 mAh at 18 V).

The power model developed during Phase I has been very helpful to evaluate the feasibility of this concept, and examine the ramifications of different assumptions and configurations. A discussion of this model follows; however, it is limited to key decisions, with a focus on component selection and preliminary thermal considerations. The derivation of the equations used is covered in Appendix A, and the Excel VBA script used to build the power model spreadsheets is located in Appendix B.

To create a model that outputs achievable depth, we focused on power demands compared to battery capacity and battery life. Commercially-available lithium-iron-phosphate battery systems provided a solid foundation of high power density and reliability to work from. These have well understood heat generation, capacity, and ageing functions that we incorporated into both our thermal analysis and mechanical models. The battery capacity is affected in large part by discharge rate, so our power modeling targeted rates below 0.5C to avoid excess capacity loss and accelerated ageing. A linear ageing model for capacity reduction was chosen for simplicity. A conservative starting capacity of less than 100% (93%) was chosen for modeling to reflect the variability of low cost 18650 cells. Additionally, the minimum allowable state of charge was limited to 25% for reliability and increased battery cycle life.

The thermal characteristics are still poorly constrained. However, the heat generated from battery discharge, combined with heat loss from a simple cylinder, does put us within a single-watt order of magnitude from equilibrium at 0°C. So, depending on battery chemistry and drive speed, heaters will not be required to maintain 0°C, or will be watt-order. The thermal analysis is more difficult to constrain and justify than the mechanical considerations. Since breadboard components, insulation, and surface coatings have not yet been selected, we decline to offer a numerical example of thermal considerations.

The power demand part of the model was approached from commercially available information as well. Electrical component characteristics for the control systems, Micro Electro-Mechanical System (MEMS) sensor suites, voltage converters, heaters, and motors were chosen based on their expected energy needs and efficiencies (control systems being Arduino, STM32, Teensy, etc.). Notably, these components are less sensitive to low temperatures than the batteries. Heaters were assumed to be simple watt loads. Minimum motor energy demands were estimated with vehicle mass, speed, and expected gravity information. These minimums were then scaled by conservative estimates of overall mechanical system efficiencies. Additional friction loads were added to the energy demands based on experimental data from early prototyping.

Targeted vehicle speed was determined through iterative analysis of maximum expected depth range and by imposing careful limits on battery discharge rates. Generally, the higher drive speeds resulted in deeper ranges, but this effect had diminishing returns. High drive speeds avoid some hotel load duration (loads from baseline operating conditions e.g., CPU, sensors, etc.), and increase heat production from electrical components (reducing the need for heaters). Low speeds, on the other hand, decrease mechanical stresses and the battery discharge rate, which can increase reliability and vehicle life. We feel the drive speed range covered in this report balances these concerns while remaining physically achievable with our chosen system architecture.

When selecting motors and gearboxes to power the drivetrain, efficiency is extremely important (as shown with Figure 82). As noted previously, the borebot track system faces optimization challenges. Therefore, it is important to maintain as high of an efficiency as possible upstream of the track system. A high-power-density, redundantly-wound brushless DC motor (Faulhaber, n.d. a), and a gear reduction system was chosen as a preliminary step for the TRL 3 prototypes (Table 3). For details about the use of Faulhaber COTS motors to enable redundant drive architectures, see Jadhav (2017).

Components with a cylindrical form-factor are required due to the small diameter, so pancake-type torquers are not a good option. This results in the need for gear reduction in order to bring the RPMs down and increase the output torque. Minimizing losses during the gear reduction stages is an important consideration. Due to the limited space, it is desirable to have the motor on the centerline of the cylindrical structure. A 90° gearbox is required to redirect power away from the centerline prior to delivery to the track system; the efficiency of this 90° gearbox is also critical. If COTS parts are used, harmonic drive units appropriate for the 64 mm borebot are not available. This is simply a miniaturization challenge, due to the required size of the tooth profile. This makes a planetary gearbox the best option for the 64 mm borebot. A 23:1 gearhead for the motor listed in Table 3 is available, and has a published efficiency of 80% (Faulhaber, n.d. b).

Drivetrain Electromechanical Components Prior to Track System (64 mm)					
Supplier	**Part #**	**Type**	**Description**	**Efficiency**	**Cost (USD)**
Faulhaber	4490H024BS	Motor	24 V / 183 mNm	87%	803
Faulhaber	44/1 23:1	Gearhead	23:1 Planetary	80%	908
Onedrives	PF15-10AR	Gearbox	10:1 Worm Drive	84%	504
				58.5%	**2215**

Drivetrain Electromechanical Components Prior to Track System (108 mm)					
Supplier	**Part #**	**Type**	**Description**	**Efficiency**	**Cost (USD)**
Faulhaber	4490H024BS	Motor	24 V / 183 mNm	87%	803
SureGear	HPGCN17-505M	Gearbox	50:1 Harmonic Drive	90%	1011
Onedrives	PF15-6AR	Gearbox	6.66:1 Worm Drive	86%	504
				67.3%	**2318**

Table 3: Prototype components (prior to track system) for TRL 3 borebot prototypes.

The borebot sized for a 108 mm bore could likely see an efficiency gain of around 10% prior to the track system, due to the availability of 50:1 harmonic drive units (with a max efficiency of 90%; Fusaro, 1999, Table 13.1). A more efficient 6.66:1, 90° gearbox could then be used, allowing for close to 67% efficiency prior to the track system. This is a strong argument for the 108 mm size. However, missions targeting tens or hundreds of meters of depth from smaller, low-cost landers could still be successful using borebots sized for 64 mm, as these efficiency losses wouldn't impose as much of a penalty. To keep things simple, it is desirable to keep the two sizes of prototypes similar in methodology, so the 23:1 planetary gearhead should be tested in the 108 mm borebot prior to switching to the harmonic drive unit.

Borebot Instruments / Downhole Science

The state-of-the-art for downhole instrumentation in a planetary science context is well-represented by the WATSON Deep Ultraviolet (DUV) fluorescence mapping spectrometer instrument (Wireline Analysis Tool for the Subsurface Observation of Northern ice sheets; Eshelman, 2019; Malaska, 2020). As described in Malaska, et al. (2020):

> "WATSON incorporates DUV fluorescence spectroscopy along with a fine-scale 2D mapping capability to search for and determine the spatial distribution of organic material. WATSON leverages technology developed for SHERLOC, the Mars 2020 DUV Raman and fluorescence spectrometer, repackaged into a 101.6 mm diameter tube 1.2 m long that can be lowered into an ice borehole. Like SHERLOC, WATSON scans a pulsed 248.6 nm laser across a sample surface, collecting fluorescence emission in a backscatter geometry and producing a spectral map of fluorescent materials."

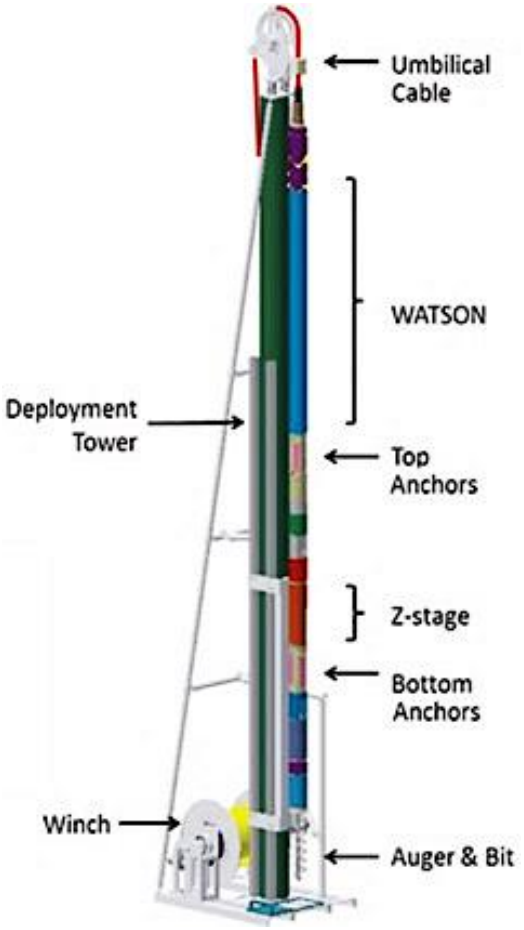

Figure 83: Figure 1-A from Malaska, (2020), showing the integration of WATSON into the Planetary Deep Drill (PDD), ref. Figure 25.

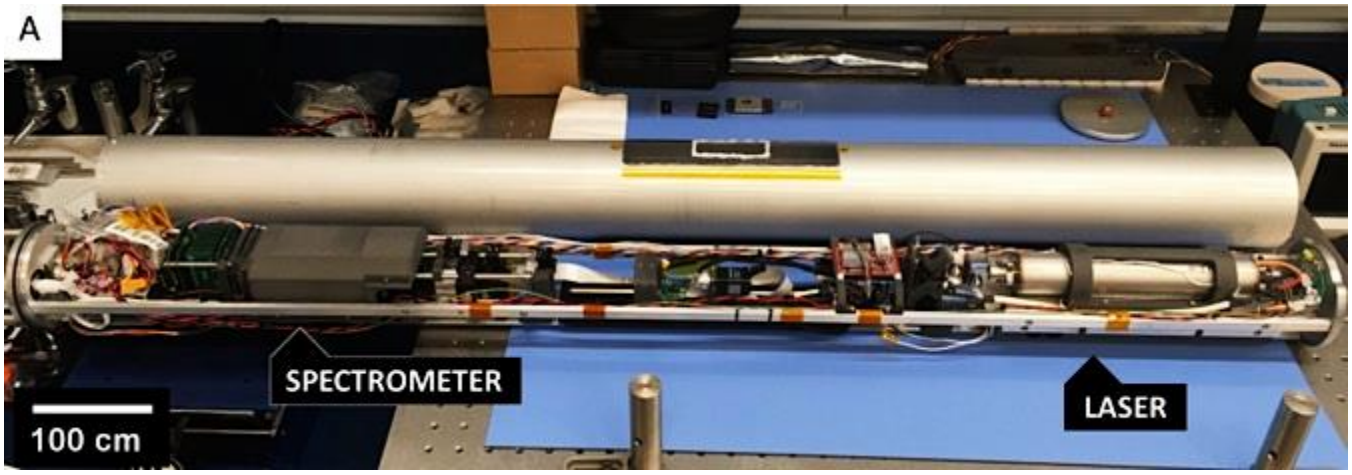

Figure 84: Figure 2-A from Eshelman, (2019), showing the 101.6 mm (4 in) x 1.2-m WATSON instrument with the external tube casing

The WATSON instrument also features a sub-30-μm-pixel-scale optical microscope (Malaska, 2021). WATSON can be seen in Figure 84, and in Figure 83 integrated into the PDD drill string (Eshelman, 2019). Note the similarity to Figure 25. WATSON can detect and classify organic signatures embedded ice, including Polycyclic Aromatic Hydrocarbons (PAHs), on par with laboratory spectrometers (Malaska, 2021). This capability is important to detect possible areas of frozen (preserved; non-fossilized) organic material that may be concentrated into discrete layers by sublimation processes over time:

> "The sublimation of the ice would leave any organic material behind. Only if the ice melted to form liquid would the organics be removed. Subsequent replacement of the ice by diffusion would also not alter the organic record. The presence of ice is important because it is likely to help protect organic material against decomposition due to soil oxidants" (Smith & McKay, 2005, section 5).

The Raman spectroscopy capability of WATSON can potentially be used to classify the type of salts present in the ice (Mason & Elwood Madden, 2021), as well as examine the Raman spectra of the O-H stretching bands of water in order to "…provide morphological information about the physical makeup of the ice matrix (e.g., features including bubbles, cracks, and veins) while not overlapping with fluorescence signals from other materials" (Eshelman, 2019).

Other leading downhole science options would include optical-only precision instruments (Carsey, 2003), or an array of simpler optical instruments to favor greater radial coverage over finer resolution. Optical coverage is valuable because volatiles (including water ice) can sublimate out of the borehole wall over time, enhancing the contrast and making greater layer detail more detectible (Smith, 2020, section 2.2.2.1). An interdisciplinary Mars polar science workshop discussed these issues, recommending a sub-1 mm optical resolution capability for detecting individual layers in the PLDs, and a 100 μm resolution if grain-size classification is desired (Smith, 2020, section 2.2.2.1). Another recommendation was fish-eye lenses for non-microscopic imagers; it seems that an array of sensors was not considered as an alternative to this (Smith, 2020, section 3.2.1). Near-IR spectrometry was also recommended for grain size determination, although it was recommended that the spectrometer is integrated into the lander, with a fiber optic connection to the downhole instrument. The lack of a standalone downhole recommendation is due to the challenges of miniaturization, and the sensitivity of the instrument to shock and vibration from drilling activities (Smith, 2020, section 2.2.2.1). These concerns are ameliorated to an extent in the borebots context, since the battery storage requirements already favor a 4" vehicle/instrument diameter, and the redundant capability means the dedicated science payload will not be present during drilling itself (the borebot with the attached spectrometer payload would be stowed while the other borebots perform drilling activities, Fig. 85).

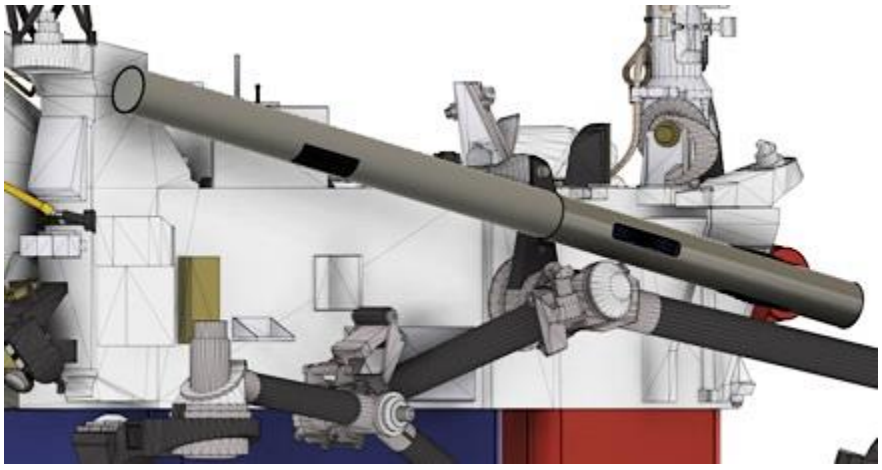

Figure 85: 4" x 2-m "WATSON-bot" in a possible stowage location between uses.

This instrument opportunity is a prime example of how the borebots architecture opens new channels of thought by trading tether constraints for battery constraints. Taken to the extreme, four different advanced spectrometry instruments could be stowed in the frunk area (Figure 13), and borebots could be incrementally retired and assigned to an instrument. Thus, four or five borebots can drill full-time, while four are dedicated to extensive and specific science payloads once they reach some odometry value. This potential capability is unheard of; or better said, unimagined, until now.

Laser-Induced Breakdown Spectroscopy (LIBS) and Near-infrared Spectroscopy (NIRS) could possibly be incorporated into a combined downhole suite, leveraging the heritage from ChemCam and SuperCam, which are in service on the Curiosity and Perseverance rovers, respectively (Lakdawalla, 2018, section 9.2; Maurice, 2021). This can offer the ability to ablate holes into the substrate (LIBS), offering physical penetration; or photonically penetrate into certain types of substrates with the Near-IR offered by NIRS. This combination would have an advantage in layers that are opaque to the DUV of WATSON, which (generally) can see one-to-two cm into clean ice (Eshelman, 2019; Malaska, 2020). Other instrument options are discussed in Smith, et al. (2020, section 3.2.1).

It is likely that a basic instrument like the Optical / UV microscope (Figure 86) integrated into the structure of the Planetary Deep Drill (Zacny, 2016) can be integrated into every borebot; therefore, more advanced downhole science instruments are considered here as end effectors, and are assumed to attach in the same manner as the drill heads and sampling devices. Although this reduces the number of borebots available for drilling from a given lander, it increases system flexibility overall by keeping the drilling borebots nimble, yet still numerous. Instruments integrated into the borebot itself should be as minimal as possible in order to avoid the borebot length getting prohibitively long. The other advantage to this approach is the availability of the down-direction to instrumentation. This allows for downward-facing sonar (for depth sounding, density, layering, etc.) and conductivity instruments in addition to downward-facing optical and UV cameras or microscopes. This benefit was noted, yet unexplored, during Phase I.

Figure 86: Optical / UV microscope integrated into Planetary Deep Drill (Zacny, 2016, Fig. 4).

Using WATSON (or a similar 1-m-long, 4” diameter spectrometry instrument) with the borebots architecture requires some finesse to maintain a high system efficiency. WATSON would be used as an end effector (in place of the drill head), allowing for a “surgical” use of WATSON that may make for an interesting implementation. For example, the top 50 meters of the borehole could likely be scanned on a single charge of a borebot. If the batteries reach a critical level before scanning is complete, the bot can stop the scanning procedure and return to the surface to charge. The scanning workflow would consist of discrete scanning depths, which are broken up into discrete sectors. Rotation of WATSON from one sector to the next can be accomplished using the main drilling motor, and it would be possible to

lock WATSON from rotating with the deployable forward pins if desired. Depth can be known to a high certainty using both borebot odometry and a downward-facing ranging instrument, measuring the approach of the bottom of the hole. If WATSON is only used for "milestone" depths (i.e., 50 meters, 100 meters, 200 meters, etc.), the "next" WATSON deployment could be used to only scan layers of interest, allowing an operational focus on building a complete log of the borehole using WATSON's continuous logging mode (as opposed to the scanning mode; see Eshelman, 2019 and Malaska, 2020). As an example, the second logging run could treat the depth range of 40-m-to-60-m as an area of interest, to compare the sublimation of the 40 m - 50 m region (drilled & logged earlier) to the 50 m - 60 m region (drilled more recently) to evaluate any sublimation that may occur (which can potentially enhance the contrast between the layers, and reveal grain boundaries; Smith, 2020, section 2.2.2.1). If the second logging run identifies other interesting targets with the continuous logging mode, the third logging run can stop and perform full scans at the depths of interest – and a few meters above/below those depths – before continuing to the bottom of the borehole in the continuous logging mode. This technique would be adaptable to competing wireline architectures, although they would require a separate motor to rotate WATSON for control of the discrete sector scanning (or possibly design the instrument to feature an annular window). WATSON is likely destined to be a permanent part of the drill string if used in competing architectures. This imposes higher mass and energy requirements on wireline drill systems, thereby increasing risk in a system that already has several single points of failure.

Each borebot will need to be equipped with a variety of non-science instrumentation, and some contingency benefits will be available from the drilling motor, drive motor, and the frequency at which the heaters need to be ran, among other available data. It has been suggested that the substrate hardness can be determined to within a 20% margin of error merely by logging the power used for a given drill RPM and WOB (Smith, 2020, section 2.2.2.1). The small microscope shown in Figure 86 will be able to provide a tremendous amount of data on layering, and grain size. This may be augmented by the presence of a camera inside the drill head (which will likely be required for data collection as part of the autonomous drilling process). Chips that are routed to the area above the core (by the flutes) will be visible by this camera as the drill head fills up. When compared with side-on microscopic data and hardness estimates, much will be known before deploying a spectrometer instrument.

Borebots will also require a Micro Electro-Mechanical System (MEMS) sensor suite, onboard thermistors or thermocouples, and various other sensors that were lumped in to the "hotel loads" category during our power analysis. The drill deflection during operation (as measured by the MEMS suite) combined with the expended effort from the variable-pressure drive system may provide contingency information as well. Although borebots are expected to be autonomous when downhole, they will have a communications system for interfacing with the rover when nearby (analogous to the one used by Ingenuity). A supplemental laser-based communications system for low-bitrate commands and/or status updates may be a reasonable idea, and would provide a contingency benefit for analyzing the atmosphere in the hole. If the rate of sublimation due to drilling can be estimated (see Bar-Cohen & Zacny, 2009, p. 523), the sublimated gasses from the substrate could potentially be analyzed. One implementation may be to have a high-powered laser on the rover to power the two-way communications method, combined with a mirror/shutter system on the borebot. The laser module on the rover could house a spectrometer, or route the return beam to SuperCam, etc. via a fiber optic cable.

Rover Sample Handling & Science Payload

In a perfect world, a rover could be built that had the combined powers of Curiosity and Perseverance. This machine would be the ideal platform for a mobile borebots drilling mission. Perseverance is rather light on science, with most of the science instruments being located on the mast and turret. This was done to accommodate the very impressive Adaptive Caching Assembly (ACA). However, the boon offered by a polar drilling mission requires a physical-sample-processing instrument.

The advantage to physical sample processing in this context is the ability to check findings detected with the downhole suite, combined with logging the climate record through precision gas analysis of ice core material. Since WATSON is capable of performing a vast array of measurements and classifications, the physical sample processing needs to do three things. First, it must be capable of concentrating and identifying compounds that may have an organic origin (samples taken from depths identified as areas of interest by WATSON). Second, it must be able to quantify the oxidant nature of the substrate to provide context for positive results that may have organic origins. Third, it must be capable of analyzing evolved gasses from our ice core analysis tool (described later in this section).

Luckily, there is a little room available on the Perseverance platform. The technology demonstrator called MOXIE (Mars Oxygen In-Situ Resource Utilization Experiment) was included as a stepping-stone to a human Mars mission, in order to prove the viability of *in-situ* oxygen production (NASA Mars 2020, n.d. a). This instrument would not be required on the next mission, so this internal volume is up for grabs. The problem is that the physical processing suite flown on Curiosity – known as the Sample Analysis at Mars (SAM) – is very large (about the size of a microwave oven; Lakdawalla, 2018). One option may be the Urey instrument (Figure 87), which was developed by NASA (Aubrey, 2008; Skelley, 2007). Urey was selected for the Pasteur payload of the Rosalind Franklin rover but was subsequently descoped. Figure 88 shows the size of the MOXIE instrument (clear, wireframe) with the Urey instrument placed into the MOXIE volume (red, solid). Figure 89 shows the same, with the SAM instrument from Curiosity looming over the pair.

Figure 87: The Urey instrument (Figure 4 from Aubrey, 2008).

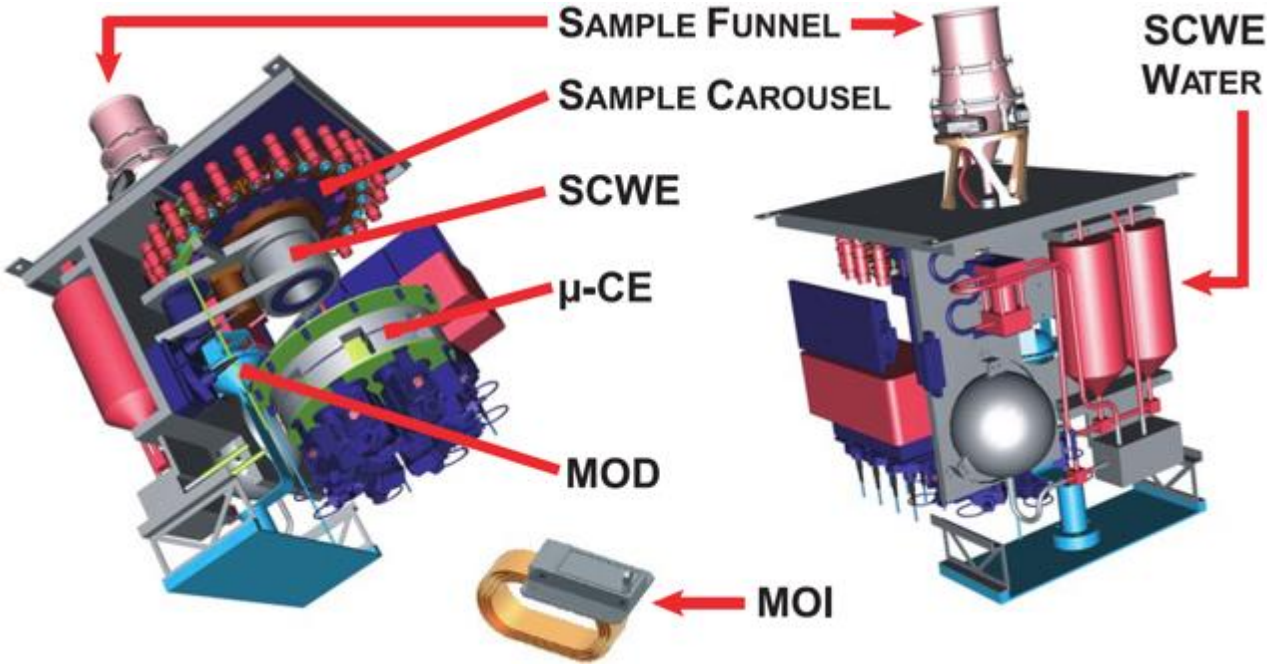

SAM could be reduced in volume some because it was designed around a modular construction strategy to facilitate testing (the modularity could be abandoned to reduce volume), and components were spaced to thermally isolate them from other components. However, SAM was not built for a polar thermal environment, and it is likely that the thermal system on the deep drilling rover could be modified to reduce some of the burden on SAM. With a more active thermal management system, the size could likely be reduced. If this could be combined with judicial downscoping of both SAM capability and other internal rover payloads, a SAM-esque suite could be feasible (i.e., some heritage could be maintained). If the Urey instrument is favored instead, there will still be some "extra" volume available. Perhaps this volume could be used to make the instrument redundant, with one sample carousel for the primary mission, and another sample carousel to support extended operations.

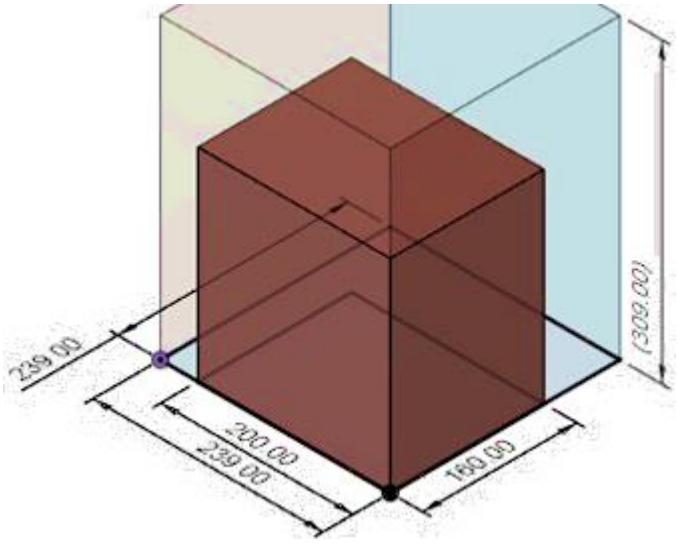

Figure 88: The Urey instrument (red) inside the volume occupied by MOXIE on Perseverance (clear / wireframe).

Figure 89: Urey inside the MOXIE volume, with SAM's volume adjacent.

The Thermal and Evolved Gas Analysis (TEGA) suite from the Phoenix lander is another option (Figure 90), although the single-use-ovens strategy used for the TEGA doesn't make a lot of sense in this context. Urey and TEGA are both highly capable and very small, meaning the remaining MOXIE volume could potentially be used to augment either instrument's capabilities by adding a precision gas analysis system designed for processing many samples (or in the case of TEGA, interfacing the evolved gas suite for pneumatic sample delivery). The National Academies lists other instrument options (2003, p. 95).

Additional community feedback is sure to shape future strategies for *in-situ* ice core analysis. To support science payload development, it is likely that some space inside the rover could be freed up. Radiation-hardened electronics continue to reduce in size and increase in computing power (McHale, 2011). It may also be possible to offload the SuperCam spectrometer entirely to the mast, perhaps foregoing the telescope for a fixed-focal-length optic (set at the distance to the borehole). Thermal management of the mast will already need to be re-evaluated in order to prevent CO_2 ice buildup over the winter, and to prevent low-temperature damage to other parts of SuperCam. Future work on the ice core analysis strategy (this strategy is discussed later in this section) will help to refine instrumentation requirements.

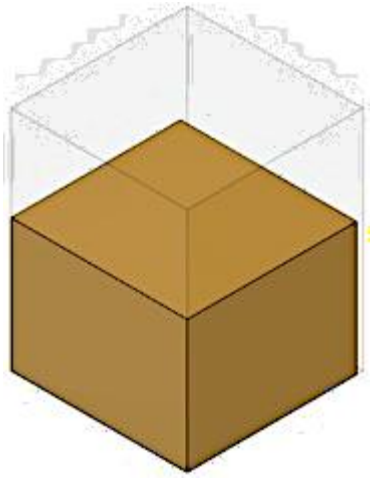

Figure 90: TEGA inside the MOXIE volume.

It is anticipated that thousands of samples will be available, yet the instruments discussed all possess a numerical limit imposed by the number of hardware items (eight ovens for TEGA, and 22 – 24 sample cells for Urey, and 74 sample cups for SAM [Hoffman, 2008; Aubrey, 2008; Lakdawalla, 2018]). The amount of available reagent is also a limiting factor, although more reagent could be stored in the remaining MOXIE volume if this were the only concern. This makes any of these instruments a good choice for specific confirmatory experiments, and to explain unexpected findings with other instruments. However, it doesn't make them a good candidate for processing hundreds or thousands of samples. One mitigating technique for limited sample cup availability may be to nest the sample cups like Russian dolls and add a station near the carousel to remove and discard used cups, revealing virgin cups below. Another technique may be to introduce a plasticizer to form an inert mass in the bottom of the cup, effectively creating a new cup-bottom that could withstand the requirements of subsequent sample processing. For true "unlimited" processing, *in-situ* solvent would need to be used (recall that the substrate is more than three-quarters water ice), and a system would need to be developed that doesn't rely on sample cups. In this case, the quantity of reagent allotments would need to be sufficient to match the expected life of the instrument's mechanical system.

To leverage the ACA for use in polar drilling, a method was developed to "re-core" the center of our ice cores with the drill bits and sample tubes used by Perseverance (Figure 8 & 9). Re-coring is a technically challenging process (Zacny, 2021; Dreyer, 2021), but is temping in this context due to the position of the deployment tube relative to the ACA. The drill chuck from the turret corer (Figure 91; Barletta, 2020) can be mounted to a chuck holder on the rover deck (it may also be possible to locate the turret corer in this position, permanently fixed). Currently it is envisioned that the chuck holder would remain static and the borebot would provide the rotation. After re-coring, an automated manipulator would remove the drill bit from the chuck and insert it into the ACA, with a 180° swing (we are calling this the "flipper," visible in Figure 8 & 9). Originally, we had imagined adding an ice-core-melting station in the ACA volume, with the sample tube inserted directly into the melting station (allowing mission planners to cache a core or analyze it). However, due to the strong recommendation against the re-coring process by our mentors, we developed two other strategies for handling ice cores. The second one may preclude the need for a full-on ice-core-melting station.

Figure 91: Chuck from the Turret Corer (Figure 2 from Barletta, 2020).

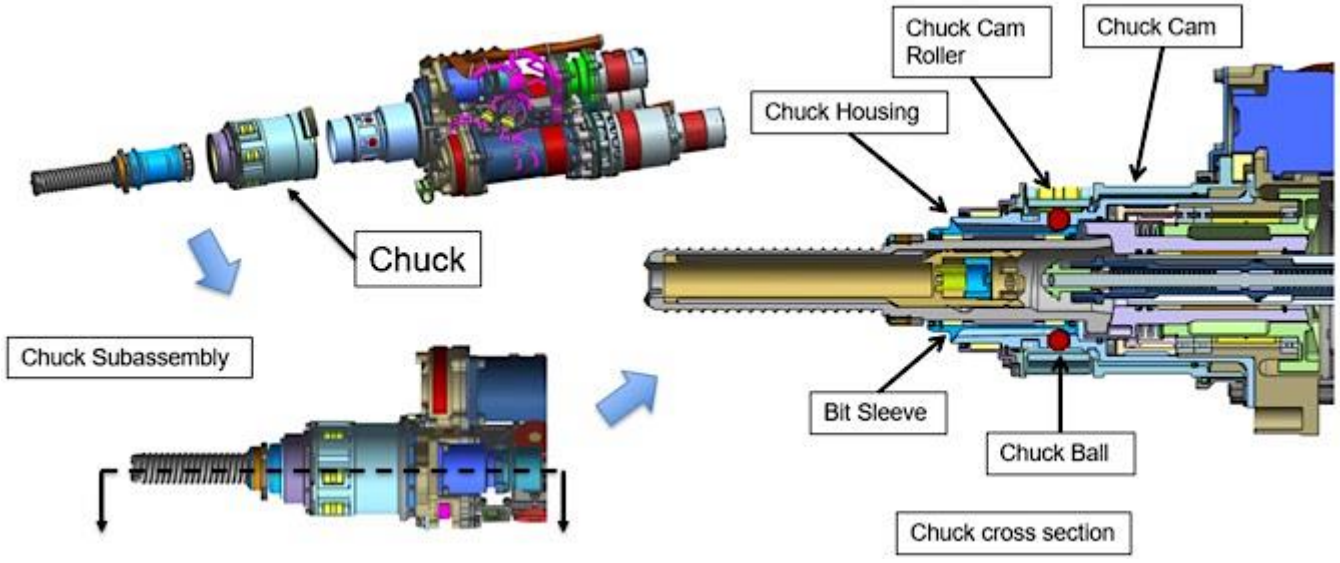

To provide ice core samples for caching and to avoid re-coring entirely, the chuck from the turret corer can be adapted to fit on a borebot and can be used to perform sub-sampling. This will require re-design of the chuck to reduce the diameter by about 15 mm for the 64 mm borebots, which allows credit for some of the design heritage (Rodriguez, 2021). A full-heritage chuck can fit directly onto the larger 4" borebots. The forward deployable pins can be used to provide the mechanical input to operate the chuck release mechanism, perhaps with a low-profile adapter plate, designed such that no modifications of the chuck are required. The robot arm would then be used to retrieve a drill bit from the ACA and fit it into the chuck. If it is desirable to use a flipper mechanism for this task (instead of the robot arm), it will need to reverse the direction of the drill bit mid-flip, so the correct end is facing the borebot prior to coupling. With the fresh drill bit installed (Figure 92), the borebot drives down to the bottom of the borehole and takes a core sample. This would most likely be performed at milestone depths, probably with two or three cores at each milestone.

To analyze the ice cores, we struggled to find an alternative to a melt-station (which would have approximated what is used on Earth to release trapped gasses from ice). Ultimately, we came up with a strategy to leave the core in the drill head and pierce the center of it lengthwise with a hot needle instrument (Figure 93). The released gasses can be routed pneumatically to the internal science payload. This has the advantage of creating a pilot hole for the cleaning station (i.e., the hot needle and the primary cleaning tool can be designed synergistically). The hot needle instrument can be mounted in approximately the location as the previously-shown chuck holder (next to the mast, on the rover deck). This location is within convenient reach of the deployment tube. During the piercing process, solid materials contained in the ice will be ingested. These solid materials can be captured using a diverter device and routed to the physical processing instruments

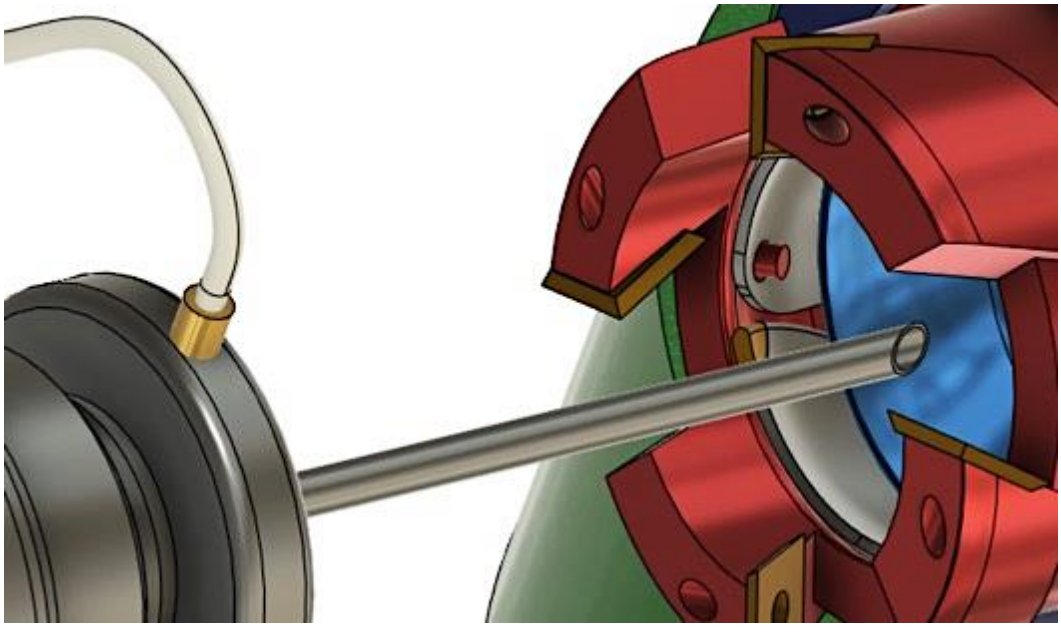

Figure 92 (above): Mockup of a re-sized chuck on a 64-mm borebot. Figure 93 (left): Hot needle ice core analysis tool. Shown is a standard medical-grade 7 gauge needle. Heating method TBD; likely an Inconel needle with a tapering thickness and an induction heater at the base of the needle.

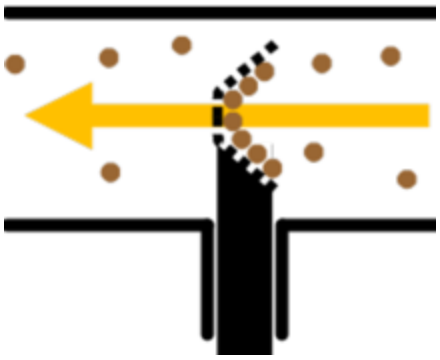

Figure 94 (right): "Lacrosse Stick" catching fluidized solid cryogenic material traveling at a very high speed through a vacuum tube. From NASA SMD, 2020.

inside the rover. Pneumatic handling of fluidized cryogenic particles was developed by Honeybee Robotics, and is shown in Figure 94 and Figure 95. This system will fly on DragonFly in 2026. For a description see Zacny et al. (2019a; 2020) and NASA SMD (2020). The material extracted by the hot needle tool should be very pure since it is from the center of the ice core. Using the core centers as sample material was recommended in Bar-Cohen and Zacny (2009, p. 488). A method could be developed to abrade the end of the ice core before piercing is started to further ensure the integrity of this sampling method. Another strategy may be to route the first and last parts of the sample overboard, instead of into the instruments. The hot needle may be a good option for creating a pilot hole even if a sample isn't desired from the particular core being processed, in order to facilitate cleaning of the drill head.

The pneumatic system could also route chips and fines from the cleaning station to the science payloads for analysis of the material in the cryogenic state. A special cleaning tool could be used to extract material from the center of the core if desired, or the chips and fines created from the original downhole drilling process could be sampled. An inlet could be added to the robot arm for selectively sampling debris of interest during or after the cleaning process. Such an inlet could also be used to sample loose material on the surface, or material disturbed by the wheels. It is envisioned that most of the turret will be removed in favor of a tube-grasping end effector, so it may be wise to add a scoop to the side of the end effector for examining the surface material to help provide insight into the properties of the sublimation lag layer. When descoping the turret, it is imperative to retain the SHERLOC instrument (Bhartia, 2021) in some capacity – either in a fixed position on the robot arm, or moved to the rover deck. WATSON evolved from SHERLOC (Eshelman, 2019), so having the ability to scan excavated material to compare the spectra with the downhole result is very important. This also allows context to be captured for a specific sample, instead of referencing the WATSON results for the depth the sample was taken at. SHERLOC also provides a good measure of redundancy, given the importance of spectrometry work in a PLD mission context.

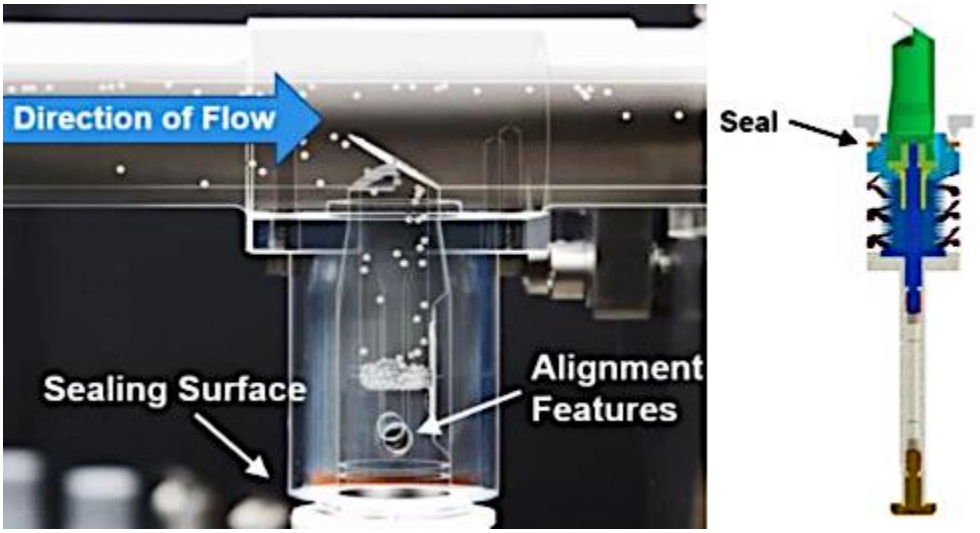

Figure 95: Pneumatic sample handling system used on DragonFly (Figure 2 from Zacny, et al. 2020).

Sampling Subglacial Liquid

During the Phase I study, a water-sampling device was developed to mitigate the risk of the "breakthrough" process into the subglacial environment, if indeed the wet hypothesis prevails. This is considered a "hedge" against the dry hypothesis, and was given a relatively small amount of attention due to the current scientific climate surrounding the wet hypothesis. If only thick mud or solid material is present instead of liquid water, the iris drill head could take the subglacial sample. Ultimately, mission planners will have to decide if breakthrough into a liquid environment is likely, and will need to choose a risk-mitigation measure to deal with that situation. We present our water-sampling device here in the hopes that it will be helpful in that decision-making process. Anyone working on a similar type of device should reference Mowlem, (2015) and Bulat, (2015, 23:50 & 35:40; 2016).

The fundamental idea with this device is to leave an "ice plug" in the borehole, i.e., stop drilling just shy of the point where the subglacial liquid would rush into the hole. The remaining thickness would then be penetrated by a "mosquito probe," offering a more surgical approach to subglacial lake access. On Earth, the hydrostatic pressure in subglacial lakes comes mainly from the weight of the ice sheet on top of the ice (Cuffey, 2006). There are several other factors that can modify this pressure, but this is the main driver (i.e., $\kappa = 1$; ref. Arnold, 2019, methods section). If this is applied one-to-one to the SPLD, the pressure in a subglacial lake would be 3/8 that of a corresponding lake on Earth with an equal ice thickness covering the lake. It follows that the required "ice plug" would be 3/8 of the required ice plug on Earth – except, the colder ice on Mars is stronger, and strengthened again by the presence of admixed dust on the order of 15% (strength vs. dust: Arthern, 2000; dust content: Zuber, 2008, & Li, 2012), although we can't know the *local* dust content until staring at it *in-situ*. It turns out that this results in a very thin ice plug. The calculation is shown below.

Figure 96: Water sampler with the penetrator probe in the extended position.

$$\Delta P = P_{H_2O} - P_{atm} \quad \rightarrow \quad \Delta P \approx P_{H_2O}$$

Shear strength S for water ice at 200 K: 3.0 MPa (conservative)

Punching Force Equation: $F = L \cdot t \cdot S$

L is the perimeter, t is the material thickness, S is the shear strength.

$$t = \frac{F}{LS} = \frac{P_{H_2O} \cdot A}{\pi \cdot D \cdot S}$$

$$t = \frac{P_{H_2O} \cdot \frac{\pi}{4} D^2}{\pi \cdot D \cdot S} = \frac{P_{H_2O} D}{4S} = \frac{\kappa \rho_{ice} g h D}{4S} = \boldsymbol{\frac{\rho_{ice} g h D}{4S}}$$

$$t = \frac{\left(1200 \frac{\text{kg}}{\text{m}^3} \cdot 3.71 \frac{\text{m}}{\text{s}^2} \cdot 1{,}500 \text{ m}\right)(0.064 \text{ m})}{4(3 \cdot 10^6 \text{ Pa})} = \boxed{\mathbf{0.036\ m}}$$

Notes: the punching-force equation comes from the manufacturing industry. Shear strength data for ice at these temperatures are hard to come by. The available choices were poorly-constrained data from Voitkovskii (1960), or

creating our own estimate based on the lack of glacial flow over the recent epoch (Byrne & Ivanov, 2004, section 6.2; summarized in Whitten & Campbell, 2018, section 1). Since Smith (2017) indicate that the "no creep/flow" situation may have more ambiguous causes than simple strength numbers, the laboratory data seemed preferable than relying on orbital observations in this case. From the laboratory data, an estimate was made which factored in the lower temperatures and higher admixed dust content. The mechanical properties of ice at very cold temperatures require further study to support planetary science deep ice drilling research in general. We recommend that the science community works to support this. See the South Polar Layered Deposits section of this report for more on ice density, composition, and strength.

The resulting plug thickness of 36 mm is quite surprising. To be cautious, a thickness of 75 mm to 100 mm could be used. This seems appropriate since they bottom-condition of the ice, and the effect from any brines present, would likely remain unknown until after breakthrough. Down-facing sonar and conductivity instruments could help fill the picture in so mission operators can make an informed decision. The initial probe length was then set at 150 mm. For the 108 mm bore, the required plug thickness is 60 mm. The 150 mm probe length still seems reasonable. For a 1 cm hole, the value is 6 mm.

Figure 97: Cut view of the water sampler, with the penetrator probe in the extended position.

The water sampler is shown in Figure 96, with the penetrator probe in the extended position. The penetrator probe itself is extraordinary; we decided to innovate first and scale back later (for example, the probe probably won't need to telescope). Telescoping screws are pretty rare, and this device would also have to anchor itself into the ice – thus the taper. The stowed penetrator probe can be seen in Figure 98. Drilling and excavation of material out of the tapered threaded hole in the ice will

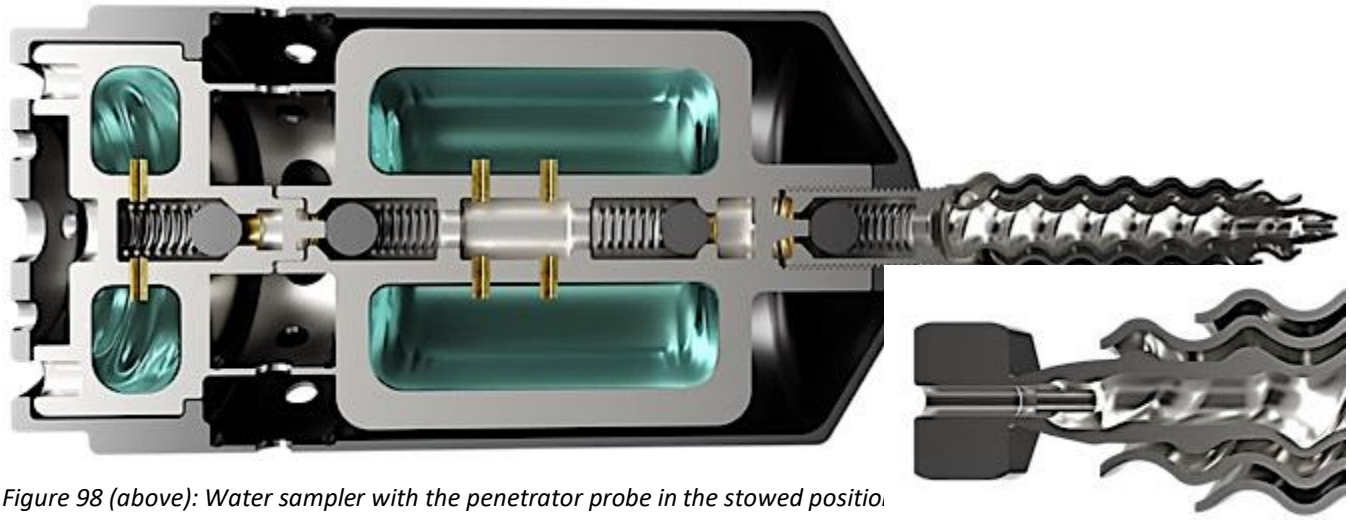

Figure 98 (above): Water sampler with the penetrator probe in the stowed positio
Figure 99 (right): Detail of a shear-nut to ensure proper setting torque during penetrator probe deployment.

be very complicated (and is torque-limited by the friction-fit of the telescoping section). It is envisioned that the outer surface of the probe would be coated in an abrasive, to facilitate widening the cut threads with a forward-back motion as the penetration progresses. It is likely that a probe closer in form to the hot needle ice core instrument would be a more desirable implementation. The problem with a straight and smooth device is anchoring to the borehole. The idea with the tapered and threaded penetrator probe is that it would be permanently installed, holding itself in the hole with the tapered thread, almost as if it were a pipe thread. The rest of the water sampler would then be removed after sampling, and the borebot would return to the surface with the water sample. If this was performed successfully, but for some reason the penetrator probe needed to be removed (if, perhaps, the sequence was performed too early because the remaining ice thickness was miscalculated), it could be "cored out" of the ice at the bottom of the hole, since the penetrator probe is smaller than the core diameter and about the same length, see Figure 100. This is the primary advantage to a detachable probe that locks into the substrate via threading. The lack of a separate anchoring device is also significant.

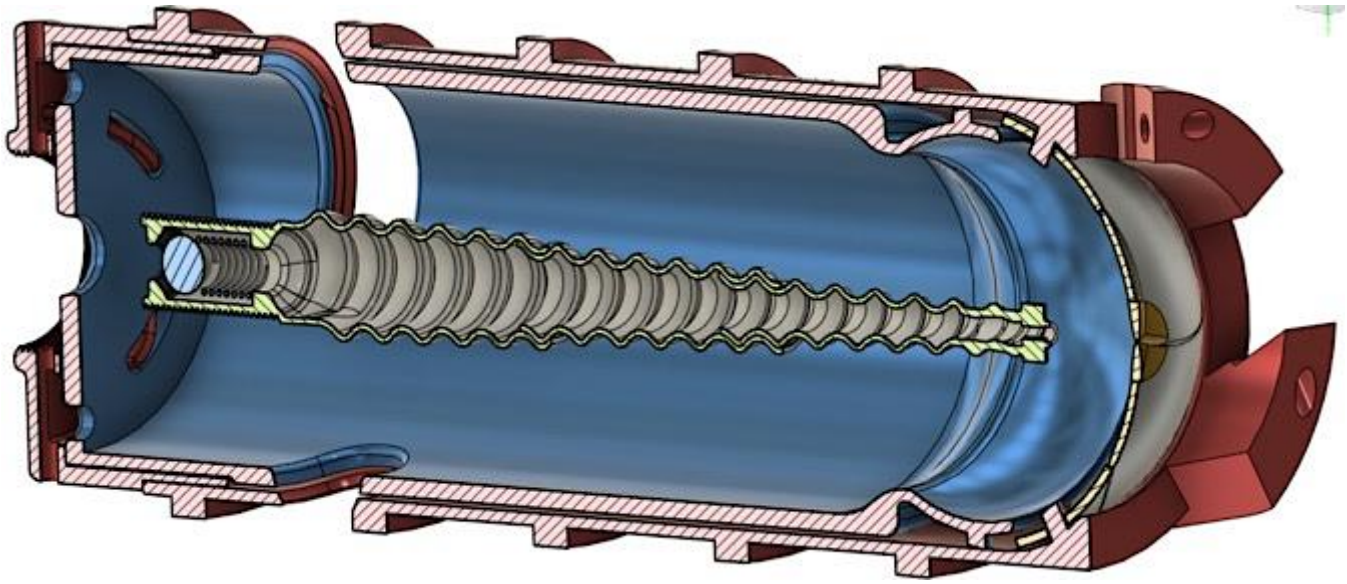

Figure 100: The penetrator probe inside the iris coring head, showing that probe extraction is theoretically possible.

The sampling device itself was envisioned to function as a simple mechanical system with only one input, the pressure from the subglacial environment. When this pressure is higher than the spring-pressure of the check valves, the bladders fill. When pressure equalizes, the check valves close. At this point, the bladders could self-seal as well, which may eliminate the need for the main bladder valve and allow the center manifold to drain after the penetrator probe is disconnected. The disconnection procedure comes next, which is accomplished by locking the forward deployable pins into receptacles in the back of the water sampler (Figure 61), and using the drill motor to loosen the double-nut retention on the penetrator probe (seen in Figure 101). Once loose, the deployable pins can be retracted, and the entire water sampler can be rotated counterclockwise to remove it from the penetrator. This may be aided by a ratchet device to lock the position of the "inner barrel" and "outer barrel" relative to each other when the forward pins are retracted. Although this seems complicated, it is purely mechanical, and is all powered by the borebot while using the ample torque of the drilling motor. The borebot and water sampler then return to the rover.

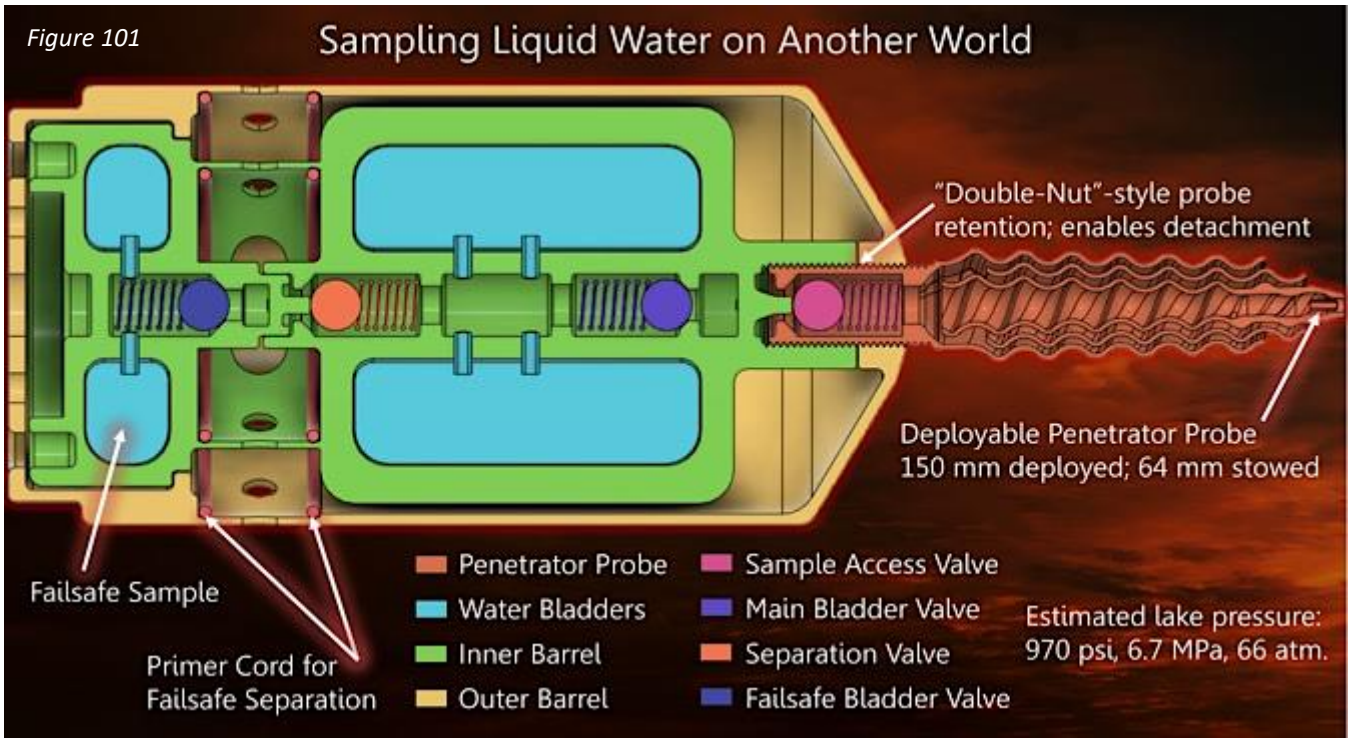

The valve strategy includes two valves that are held open until needed, and two valves that are opened by lake pressure and closed when the pressure equalizes. The main bladder/fill valve is the valve that could be removed if the bladders were self-sealing. It is also a candidate for replacement with an actuated valve, like a ball valve (discussed more below, regarding purging the probe). The valve in the penetrator probe itself is intended to withhold the water pressure from the subglacial lake when the water sampler is disconnected. The water sampler could subsequently be reattached. Another water sampler could draw additional samples from this valve using a "rabbit feeder" strategy, or by disconnecting its pre-loaded penetrator probe prior to being deployed down the hole.

The aft section of the water sampler is a "failsafe module" that can be decoupled from the rest of the unit via pyrotechnic devices (Figure 101). This would be used in two cases: the first being the penetration sequence has failed, water is filling the hole, and no sample was taken; the second being the bladders were successfully filled, but no time remains to decouple from the penetrator due to water filling the hole. This concept helped to inspire simpler versions of the water sampler itself, which will be covered at the end of this section. If the hole is indeed flooding, it is unlikely that a borebot could outrun the fill rate; however, the farther the borebot gets from the lake, the lower the risk of contaminating the lake. Water would flow around the borebot and freeze. Core samples of lake ice could then be taken.

Sampling subglacial liquid on Mars is a massive planetary protection concern (Category IVc, and Restricted Category V; COSPAR, 2002, pp. 8, 10). This is the highest standard on the books. The sample quality is also important to ensure confidence if any organic material is found. Holding the water sampler to the most stringent planetary protection standards is not really the problem; the device can be stored in a hermetically sealed container until attached to a borebot. Returned samples can be irradiated in the capsule on their return to Earth (Morrison, 2021). The largest contamination risk is the material at the bottom of the hole, before the final breakthrough process is initiated. There is no guaranteed solution to this problem, although dry drilling does help reduce the variables. Excavated material that remains at

the bottom of the hole would be the first material that the penetrator probe comes into contact with. If this challenge is mitigated, the probe may also ingest materials while performing the final penetration (initiating breakthrough). It may be possible to eject this material into the subglacial environment after breakthrough and before sampling begins. One way to mitigate exposure to excavated material may be to enclose the penetrator probe in a sheath that has a front cover analogous to the "launch abrading bit" that flies attached to the Perseverance turret corer drill chuck (Moeller, 2021, fig. 18). This abrasion tool could have a small chamber for containing a volume of debris cleaned from the bottom of the hole, and could then be moved to one side as the sheath retracts to expose the penetrator probe. The probe will still ingest materials during the drilling process, but if they are virgin materials local to the lake/ice-sheet system, this isn't as much of a concern as debris introduced during the drilling process.

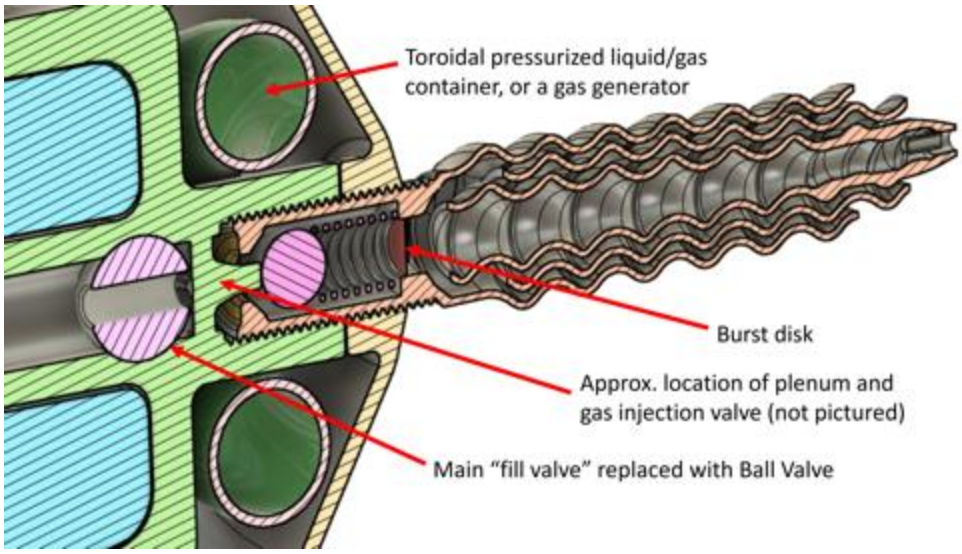

Figure 102: A method to clear the penetrator probe of debris prior to taking a sample.

The penetrator probe can be cleared of debris by a high-pressure blast of air or liquid. If this functionality is desired, it is recommended that a burst disc be placed in a plenum area where the penetrator probe is attached to the rest of the water sampler. This disc should be strong enough to withstand the pressure from the subglacial lake, but should rupture when the high-pressure gas clearing process is initiated (either due to the introduced gas pressure or a puncture mechanism that operates shortly after the pressurized gas is released). One layout for this is shown in Figure 102. The volume of gas generated should be sufficient to clear the entire volume of the probe with some factor of safety. A ball valve can be used to protect the rest of the water sampler from this cleaning event. Once exhausted, the penetrator would fill with subglacial water, and the ball valve can then be opened to fill the sampler. The penetrator can then be disconnected in the manner previously discussed.

After development of the pyrotechnic-failsafe strategy and the burst-disc-probe-evacuation strategy, it began to make sense to re-design the whole unit around these two concepts instead of using the failsafe separation shown previously. The threaded probe would also be replaced with a needle-type penetrator (possibly heated). The forward pins could be used to fire individual pyrotechnic devices: the first, to fire an explosive anchor into the wall of the borehole, to ensure the smooth probe does not get forced out of the ice. The second to destroy a burst disc, cleaning out the needle and filling the water sampler. The pyro-firing electrical circuit common-to the main coupler on the borebot could be used to fire a third pyro device that separates the penetrator from the sampler, and the borebot can return to the rover with the sample. The electrically-actuated separation device could be a magnetic coupling instead of a pyro device, which has been used in subglacial sampling instruments on Earth (Mowlem,

2015). This may allow for re-attachment by another borebot to retrieve another sample. This type of system is simpler to implement than the purely mechanical system, and would be easier to test in a laboratory (although each test will require several replaced components). A more advanced electrical connection on the front of the borebot may allow it to be simpler yet. It may also be possible to detonate different pyro devices through the same circuit with by varying the current-sensitivity of the devices. This could be done by including higher-rated resistors on the devices that are to be fired later in the sequence, thus requiring an increase in the applied voltage to achieve the necessary current draw in order to activate the subsequent devices.

When presenting the water sampler to the community we often get questions like "what happens if it fails and the hole floods." That is the *normal* approach (used on Earth) – break through, flood the hole with water (submerging your downhole equipment), and then try to escape before the hole freezes. This is a perplexing state of affairs, and has no place in a highly-planned planetary science mission. Furthermore, such an escape plan relies on high-speed, high-powered winches, which are likely outside the scope of what could even be used on a wireline system for Mars (assuming a Mars-2020-type mission and launch mass). The first breakthrough into lake Subglacial Lake Vostok, East Antarctica, in 2012 was a truly fantastic event (by any measure), described here by Lukin and Vasiliev:

> "On 5 February at 20:25 Moscow time, at a depth of 3769.3 m (by the ice-core length), contact between the drill boring bit and the lake water body was registered by the load sensor on the bottom and the momentum sensor on the boring bit in the process of ice cutting. The main objective of the drill operators was immediate recovery of the drill to the surface. The boring bit diameter is 135 mm, while the diameter of the ice borehole is slightly larger. However, there is a small clearance between the coring tube surface of the drill and the sides of the borehole, which will immediately be filled with water under pressure. The ice borehole sides are below freezing temperature everywhere above the ice/water interface, so the seeped super-thin water layer would freeze almost immediately and then it would be impossible to recover the drill to the surface. The operation regime of the drill winch was changed from 'descent' to 'ascent' within 4 s of contact with the water. At a height of about 30 - 40 m from the bottom of the borehole, the drill rose at a faster rate than the lake water. Simultaneously the drilling fluid level began to rise. About 1.5 m^3 of fluid poured over the upper edge of the borehole into special collecting pans from where it was pumped into empty barrels. After several minutes the overflow stopped and the fluid level began to drop. Measurements made on 29 February 2012 showed the upper level of the borehole fluid was 43.5 m, and the drill with a borehole caliper could not descend below 3176.7 m. This meant that water from the surface layer of Vostok Subglacial Lake had risen by 592.6 m, rather than by 30 - 40 m as previously calculated" (2014).

Back on Mars, if the hole were to freeze with a wireline drill string still in the hole, that would be the end of the drilling mission. Things are different for the borebots architecture. If "conventional" breakthrough is performed, you simply "write off" the borebot at the bottom of the hole. The hole freezes, the borebot is lost, and new ice forms farther up the hole, which is subsequently *cored by another borebot*. This is "Plan B" for the Borebots architecture, and we think it is very competitive.

South Polar Layered Deposits

Starting at the bedrock, the astronomical age of this region is very apparent. Areas adjacent to the SPLD have been determined to predate heavy bombardment based on crustal magnetism data, and may possibly still contain ice or permafrost from that period. From Smith & McKay:

> "…this indicates that the magnetic features predate the heavy bombardment, predate the crustal dichotomy between the northern and southern hemisphere, and predate the formation of the large geological features such as Tharsis and Valles Marineris. Thus the magnetic crustal features may be sites of the oldest undisturbed terrains on Mars providing a window into the early environments that may contain material dating back to an earlier wetter Mars. These locations experienced the heavy bombardment, but not impacts large enough to erase magnetism. Sites in the southern highlands between 60° and 80° S, near 180° W containing the previously mentioned magnetic crustal features may be the oldest permafrost on Mars and the best target when searching for Martian life" (2005).

The area targeted for the mission context during this Phase I study is farther south than the area investigated by Smith and McKay, but is covered by the SPLD. This can make crater dating and this type of crustal analysis more difficult (the latter making density determinations a challenge as well, Li, 2012).

On the other side of the pole, there is evidence that dramatic glacial retreat around 3.5 billion years ago changed the landscape leaving eskers behind (Head & Pratt, 2001). It is estimated that layered ice from this period (known as the Dorsa Argentea Formation or DAF) remain preserved and extend under the SPLD (Head & Pratt, 2001; Whitten, 2020; Buhler, 2021). From Head & Pratt:

> "The Dorsa Argentea Formation and [Hesperian-Noachian-aged undivided terrain] as presently exposed over a combined surface area of $1.52 \cdot 10^6\ \mathrm{km}^2$, slightly larger than the present south polar deposits. If they underly the present south polar deposits … which seems plausible given the geometric relationships documented by the MOLA topography data, then the total area covered could be about $2.94 \cdot 10^6\ \mathrm{km}^2$, slightly over 2% of the surface of Mars. This is approximately 50% larger than the present Greenland ice sheet … and about 22% of the area of the Antarctic ice sheet…" (2001, p. 21).

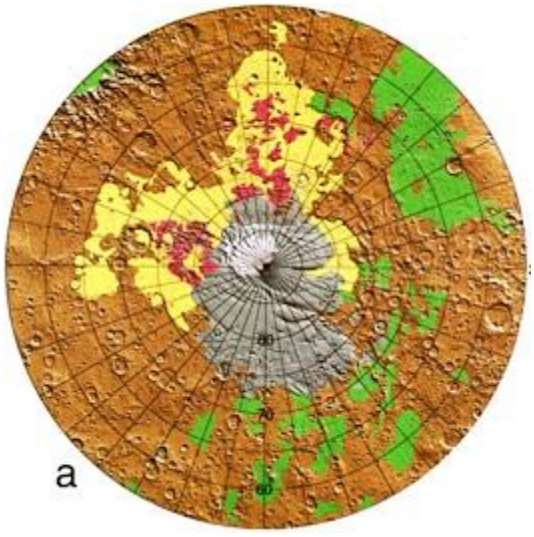

Figure 103: Plate 1a from Head & Pratt, 2001. Hesperian DAF is yellow, with older Hesperian-Noachian-aged undivided terrain in purple. The Amazonian SPLD is indicated in gray.

In contrast, the North Polar Layered Deposits (NPLD) are younger and have experienced more dramatic reductions in size over the eons. The basal unit is estimated to be between 2 and 3.5 billion years old, with evidence of major periods of resurfacing over the past few hundred million years (Nerozzi, 2021). Since the SPLD is much higher in altitude and more resistant to mass wasting during obliquity cycles, this helps to confirm that an older formation (i.e., the DAF) underlying the SPLD is reasonable. For more on the NPLD, see Byrne, 2009; and Byrne & Ivanov, 2004.

New questions about the basal unit continue to be raised by orbital observations, like the announcement of a bright subglacial radar reflection that may be associated with a liquid water lake (Orosei, 2018a). This sparked off quite a debate, and was also the motivation for the synthesis of this concept. The planetary science community was quickly divided into the "wet hypothesis" crowd and the "dry hypothesis" crowd. Those skeptical of the wet hypothesis have developed explanations for the bright basal reflections which don't rely on a wet explanation (Bierson, 2021; Khuller & Plaut, 2021; Lalich, 2021; Smith, 2021a, 2021b). Notably (for the borebots context), if a thick mud (frozen or otherwise) is present at the basal unit, the iris core catcher would be well-suited to retrieving the material. Arguably, this could make the mission more scientifically productive (by way of sediment cores from the subglacial material) than if the wet hypothesis is correct. Other skeptics of the wet hypothesis have tried to show that the *formation* of liquid is impossible by careful thermal modeling (Sori & Bramson, 2019). The thermal modeling method used by Sori & Bramson helped us with our estimate of ice temperatures that the borebot would be exposed to, and it has been recommended that we build on this type of model to more accurately predict these temperatures (Buhler, 2021). Others are also performing follow-up thermal modeling, examining the effect of porous layers in the stratigraphy, as well as sublimation lag layers of varying thicknesses (Orosei & Mitri, 2021). One interesting theory favoring the wet hypothesis (seemingly written as a response to the conclusions of Sori & Bramson) is introduced by Lauro, et al., and doesn't require modern formative conditions:

> "The process of absorption of atmospheric water by perchlorates and the subsequent formation of hypersaline solutions (i.e., deliquescence) was directly observed at the Phoenix Landing Site. Considering that Ca-, Mg-, Na- and K- perchlorates, chlorates and hydrated chlorides are globally ubiquitous in the Martian regolith, we posit that deliquescence and the formation of brines could plausibly occur at the south polar latitudes as well. Experimental work has shown that soluble salts with low eutectic temperatures deliquesce at low relative humidity values over a wide range of temperatures, overlapping with those expected on Mars, suggesting that brines may readily form in sub-polar regions when the temperatures are in the higher range (e.g., at noon). Re-crystallization of brines (efflorescence) when temperatures drop, however, is often kinetically inhibited because high activation energies are required for the transition from liquid to solid (ordered) states. Freezing experiments conducted under conditions similar to those on Mars have shown that perchlorate and chloride brines may exist for long times after their formation without effloresing. It is therefore plausible that once formed, brines may exist on Mars in a metastable state for geologically significant periods of time" (2021, p. 10).

If this hypothesis were true, not only would the ice sheet have logged the existence of life that could have been transported by wind to the polar regions (Smith and McKay, 2005), but life could be present in the brine under the SPLD, at a depth of 1500 m. Bright subsurface reflections were found elsewhere in the SPLD (Plaut, 2007), which may indicate an unrecognized phenomenon common to the SPLD (although liquid couldn't be ruled out; Plaut, 2007, p. 2). These are questions that can only be resolved to a high degree of certainty with deep drilling, which McKay again recommended in 2018 (Kaplan). Deep drilling also enables us to refine existing orbital observations by collecting ground truth.

Before moving away from the basal unit, it is worth considering the concept of hydraulic potential surfaces and their role in predicting locations where subglacial melting, flowing, and pooling can take place. This form of analysis is frequently applied to subglacial hydrology on Earth (Shreve, 1972). In Antarctica, lakes have not been found where they were expected to be, based on glacial flow characteristics and altimeter data (Humbert, 2018). Modeling of subglacial hydrology was used to explain and understand the discrepancy. However, subglacial lakes in the Arctic have been found in areas where the glacier was believed to be frozen to the basal unit (Rutishauser, 2018), which shows that our understanding can be lacking even on Earth. Currently, potential surface modeling does not indicate subglacial flow and pooling in the High Reflectance Area (HRA) common to the proposed location of a subglacial lake (Arnold, 2019). However, local melting is a possibility in this location, according to the authors. The topic is discussed again in Lauro et al. (2021, pp. 10-11). The shortcomings of our knowledge of glacial processes on Earth is highlighted again in Arthern (2010), when long-held beliefs about glacial densification were shown to disagree with empirical data (discussed again later in this chapter). It is also worth noting that Humbert (2018) experienced challenges defining the radar absorption properties of Recovery Glacier, resulting in a poorly constrained basal reflectivity. This is a problem shared by orbital science teams examining Mars polar data. These are strong reasons to be skeptical about firm claims in Mars polar science studies (especially ones which relate glacial processes on Earth to Martian processes), since even our fundamental understanding of Earth is in flux. Hopefully, surface operations in the polar regions of Mars can help us to evolve our understanding of both planets.

Moving on to the layered structure of the SPLD, it appears that the main drivers of accumulation are obliquity, eccentricity, and longitude of perihelion cycles that Mars goes through. Each obliquity cycle takes about 120,000 years (Buhler, 2020; Buhler & Piqueux, 2021; Byrne, 2009). See Figure 104, which is from Buhler & Piqueux (2021), and shows the transfer of CO_2 (on a global scale) during obliquity cycles. Note that we are not overly concerned with CO_2 deposits in our location of interest (the HRA), but looking at the evolution of CO_2 deposits can help us understand the powerful effect obliquity changes can have (since water is also a volatile in this context). Within each obliquity cycle, annual cycles occur that help transfer volatiles between the poles. Today we believe that there is a fine-scale layering caused by these annual cycles (that we can't see, but can infer, from orbit; Campbell, 2018) and a larger-scale layering that is likely obliquity-driven (which we can clearly see). The farther we look into the past, the more difficult it is for us to piece things together from orbit. The large-scale melting events that have obviously occurred (as evidenced by the eskers pointing to large-scale DAF retreat; Head & Pratt, 2001), washed away much of the evidence. However, we hope that areas of the ancient SPLD (i.e., the DAF) contain evidence of this warmer period, protected under the SPLD that we see today. This would help us unravel the mystery, and give us insight into the solar conditions that Earth was exposed to at the same time.

At some point the dramatic glacial retreat ceased, leaving the DAF as we see it. In the intervening billions of years, Mars went through several more accumulation phases (possibly with large-scale retreat phases interspersed). Eons that experienced interrupted periods of glacial formation (i.e., glacial retreat) were likely to have left sublimation lag layers in the SPLD stratigraphy, similar to the lag layer we see today at the surface (Buhler, 2021). Lag layers are discussed more later in this chapter. The obliquity, eccentricity, longitude of perihelion, and annual cycles continued for millions of years, resulting in the layered formation that we see today, which is about 3 km thick at a maximum (Byrne & Ivanov, 2004).

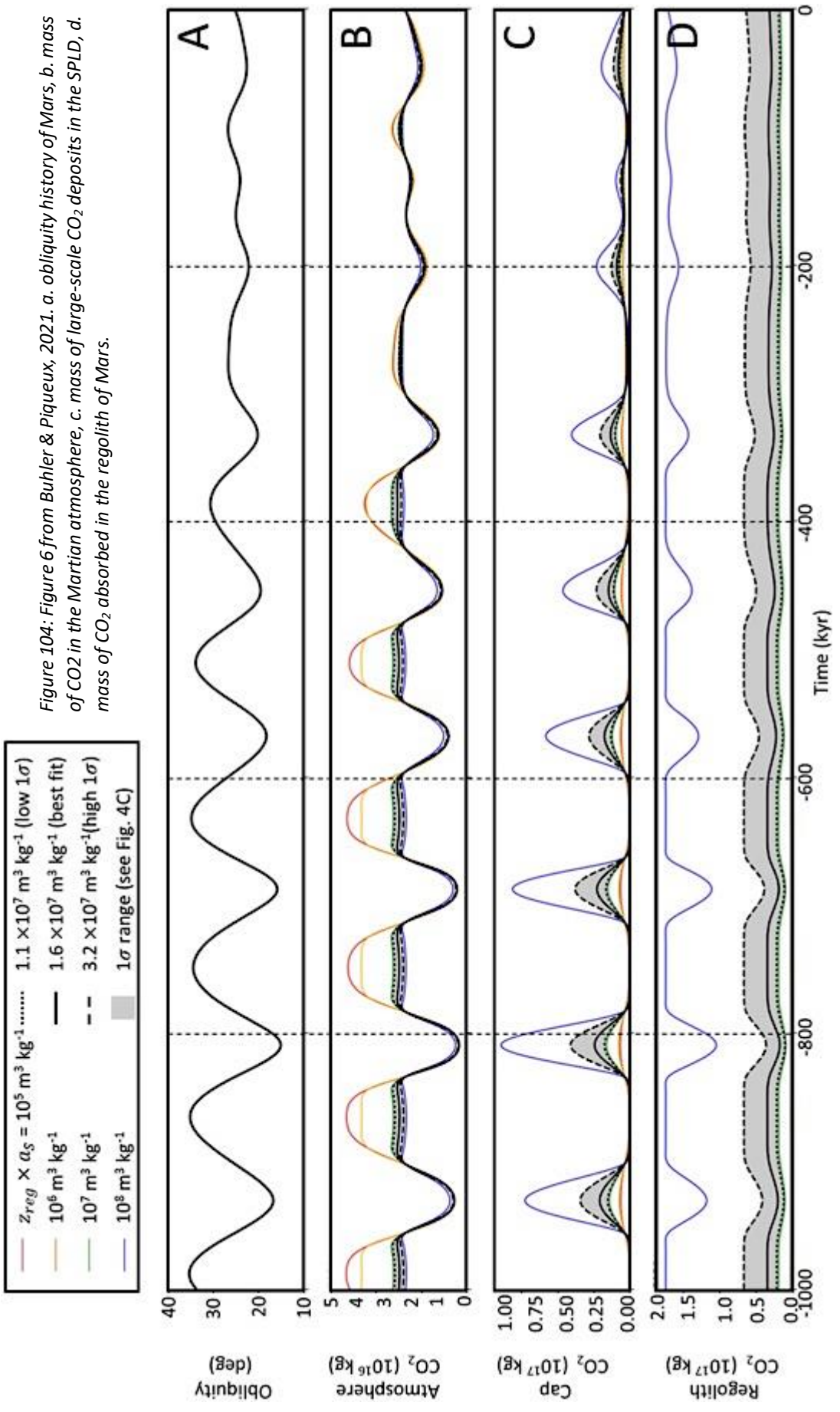

Figure 104: Figure 6 from Buhler & Piqueux, 2021. a. obliquity history of Mars, b. mass of CO2 in the Martian atmosphere, c. mass of large-scale CO_2 deposits in the SPLD, d. mass of CO_2 absorbed in the regolith of Mars.

As we move into the meat and potatoes of the SPLD – or "s'mores" if you ask Isaac Smith (2017) – we are concerned with the physical properties of the formation as a whole (which is best imagined as an ice sheet in this context). However, the layered substrate introduces some potentially unusual challenges. This is where Smith's s'more comes in to play: instead of one uniform ice sheet, he posits that each layer can be treated as an ice sheet sandwiched between two less icy layers, that are considerably harder than the ice sheet in the middle (Figure 105 and 106). This explains why we don't see large-scale flowing of the ice sheet, which actually impairs our ability to estimate the bulk shear strength of the ice (which is unfortunate in our drilling context).

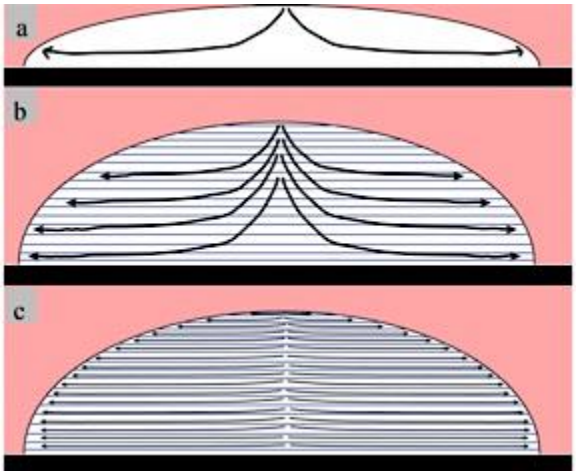

Figure 105 (above): Figure 3 from Smith, 2017. Three flow scenarios, a. is "generic," b. represents an older SPLD model. Smith posits that c. is most akin to SPLD.
Figure 106 (below): Smith's s'more (2017, fig. 4).

Byrne and Ivanov performed an excellent analysis in 2004, carefully following specific layers through as much of the SPLD as possible using orbital imagery (Figure 107). Whitten and Campbell did a similar layer-tracing analysis using SHARAD radar data (2018), see Figure 108. The discipline and enthusiasm that the planetary science community shows for this type of work is inspiring, and highlights how informative surface operations can potentially be. The value provided by carefully identifying the continuity of the SPLD layers resonates well with the Clifford et al. report, which recommended traversing down one of these slopes drilling shallow boreholes along the way (2013, section 3.1). Performing spectroscopy work on excavated material (as recommended in Calvin, 2010, p. 21 para. 5) from the specific layers traced by Byrne and Ivanov (as an example) would also be a boon to polar science, helping us refine previous analyses and better understand deeper radar data. In effect, we need to go see what the s'more tastes like.

Figure 107: Figure 4 from Byrne & Ivanov (2004), showing their excellent attention to detail. BFL is Bench Forming Layer, WL is Wavy Layer; SS is Steep Sequences. Layers are matched up in various locations to map the internal SPLD structure.

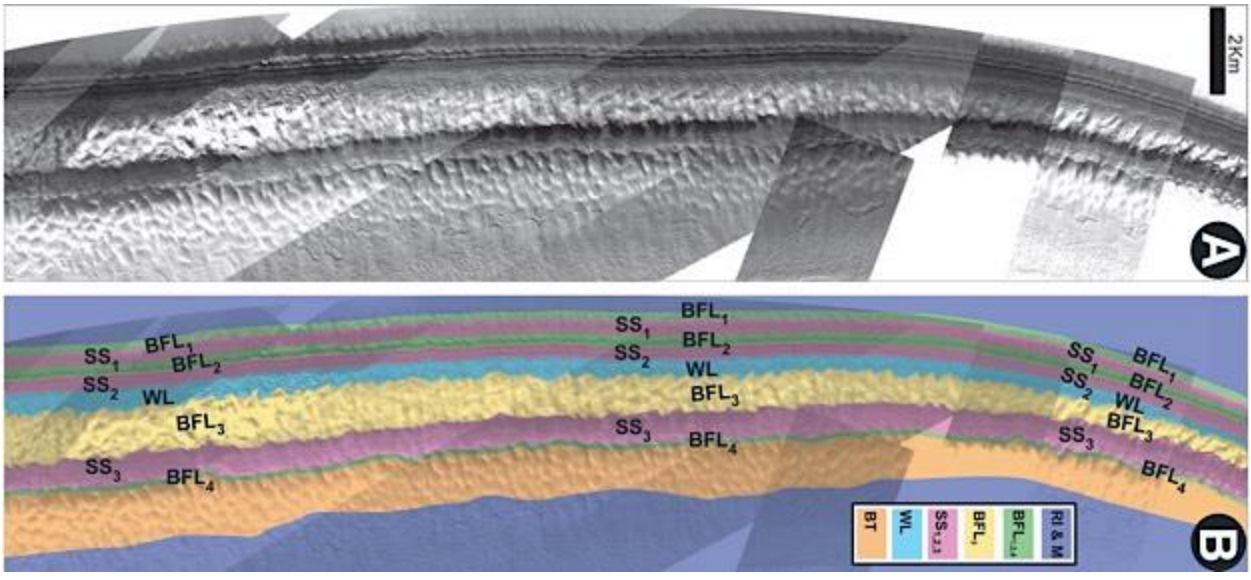

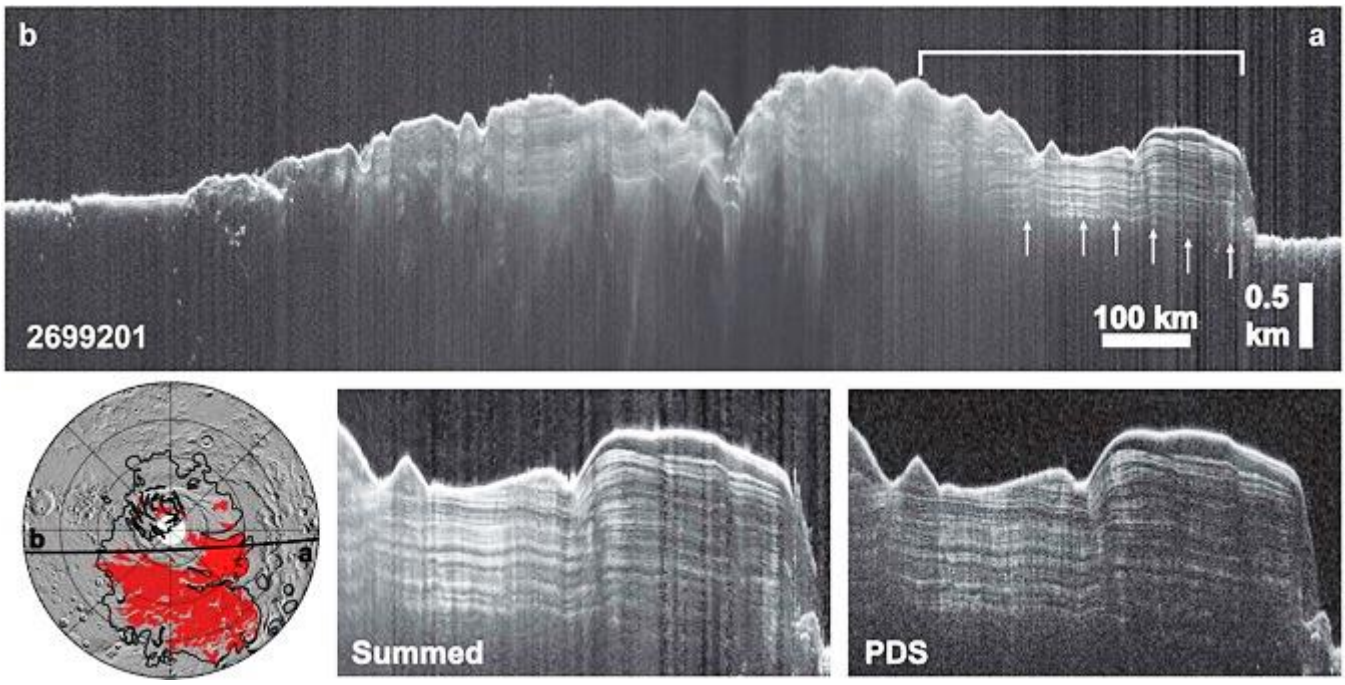

Figure 108: Figure 7 from Whitten & Campbell (2018), showing a Shallow Radar (SHARAD) sounder radargram. Layers can be traced through the SPLD stratigraphy to map the internal structure. Note that layers are not always visible due to a "fog."

There are areas in the SPLD that contain massive amounts of buried CO_2. This was revealed in 2011 by the influential work of Phillips et al., and changed our understanding of the way the planet responds to obliquity cycles. We now know that the CO_2 atmosphere can almost completely collapse, depositing most of the atmosphere into solid CO_2 accumulations at the poles. Phillips also points to areas where these massive CO_2 deposits have wasted away, indicating that the present atmosphere is not an example of the maximum extent of atmospheric collapse (2011). A radargram showing the most significant "Reflection-Free Zone" (RFZ) is shown in Figure 1 of this document (p. 5). RFZs indicate solid CO_2, and the authors eliminate porous water ice or clathrates as a cause with a high degree of confidence (Phillips, 2011). It is important to note that porous water ice, clathrates, and solid CO_2 (below the seasonal surface layer, discussed later in this chapter) are significant threats to the feasibility of a borebots SPLD mission. This is the reason for our focus on these issues during Phase I. Other than in the upper meters, it is extremely difficult to mitigate the threat posed by these compositions encountered at depth. Locations containing highly porous water ice, clathrates, and CO_2 ice in the stratigraphy should be eliminated as potential borebots deep drilling sites.

Note: we developed a strange mitigation measure if very thin (10-cm-order) layers of solid CO_2 are encountered during drilling (which would sublime away at a significant rate, i.e., day-order, creating a gap extending horizontally away from the borehole), but have deemed it both too technically challenging and unnecessary. Basically, a borebot loaded with a drill head that contains a capsule of foaming agent is sent down the borehole upside-down, and is charged with the task of anchoring a plug above the affected layer in the stratigraphy, and driving / falling to a level below the layer. The foaming agent would be deployed. After curing, the borebot would have to drill upwards through the cured foam, effectively restoring the borehole, removing the plug on its way up. Due to the improbability of encountering this type of situation, this strategy won't be developed or further described.

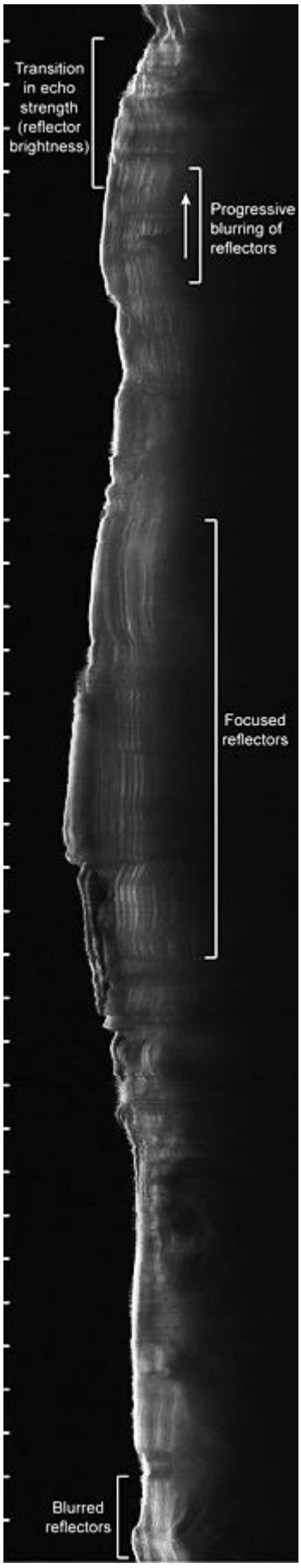

As mentioned in the Primer, there is no evidence for large quantities of buried CO_2 ice near the area being considered in this study (Putzig, 2011). No clathrates (except perhaps at the top/bottom of a CO_2 surface layer) are expected either (Buhler, 2021). For a review of clathrate possibilities, see Longhi, (2006), but note that orbital observations do not support widespread CO_2 layers in the substrate (Putzig, 2011). Longhi, 2006 was written when MARSIS was still going through its first weeks of science, and before the SHARAD instrument was operational at Mars. We do expect to deal with thin surface CO_2 deposits, although we believe they can be avoided entirely during landing site selection. If that is not the case, the mobility capabilities of the rover can allow us to find a site with little to no surface CO_2. Generally, the CO_2 It is only trapped permanently when buried under a thick, nonporous layer at a sufficiently fast rate (Manning, 2019). Also, it is believed that the RIMFAX ground-penetrating radar on Perseverance could detect any threatening layers in the upper hundred-meters of the substrate (Orosei, 2021). If surface CO_2 layers are unavoidable, the best thing to do is to bring extra lengths of drill pipe (i.e., tubes like the deployment tube, that can be inserted into the ground until below the CO_2 layer). This is important to ensure the stability of the upper portion of the borehole during drilling operations (since CO_2 likes to sublime in the summer). A top-anchor (which would look like a Christmas-tree stand) for these drilling pipes could be used to make it easier to autonomously couple the deployment tube with the drill pipe on a regular basis. This would also represent a more significant investment in one drilling site, which adds mission risk and makes borehole abandonment a tougher decision.

We've already touched on some surface-layer considerations, but the situation at the surface is actually quite complex and poorly understood. Continuing with the bottom-up approach to this section, as we approach a depth of 50 m below the surface we expect to encounter a significant, dense, and hard sublimation lag layer. It is logical to expect this layer to extend to 30 m or 45 m deep. These estimates are multiples of the SHARAD sounder wavelength of 15 m. Whitten & Campbell (2018) introduced the hypothesis that the "fog" effect seen by the SHARAD instrument in the SPLD could be caused by a 30-m sublimation lag layer (sect. 4.2, para. 4). We think it wise to extend this to a range of between about 15 m and 45 m, and with our primary mission goal of 50 m, we hope to find out for sure. The lag layer would be made out of ice-cemented dust, formed as duricrust, as water sublimated from the SPLD. This material would generally be very hard and stable, and is likely topped with a cm-order layer of dry dust or regolith.

Figure 109 (left): SHARAD radargram showing fog throughout the SPLD. Towards the center, the fog seems to ease up a bit allowing subsurface layer reflections to be seen more clearly (Whitten & Campbell, 2018, Figure 3).

These conditions are favorable in our borebots context. RIMFAX is expected to see through such a lag layer, and could see farther in higher-water-ice-content scenarios (Orosei, 2021). For this reason, RIMFAX may be the most important instrument on the rover, as over 15 years of orbital radar polar science could be improved dramatically with the first RIMFAX soundings (especially given the instrument's ultra-wideband design [NASA Mars 2020 Mission, n.d. c], making it easier to nail down the permittivity of near-surface layers). RIMFAX could also operate synergistically with future orbital radars.

The density of the SPLD is semi-constrained, but affected by crustal gravity anomalies. Zuber et al. (2007) fond that the bulk density of the SPLD is about $1220\ \mathrm{kg/m^3}$, which translates to a composition of about 15% admixed dust. Li et al. (2012) was able to provide a 2D density map, although the authors emphasize that their model is sensitive to gravity anomalies (and they do believe that has affected their results). Gravity anomalies in this case would mean varying crust composition of the bedrock, or perhaps the bedrock terrain not agreeing with terrain data from MARSIS soundings. We used the density map from Li et al. to create the context map shown in Figure 110, with the HRA indicted with a star.

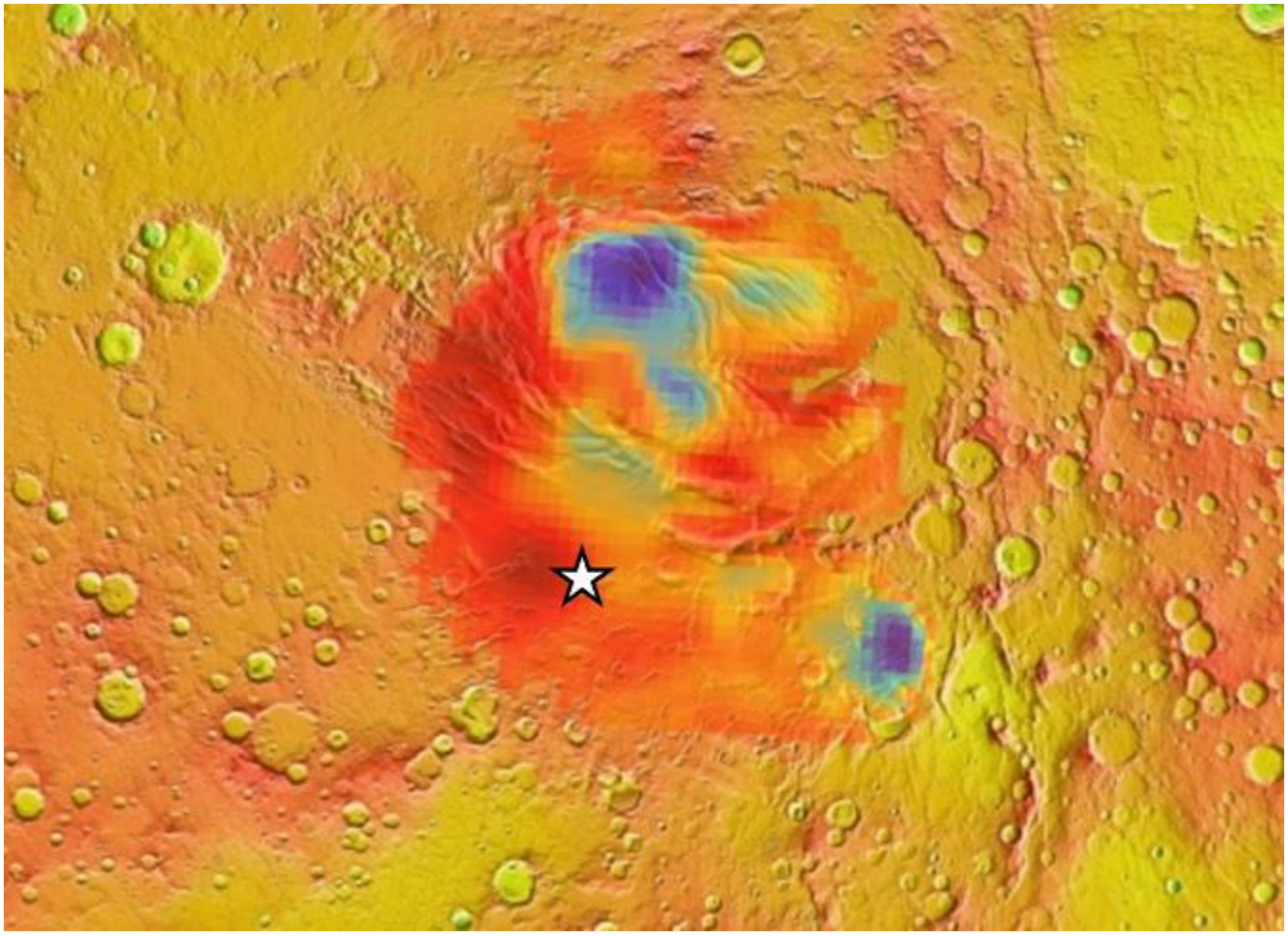

Figure 110: Regional map w/ density overlay (density from figure 6-d, Li, 2012). Density at HRA: 1200 kg/m³ ± 100 kg/m³

The density measurements indicate that the PLDs are mostly dusty water ice, and that the upper layers of the PLDs are denser than accumulation and densification models suggest (which were heavily influenced by glaciology on Earth). Arthern, Winebrenner, & Waddington (2000) proposed a densification model that relied more on vapor exchange with the atmosphere. This process is opposed to pressure-induced sintering that happens on Earth. A modern overview of sintering can be found in

Molaro, (2018). It would be wise to expect that both processes play a role, with one process or another being favored during different geological eras (depending on the atmospheric pressure and accumulation rates). The Arthern model has been found to agree with orbital radar observations (Clifford, 2000; Sori, 2016; Langevin, 2005), although we are observationally blind below the top few centimeters (which continues to 10s of meters; Mellon, 2021), so the model can't be confirmed to a high degree of certainty with current surface radars or radar sounders. The uncertainty related to sublimation lag layers could be masking the truth about our accumulation models in the South, which is why the NPLD is usually favored for this type of analysis. The Arthern vapor exchange model is also at odds with our current understanding of the densification of mid-latitude glaciers, which seem to form a hard upper curst via a vapor exchange process, halting densification of the firn layers below (Bramson, et al. 2017; Bramson, 2018). This may pose a challenge for mid-latitude resource extraction using traditional drilling techniques (or borebots).

The discrepancy in near-surface density in the PLDs, caused by poorly understood surface processes, was alarming at the beginning of the Phase I study. We tried to understand which school-of-thought was the most relevant to what we see today, and examine whether that would result in conditions amenable to surface operations. At the heart of this is the desire to avoid thick low-density firn layers, since the borebot track system could erode such a substrate relatively quickly. Bracketed estimates of density vs. depth for various dust contents were then made, with Figure 111 representing the highest density, Figure 112 the lowest (i.e., with significant annual snowfall; Arthern, 2000). Figure 113 would apply to a period of wasting. If the SHARAD fog is caused by a lag layer, the density should tend towards the ideal case, as low-density surface layers would have been removed or cemented. The longer a wasting period continued, the thicker and more dust-rich the lag layer could be (30 m of thickness would challenge our assumptions about non-permeable layers in the PLDs, which is already being done to couple the massive CO_2 deposits to obliquity cycles; see Buhler, 2020).

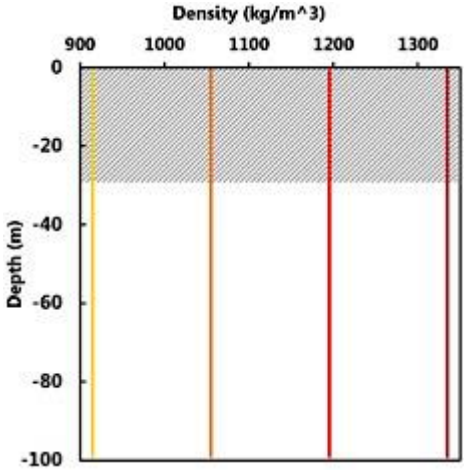

Figure 111 (left): An ideal formation. hatching indicates lag layer uncertainty.

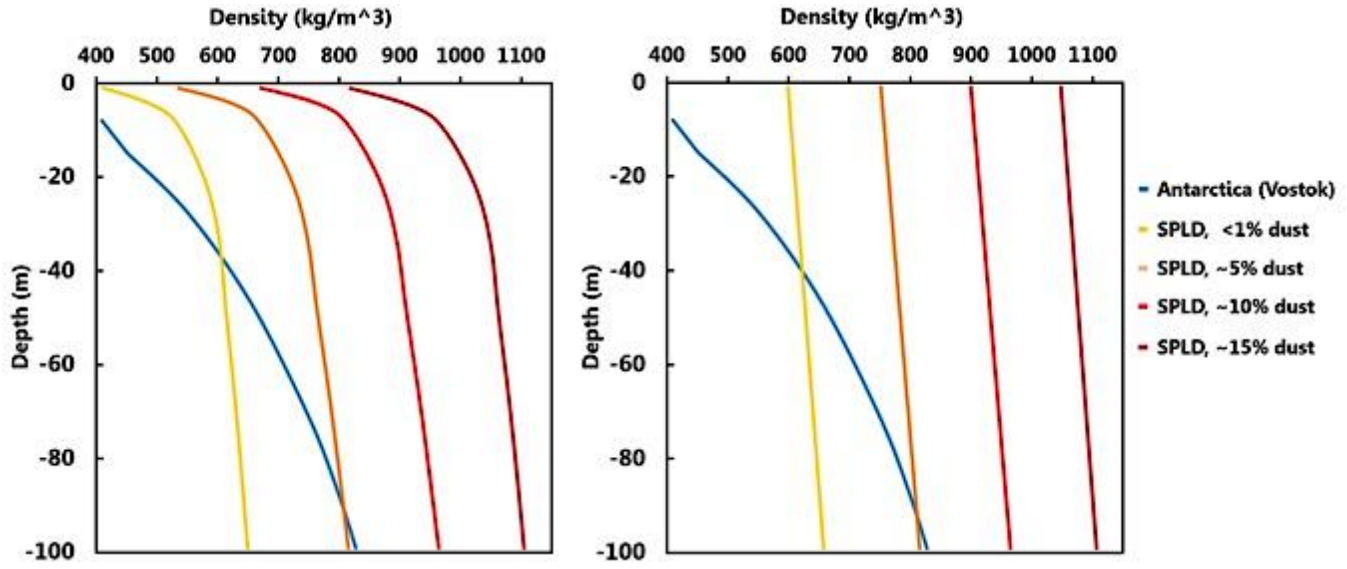

Figure 112 & 113 Pos. mass (L), wasting (R). Vostok data: Cuffey (2006, fig. 2-3).

Cryptic terrain is a common seasonal surface feature in the SPLD. It is believed that it surmounts the lag layer and is comprised of CO_2 ice that is trapped under layers of water ice. When exposed to insolation the CO_2 sublimes, breaking through the water ice (erupting as geysers), and leaves behind "spiders." In our context, we need to get to a location that is below these surface layers of CO_2, or land later in the year when the terrains are at their minimum. In some areas, large pits form as CO_2 sublimes, some of which have sloping hillsides on one or more sides. We believe that the bases of these pits would be good drill sites. Fig. 114 shows promising landing sites and drilling locations. For more on cryptic terrains, see Piqueux (2003), and Schwamb (2018). The effect of polar winter on rover operations is unknown. Heat from the RTG should prevent CO_2 icing on the rover, and may offer protection some distance from the rover. Operating statically at a drill site, <1 m of ground ice accumulation may be fine.

Figure 114: Hi-RISE imagery in the vicinity of the HRA. NASA/JPL/UArizona. https://www.uahirise.org/ESP_066074_0990

Feasibility Assessment & Technology Roadmap

Feasibility Determination

The prospect of traversing a borehole without any link to the surface is tantalizing. Surprisingly, wireline drills seem to share a lot of the same feasibility challenges with our "wireless" system – mainly, rotational force has to come from the downhole unit, not from the surface. A consequence of this is that both borebots and wireline drills must anchor to the borehole wall during drilling, which means they place a mechanical demand on the sides of the borehole. This is the largest threat to feasibility that we see for the borebots system, especially given the poorly constrained stratigraphy of the SPLD. All the winch does is raise and lower the downhole equipment. This does mean that the borebots system is expected to place additional demands and wear & tear on the borehole, compared to a wireline system. However, we are encouraged by the prospect of variable-pressure drive to reduce those demands, and feel that a rolling rubber track may be less damaging than spiked anti-torque pads. What remains to be seen is how various types of stratigraphies respond to frequent tripping. A wireline system only has to anchor at a given depth one time, yet with borebots the demands on the borehole are cumulative. Luckily, most potential targets for borebots in planetary science have very hard substrates.

Aside from demands on the substrate, there are two other primary considerations when it comes to feasibility. The first is the fundamentals of the mechanical system, i.e., does it all add up? The second is the long-term survival of COTS hardware on the Martian surface (as each borebot would spend most of its mission life at the surface). While the second consideration can be mitigated by storing borebots in a shielded environment between uses, and allayed to an extent by the success of the Mars Helicopter technology demonstrator Ingenuity, the picture with the mechanical system is much more complicated.

Our power modeling and the accompanying discussion in the Power & Components section of the Technical Discussions chapter of this report shows that 100-m-order depths are achievable even with an extraordinarily inefficient mechanical system and limited power storage. This may actually be a desirable configuration for the lower-cost alternate contexts that we discussed: a bomb-proof, non-adjustable drivetrain with a low efficiency that would struggle to get past 100 m before damaging the batteries. However, with a reasonable and prudent amount of mechanical development, we believe efficiency gains and increased power storage can allow km-order depths while increasing the redundancy of the drilling mission several fold over a wireline drilling system. At the same time, we believe that it is easier to accommodate borebots on existing spacecraft designs, and can potentially provide a more flexible drilling workflow. We therefore find the concept fundamentally feasible.

The next section explores direct comparisons to architectures that we perceive to compete with borebots: wirelines, melt probes, and hybrid thermo-mechanical drills. The chapter concludes with a Technology Development Roadmap, designed to take borebots to TRL 5 and beyond.

Borebots vs. Competing Deep Drilling Architectures

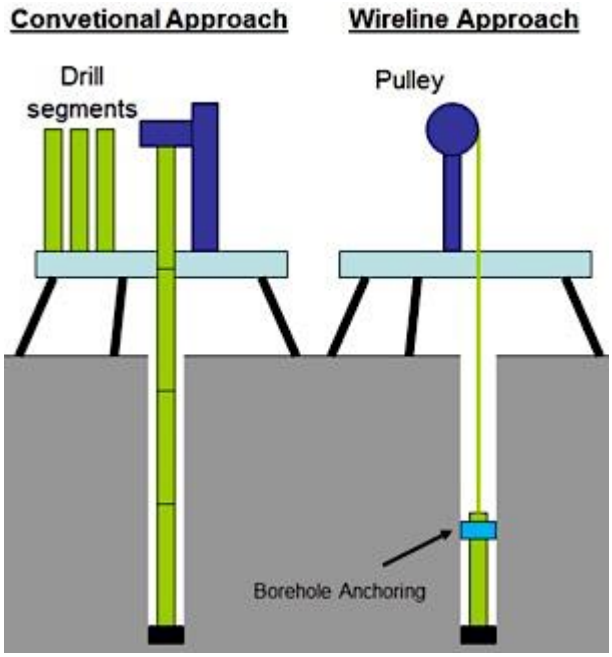

Figure 115: Conventional drilling vs. wireline drilling (Zacny, 2013, Figure 1).

In the last 60 years, thought around deep ice drilling has evolved, from methodologies employed by the oil industry to the modern wirelines (cable-suspended electromechanical drills) that we see operating in Antarctica today (Talalay, 2016, p. 109; Bar-Cohen, 2009, p. 226). Drill pipe (or any other rigid link to the surface) is generally relegated to meter-order ice drilling. This is evidenced by the deep drill that is ready to fly with the ESA Rosalind Franklin Rover, with a maximum depth of 2 m using drill pipe (Magnani, 2004; Bar-Cohen, 2009, p. 506), with wireline concepts favored for any deeper extra-terrestrial surface-linked work (Zacny, 2013). Several competing wireline designs have been pushing up through the NASA technology pipeline, but many of these designs seem to stall out around TRL 5 (Zacny, 2018a). The WATSON / Planetary Deep Drill combo appears to be the leader in this area (Eshelman, 2019). We believe the difficulty with getting to / past TRL 5 is because wireline drills are difficult to integrate into a spacecraft and difficult to automate, making potential mission customers hesitant. This relegates these systems to technology development projects without a clear path to a mission. The current leading wireline space technology concepts are all produced by Honeybee Robotics. For a complete history of cable-suspended ice drills, see Talalay (2016) and Bar-Cohen & Zacny (2009); we highly recommend these books for anyone even tangentially involved with ice drilling. For recent developments, see Zacny (2018a) and Eshelman (2019).

Until this Phase I study, nuclear-powered melt probes were the only concepts that had no physical link to the surface. To achieve this, they sacrificed the ability to go back to the surface at all, instead relying on wireless links (with “puck” relays) to relay data back to the lander, meaning all of the science had to be performed in the melt probe. Some of these devices even involved tethers, to eliminate isotope reliance and provide for easier data transmission. Work on steerable and recoverable non-isotope versions has been performed (Kowalski, 2016). One concept used a high-power laser to beam power down the hole (Stone, 2018). The same paper discusses the “starting problem” for melt probes (sect. 4.2), which we address on p. 72, para. 3. For more on the current status of melt probes, see Schmidt (2021, tbl. 1; note the max TRL is 5, Stone claims this is due to a lack of testing facilities [2018, sect. 4.2]).

Recently, hybrid systems have begun to emerge, exemplified by Honeybee Robotics’ SLUSH drill (Zacny, et al. 2018b; 2019b). JPL has a similar concept in-work, tentatively called Probe Using Radioisotopes for Icy Moons Exploration (PRIME; Howell, 2020) however, there is quite a bit of secrecy around the concept, which makes our efforts to form a comparison difficult (a fact which we regret). Since we feel that this style of system is much more capable in our SPLD context than pure melt probes, and with no information about JPL PRIME available, our analysis of competing thermal and thermo-mechanical systems is limited to the SLUSH family of drills.

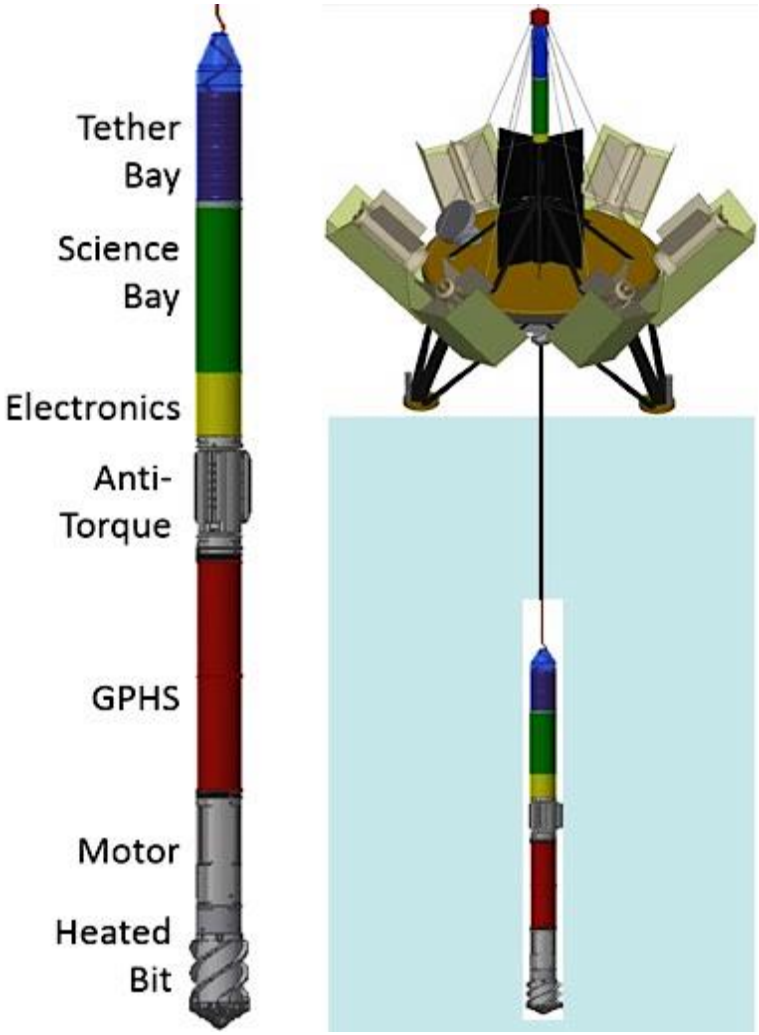

Hybrid thermo-mechanical drill systems are difficult to compare to borebots, because of the large size of the former. However, as we showed in Figure 80 & 81, the power required for subsurface ocean access in an ocean worlds context is 100-Ah order. This is not an unreasonable amount of power storage when considering the 57 cm diameter of the SLUSH drill (Zacny, et al., 2018b). A borebot that size could use massive LiFePO4 batteries, like the ones used in the marine industry, easily enabling 500 Ah of storage in a several-meter-long, half-meter-wide borebot. These large-scale borebots are not currently being considered, but are expected to have the same scaling challenges as a large thermo-mechanical drill. Perhaps an annular lander with several borebots stored around the circumference, with a short-and-stout deployment tube, could be a tetherless answer to the SLUSH drill.

Figure 116 (above): Honeybee Robotics SLUSH drill, est. to be 10x more efficient than melt probes. Note 6 RTGs. Zacny, (2018a).

Figure 117 (below): JPL PRIME, a thermo-mechanical drill that we believe to be similar to the SLUSH drill. Howell, (2020).

In a Mars PLD context, these thermo-mechanical drills are quite capable of deep drilling into the dirty / layered ice. There may be challenges penetrating lag layers if they are extremely "dry" duricrust, that has low percentages of cementing water ice. However, we believe that this could be easily remedied with technology development focused at the SPLD, to enable a pure-mechanical mode of operation when dry layers of the stratigraphy are encountered. An easier solution is to avoid the SPLD and thick lag layers (focusing instead on the NPLD), which wouldn't require any periods of pure-mechanical operation. This has the benefit of avoiding the planetary protection concern of introducing heated equipment into the subglacial liquid environment. It is likely that there would be a planetary protection concern raised by the inclusion of six RTGs in such a lander; this would be somewhat alleviated by selecting the NPLD, but would still be an issue.

Nuclear-powered melt probes are an even larger planetary protection concern, especially when targeting subglacial environments that may contain liquid water and signs of life. Melt probes (nuclear or otherwise) are also poorly equipped for dealing with relatively dry layers of the stratigraphy, without having a full-on mechanical mode (even if some have mechanical aspects of operation). However, there have been instances of non-nuclear melt probes penetrating sediment layers in ice (Kowalski, 2016), by way of a small mechanical drill. We do believe that after a preponderance of these factors, melt probes are not feasible in the SPLD context, especially in the HRA from Orosei (2018). They are a good choice for the NPLD (if planetary protection concerns can be resolved), and have been recommended for NPLD use over the years (Zimmerman, 2002; Smith, 2020, section 3.5.1).

Of special note in the context of an ocean worlds melt probe, is the use of borebots to create a "starter hole" for a 10-km-order ocean access mission. A km-order hole could be drilled with several borebots. This could allow for enough head loss (opposing the outflow of sublimed gasses), such that the hole can form its own atmospheric pressure, allowing melting of the substrate. This would allow for a much simpler probe-handling system (not requiring a sealed deployment tube, Zacny, 2021), and enable the probe to be a true melt probe (instead of subliming most of the substrate away, overcoming the latent heat of one phase change instead of two), thereby increasing energy efficiency significantly.

Returning to cable-suspended drills, this type of system seems to be the most reasonable head-to-head competitor to borebots in the SPLD context. Although thermo-mechanical drills can't be ruled out, the cost and complexity make it a ham-fisted approach to km-order deep drilling. It is likely that a wireline mission could be converted to a borebots mission, or vise-versa, relatively easily; while a thermo-mechanical architecture requires more special consideration (mainly the order-of-magnitude greater power demands, Zacny, 2018a). We believe the true advantage of borebots is the potential for a several-fold increase in redundancy without increasing the energy demands of the lander system, when weighed against a wireline drill. The only single-points-of-failure in the borebots architecture are the robot arm and the deployment tube, which can act as backups for each other to some extent (this could be explored further when working with a mission customer). The handling of equipment is also simplified. Cables, winches, cable-handling hardware, etc. are all eliminated from the system. The only large advantage wirelines have is the potential to reduce wear on the borehole wall. A secondary advantage is the ability to "winch your way out of trouble." We believe the ability to abandon a borehole and start another one (several times if necessary), combined with the reduction in single-point-of-failure items in the architecture, are advantages to borebots that far outweigh these two wireline advantages.

Technology Development Roadmap

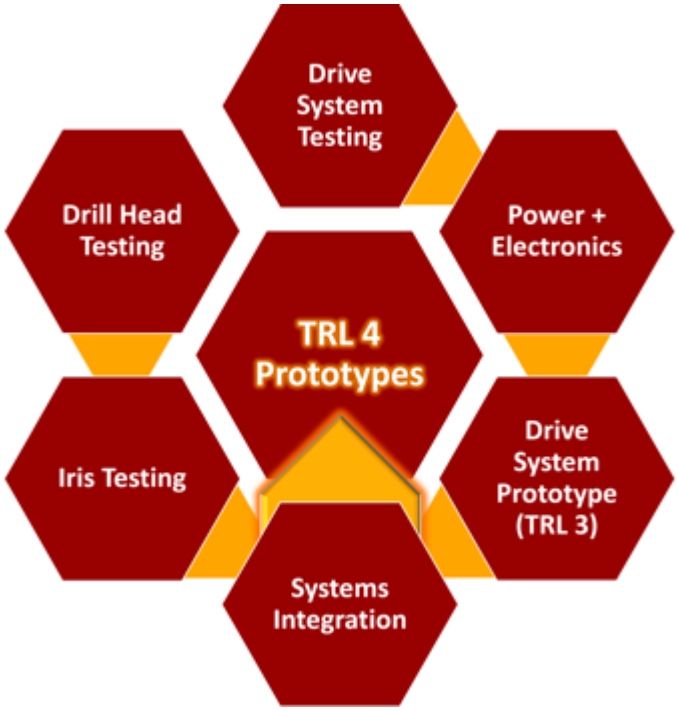

Figure 118: Recommended iterative design phase of TRL 3 & 4 hardware. 108 mm borebots should be introduced at TRL 3 to benefit from iterative design gains. 64 mm should be continued to TRL 4 before the Key Decision Point.

Due to the sensitivity of the architecture to drivetrain inefficiencies, and the strong argument for statistical component reliability (imposed by the requirement of 10,000 trips for 1.5 km depth), we recommend that the technology development process in Phase II should lay the foundation for efficient drivetrain evolution within a statistical control framework. The drill head and core breaker will also need a high level of reliability, but should be a secondary focus area since other drill heads can be used. Again, the motivation for a borebots-specific drill head is efficiency / WOB.

The drive system should be iterated in a method conducive to bench testing, and the most efficient versions should be brought up to full TRL 3 prototypes for experimentation. Tertiary focus areas should be advanced in TRL, but should not be included in system integrations work until warranted (*if* warranted for the water sampler).

Figure 119: Big-picture Technology Roadmap showing the core development stream, as well as concurrent 64 mm and 108 mm prototype testing prior to TRL 5. Risk reduction, re-evaluation, and tertiary focus areas are recommended. Design should shift from iterative to qualitative at the Key Decision Point (during the second year of Phase II). Investigators should then add a quantitative statistical context, to be maintained through the remainder of the development process.

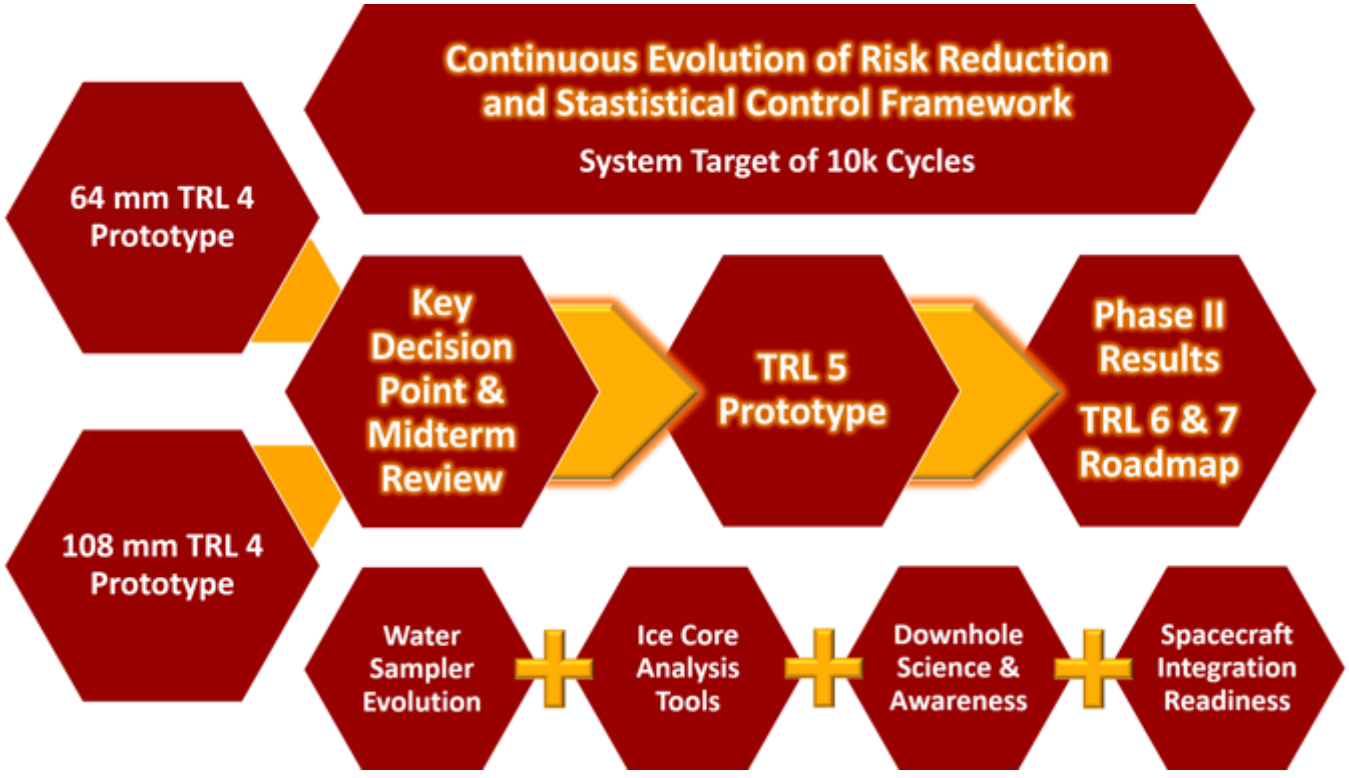

Conclusion, Key Findings, & Recommendations

Conclusion

This NIAC Phase I study covered a lot of ground, and the concept of "cutting the cord" with the surface generated a very enthusiastic community response. The versatility of the concept is much greater than originally anticipated, with surprising and inspiring applications that we had never imagined prior to the study. There is a myriad of development directions open to us because of the amazing opportunity that NASA has given us to explore this concept. We look forward to leveraging this opportunity by continuing to explore new directions, and that process has already begun. We received an invitation from The Mars Society to give a talk about borebot-equipped COTS robots performing team-based mid-latitude resource extraction. We have also been encouraged to develop an Ocean Worlds borebots mission concept targeting sub-surface life detection on Titan, and received an invitation to discuss subsurface access in an astrobiology context. All of these opportunities were unexpected, but help to illustrate the flexibility of the borebots concept. With launch prices tumbling and the demand for Mars-polar-science ground truth coming to a boil, we hope that the borebots concept is the catalyst needed to re-ignite an enthusiasm for polar surface operations within NASA and the community.

Phase I Key Findings

- Driving up and down a borehole is a fundamentally feasible alternative to wireline drilling
  - Mission-profiles are depth limited, due to battery storage & cycle life requirements
- Energy efficiency is a critical factor, affecting achievable depth and battery cycle life
  - Borebots are especially sensitive to power draw from electronics and the track system
- Iterative design methods are not only desirable, but required, to optimize drive system
  - FEA struggles with sparse, flexible, anisotropic structures; precluding bottom-up design
- Drill heads designed for low Weight-on-Bit and low power draw can add margins to power budget
  - Borebots-specific drill heads are not a requirement, increasing flexibility
- The Mars-2020-class mission can preserve most spacecraft heritage
  - Only small modifications to the external features of the rover are required
  - Optionally, a prudent level of reconfiguration could potentially boost the science payload
- Borebots architecture is easily adapted to other mission classes
  - Static landers and small rovers unlock access to Discovery, New Frontiers opportunities
  - Commercial-off-the-shelf (COTS) robots (i.e., Boston Dynamics) team-based missions
    - This finding has generated an exceptionally enthusiastic community response
- Mars 2020 Adaptive Caching Assembly (ACA) can be retained with full heritage
  - Leveraged to cache ice core samples by way of re-coring and/or sub-sampling
  - Possibly used in static lander contexts; modularity was an ACA design feature
- High-TRL downhole science instruments exist; addt'l. legacy spectrometer evolutions are possible
  - Integration of WATSON into the borebots architecture could lead to a mission customer
- Physical sample processing of excavated material (via a pneumatic system), combined with ice core evolved gas analysis offers a robust science return.

Recommendations

Due to the potential for borebots to kindle an enthusiasm in the scientific community for Mars polar drilling – and because of the immense challenges that no doubt await us there – we offer the following recommendations. It is our hope that those in the scientific community that wish to assist or support such an effort can do so. We also encourage other undergraduates to find ways to participate.

Recommendation: The ethical question of breakthrough into a Martian liquid environment should be explored further. Although the water sampler is a tertiary focus area, the fundamental design of the device is affected by philosophical decisions around sample cleanliness vs. subsurface contamination. Importantly, the concept of reversibility pertains to downhole anchoring or abandoning equipment.

Recommendation: Thermal modeling of the SPLD should be refined to include a significant sublimation lag layer, topped with the complex cryptic terrain layering most of the year. This work should be informed by additional orbital observations, and should include context for (sub)surface operations.

Recommendation: The versatility of the SHERLOC instrument on Perseverance (and the subsequent conversion into the downhole suite WATSON) has shown that future spectrometer development should be carefully considered for use on smaller landers and in downhole equipment, to increase the impact of this important technology. The design of a "common instrument" to be used on several types of missions may be high-impact, and could increase the chances of instrument selection. To emphasize this, a COTS-robot team member could be dedicated to a SuperCam-esque instrument; or an MER-class rover could benefit as discussed previously.

Recommendation: *In-situ* ice core analysis (i.e., in the drill head) should be explored further in a science context. The community may wish to weigh the value against terrestrial ice core analysis methods.

Recommendation: The polar science community should form a recommendation on avoiding the potential impacts of CO_2 ice during surface operations. For example, it can be considered advantageous to land at the SPLD during the southern spring to have a single-season, long-duration mission prior to winter (about one Earth year). However, the surface CO_2 situation is rather volatile at this time, and by Autumn, most of this surface CO_2 has sublimed. The effect of operating continuously over winter should also be considered in this CO_2-ice context.

Recommendation: During efforts to determine the composition of the stratigraphy, attention should be paid to regions that may contain CO_2, H_2O-CO_2 clathrate, or porous H_2O ice layers, in a sub-surface access context. Future missions may wish to target these areas, or in our case, avoid them. If undetectable in an area, a quantitative estimate of the maximum thickness of undetectable layers should be given.

References

Arnold, N. S. et al. (2019). Modeled subglacial water flow routing supports localized intrusive heating as a possible cause of basal melting of Mars' south polar ice cap. *Journal of Geophysical Research: Planets*, *124*:8. Wiley-Blackwell. https://doi.org/10.1029/2019JE006061

Arthern, R. J., Vaughan, D. G., Rankin, A. M., Mulvaney, R., and Thomas, E. R. (2010), In situ measurements of Antarctic snow compaction compared with predictions of models. *Geophysics Research, 115*. doi:10.1029/2009JF001306.

Arthern, R. J., Winebrenner, D. P., & Waddington, E. D. (2000). Densification of Water Ice Deposits on the Residual North Polar Cap of Mars. *Icarus*, *144*(2), 367–381. https://doi.org/10.1006/icar.1999.6308

Aubrey, A. D., et. al. (2008). The Urey Instrument: An Advanced *In-Situ* Organic and Oxidant Detector for Mars Exploration. *Astrobiology 8*. doi:10.1089/ast.2007.0169

Balaram, J., Aung, M. M., & Golombek, M. P. (2021). The Ingenuity Helicopter on the Perseverance Rover. In *Space Science Reviews* (Vol. 217, Issue 4). Springer Science and Business Media B.V. https://doi.org/10.1007/s11214-021-00815-w

Balaram, J., et al. (2018). Mars helicopter technology demonstrator. *AIAA Atmospheric Flight Mechanics Conference, 2018*. https://doi.org/10.2514/6.2018-0023

Bar-Cohen, Y., & Zacny, K. (Eds.). (2009). *Drilling in Extreme Environments*. Wiley. https://doi.org/10.1002/9783527626625

Barletta, A. (2020). Design and Development of a Robust Chuck Mechanism for the Mars 2020 Coring Drill. *45th Aerospace Mechanisms Symposium*. http://hdl.handle.net/2014/52360

Battery University. (2021). *BU-808: How to Prolong Lithium-based Batteries*. https://batteryuniversity.com/article/bu-808-how-to-prolong-lithium-based-batteries

Bhartia, R., et al. (2021). Perseverance's Scanning Habitable Environments with Raman and Luminescence for Organics and Chemicals (SHERLOC) Investigation. *Space Science Review 217:*58. https://doi.org/10.1007/s11214-021-00812-z

Bickel, B., et al. (2010). Design and Fabrication of Materials with Desired Deformation Behavior. *ACM Transactions on Graphics*, *29*(4), 1–10. https://doi.org/10.1145/1778765.1778800

Bierson, C. J., Tulaczyk, S., Courville, S. W., & Putzig, N. E. (2021). Strong MARSIS Radar Reflections From the Base of Martian South Polar Cap May Be Due to Conductive Ice or Minerals. *Geophysical Research Letters*, *48*(13). https://doi.org/10.1029/2021GL093880

Bramson, A. M., Byrne, S., & Bapst, J. (2017). Preservation of midlatitude ice sheets on mars. *Journal of Geophysical Research: Planets, 122*. https://doi.org/10.1002/2017JE005357

Bramson, A. M. (2018). Radar Analysis and Theoretical Modeling of the Presence and Preservation of Ice on Mars. *University of Arizona.* http://hdl.handle.net/10150/630533

Buhler, P. (2021). Personal Communication.

Buhler, P. B., Ingersoll, A. P., Piqueux, S., Ehlmann, B. L., & Hayne, P. O. (2020). Coevolution of Mars's atmosphere and massive south polar CO_2 ice deposit. *Nature Astronomy, 4*. https://www.nature.com/articles/s41550-019-0976-8

Buhler, P. B., & Piqueux, S. (2021). Obliquity-driven CO2 exchange between Mars' atmosphere, regolith, and polar cap. *Journal of Geophysical Research: Planets, 126*. https://doi.org/10.1029/2020JE006759

Bulat, S. (2015). Results from Subglacial Lake Vostok. *The Royal Society.* https://downloads.royalsociety.org/events/2015/03/subglacial-antarctic-lakes/bulat.mp3

Bulat, S. (2016). Microbiology of the subglacial Lake Vostok: first results of borehole-frozen lake water analysis and prospects for searching for lake inhabitants. *Philosophical Transactions of the Royal Society A, 374*:20140292. http://dx.doi.org/10.1098/rsta.2014.0292

Byrne, S. (2009). The Polar Deposits of Mars. In *Annual Review of Earth and Planetary Sciences* (Vol. 37, pp. 535–560). https://doi.org/10.1146/annurev.earth.031208.100101

Byrne, S., and Ivanov, A. B. (2004). Internal structure of the Martian south polar layered deposits. *Journal of Geophysical Research, 109*. https://doi.org/10.1029/2004JE002267

Calvin, W. (2010). *Planetary Science Decadal Survey Mars Polar Climate Concepts*. https://ia600300.us.archive.org/15/items/MarsPolarClimateConcepts/13_Mars-Polar-Climate-Final.pdf

Campbell, B. A & Morgan, G. A. (2018). Fine-Scale Layering of Mars Polar Deposits and Signatures of Ice Content in Nonpolar Material From Multiband SHARAD Data Processing. *Geophysical Research Letters*. doi:10.1002/2017GL075844

Cappucci, S., Moulton, J., & Hengeveld, D. (2018). Assessment of the Mars Helicopter Thermal Design Sensitivities Using the Veritrek Software. *Thermal & Fluids Analysis Workshop*.

Carsey, F., Mogensen, C., Behar, A., Engelhardt, H., & Lane, A. (2003). Science goals for a Mars polar-cap subsurface mission: Optical approaches for investigations of inclusions in ice. *Annals of Glaciology, 37*, 357-362. doi:10.3189/172756403781816004

Clifford, S. M., et al. (2000). The State and Future of Mars Polar Science and Exploration. *Icarus*, *144*(2), 210–242. https://doi.org/10.1006/icar.1999.6290

Clifford, S. M., et al. (2013). Introduction to the fifth Mars Polar Science special issue: Key questions, needed observations, and recommended investigations. In *Icarus* (Vol. 225, Issue 2, pp. 864–868). https://doi.org/10.1016/j.icarus.2013.04.005

COSPAR. (2002). COSPAR Planetary Protection Policy. NASA. https://science.nasa.gov/science-red/s3fs-public/atoms/files/COSPAR_Planetary_Protection_Policy_v3-24-11.pdf

Cuffey, K. M., Paterson, W. S. B. (2006). *The Physics of Glaciers*. 4th ed. Elsevier.

Darcy, E. & Scharf, S. (2015). "Safe, High Performing Li-ion Battery Designs: Summary of 2015 Findings." https://www.nasa.gov/sites/default/files/atoms/files/darcy_-_nasa_batt_workshop_2015.pdf

Davis, J. (2018). *PDD Completes Second Field Test*. The Planetary Society. https://www.planetary.org/articles/pdd-completes-second-field-test

Dreyer, C. (2021). Personal Communication.

Eshelman, E. J., et al. (2019). WATSON: In Situ Organic Detection in Subsurface Ice Using Deep-UV Fluorescence Spectroscopy. *Astrobiology*, *19*(6), 771–784. https://doi.org/10.1089/ast.2018.1925

Farley, K. A., et al. (2020). Mars 2020 Mission Overview. In *Space Science Reviews* (Vol. 216, Issue 8). Springer Science and Business Media B.V. https://doi.org/10.1007/s11214-020-00762-y

Faulhaber.com. (n.d. a). Brushless DC-Servomotors, Series 4490 BS. https://www.faulhaber.com/en/products/series/4490bs/

Faulhaber.com. (n.d. b). Planetary Gearheads, Series 44/1. https://www.faulhaber.com/en/products/series/441/

Fusaro, R.L. (1999). *Space Mechanisms Handbook*. NASA Glenn Research Center.

Garcia, I. (2013). *Sneakers with Filaflex*. http://web.archive.org/web/20131203233344/http://recreus.com/?p=1

Garcia, I. (2014). *Recreus sneakers II*. https://www.thingiverse.com/thing:285404

Goesmann, Fred, et. al. 2017. "Mars Organic Molecule Analyzer (MOMA) Instrument." *Astrobiology 17,* 6-7. https://doi.org/10.1089/ast.2016.1551

Great, D. (n.d.). *Boston Dynamics Spot*. Sketchfab.Com. Retrieved October 29, 2021, from https://skfb.ly/ooLTs

Head, J. W., & Pratt, S. (2001). Extensive Hesperian-aged south polar ice sheet on Mars: Evidence for massive melting and retreat, and lateral flow and ponding of meltwater. *Journal of Geophysical Research E: Planets*, *106*(6), 12229–12275. https://doi.org/10.1029/2000je001359

Hermann, S. (2018). *Infill Pattern and Shells - How to get the Maximum Strength out of your 3D Prints*. https://www.youtube.com/watch?v=AmEaNAwFSfI

Hodgson, G. (Ed.). (2012). *A History of RepRap Development*. https://reprap.org/mediawiki/images/a/a5/A_History_of_RepRap_Development.pdf

Hoffman, J. H., Chaney, R. C., Hammack, H. (2008). Phoenix Mars Mission: The Thermal Evolved Gas Analyzer. *Journal of the American Society for Mass Spectrometry, 19:*10. https://doi.org/10.1016/j.jasms.2008.07.015

Howell, S. et al. (2020). Diving into Ocean Worlds. *ECO Magazine, May/June 2020. http://digital.ecomagazine.com/publication/?m=9890&i=659148&view=articleBrowser&article_id=3667761*

Humbert, A., Steinhage, D., Helm, V., Beyer, S., & Kleiner, T. (2018). Missing evidence of widespread subglacial lakes at Recovery Glacier, Antarctica. *Journal of Geophysical Research: Earth Surface, 123.* https://doi.org/10.1029/2017JF004591

Ion, A., Frohnhofen, J., Wall, L., Kovacs, R., Alistar, M., Lindsay, J., Lopes, P., Chen, H. T., & Baudisch, P. (2016). Metamaterial mechanisms. *UIST 2016 - Proceedings of the 29th Annual Symposium on User Interface Software and Technology*, 529–539. https://doi.org/10.1145/2984511.2984540

Jadhav, S. (2017). Redundant Brushless Drive System. *Innovative Small Drives and Micro-Motor Systems, 11th GMM/ETG-Symposium.* https://ieeexplore.ieee.org/document/8241185

Jet Propulsion Laboratory. (2021). *NASA InSight's 'Mole' Ends Its Journey on Mars*. https://www.jpl.nasa.gov/news/nasa-insights-mole-ends-its-journey-on-mars

Joshi, D.R., Eustes, A. W., Rostami, J., & Dreyer, C. (2021). Evaluating Data-Driven Techniques to Optimize Drilling on the Moon. *SPE/IADC International Drilling Conference and Exhibition*. https://doi.org/10.2118/204108-MS

Kaplan, Matt, et. al. (2018). "Diving into that Lake on Mars." https://www.planetary.org/planetary-radio/0801-2018-garvin-mckay-mars-lake

Kerr, J. (2016). *Print-in-Place Iris Box (remix)*. Thingiverse. https://www.thingiverse.com/thing:1817180

Khuller, A. R., & Plaut, J. J. (2021). Characteristics of the Basal Interface of the Martian South Polar Layered Deposits. *Geophysical Research Letters*, *48*(13). https://doi.org/10.1029/2021GL093631

Kowalski, J. et al. (2016). Navigation technology for exploration of glacier ice with maneuverable melting probes. *Cold Regions Science and Technology, 123*. https://doi.org/10.1016/j.coldregions.2015.11.006.

Lakdawalla, E. (2018). *The Design and Engineering of Curiosity.* Springer Praxis.

Lalich, D. E., Hayes, A. G., & Poggiali, V. (2021). Explaining Bright Radar Reflections in the Martian SPLD without Liquid Water. *LPSC 2021*. https://www.hou.usra.edu/meetings/lpsc2021/pdf/2392.pdf

Lalish, E. (2013). *Gear Bearing*. Thingiverse. https://www.thingiverse.com/thing:53451

Lalish, E. (2016). *Preassembled Iris Box*. Thingiverse. https://www.thingiverse.com/thing:1811143

Langevin, Y., et al. (2005). Summer Evolution of the North Polar Cap of Mars as Observed by OMEGA/Mars Express. *Science 307*(5715). doi:10.1126/science.1109438

Lauro, S. E., et al. (2021). Multiple subglacial water bodies below the south pole of Mars unveiled by new MARSIS data. *Nature Astronomy*, *5*(1), 63–70. https://doi.org/10.1038/s41550-020-1200-6

Lauro, S. E., et al. (2019). Liquid water detection under the South Polar Layered Deposits of Mars-A probabilistic inversion approach. *Remote Sensing*, *11*(20). https://doi.org/10.3390/rs11202445

Li, J., Andrews-Hanna, J. C., Sun, Y., Phillips, R. J., Plaut, J. J., & Zuber, M. T. (2012). Density variations within the south polar layered deposits of Mars. *Journal of Geophysical Research E: Planets*, *117*(4). https://doi.org/10.1029/2011JE003937

Lockheed Martin. (n.d.). *Returning to the Red Planet*. Retrieved August 24, 2021, from https://www.lockheedmartin.com/en-us/news/features/2018/returning-to-mars.html

Longhi, J. (2006). Phase equilibrium in the system CO2-H2O: Application to Mars. *Geophysical Research, 111.* doi:10.1029/2005JE002552

Lukin, V. V., Vasiliev, N. I. (2014). Technological aspects of the final phase of drilling borehole 5G and unsealing Vostok Subglacial Lake. *Annals of Glaciology, 55*(65). doi:10.3189/2014AoG65A002

Magnani, P.G. et al. (2004). Deep Drill (DeeDri) for Mars Application. *Planetary and Space Science, 52*. doi:10.1016/j.pss.2003.08.023

Malaska, M. J., et al. (2020). Subsurface in Situ Detection of Microbes and Diverse Organic Matter Hotspots in the Greenland Ice Sheet. *Astrobiology*, *20*(10), 1185–1211. https://doi.org/10.1089/ast.2020.2241

Malaska, M. J. (2021). Personal Communication.

Manning, C. V., Bierson, C., Putzig, N. E., & McKay, C. P. (2019). The formation and stability of buried polar CO2 deposits on Mars. *Icarus*, *317*, 509-517. https://doi.org/10.1016/j.icarus.2018.07.021

Mason, D. P., & Elwood Madden, M. E. (2021). Raman spectroscopy of high salinity brines and ices. *Icarus, 372.* https://doi.org/10.1016/j.icarus.2021.114759.

Matthews, H. (2005). *Line Shaft Pulleys and Belting: Power Transmission by Belt*. Harry's Old Engine. https://www.old-engine.com/belts2.htm

Maurice, S., et al. (2021). The SuperCam Instrument Suite on the Mars 2020 Rover: Science Objectives and Mast-Unit Description. In *Space Science Reviews, 217*(3). Springer. https://doi.org/10.1007/s11214-021-00807-w

Mellon, M. T. (2021). Personal Communication.

McHale, J. (2011). Radiation-hardened electronics designers face increasing difficulty with shrinking chip geometries. *Military and Aerospace Electronics. https://www.militaryaerospace.com/computers/article/16717354/radiationhardened-electronics-designers-face-increasing-difficulty-with-shrinking-chip-geometries*

McKay, C. P., & Stoker, C. R. (1989). The early environment and its evolution on Mars: Implication for life. *Reviews of Geophysics*, *27*(2), 189. https://doi.org/10.1029/RG027i002p00189

Milanowski, M. (2021). Curiosity found a new organic molecule on Mars. *Popular Science.* https://www.popsci.com/science/curiosity-new-organic-molecules-mars/

Millan, M., et al. (2021). Organic molecules revealed in Mars's Bagnold Dunes by Curiosity's derivatization experiment. *Nature Astronomy*. doi:10.1038/s41550-021-01507-9

Moeller, R. C., et al. (2021). The Sampling and Caching Subsystem (SCS) for the Scientific Exploration of Jezero Crater by the Mars 2020 Perseverance Rover. In *Space Science Reviews, 217*(1). Springer. https://doi.org/10.1007/s11214-020-00783-7

Molaro, et al. (2018). The microstructural evolution of water ice in the solar system through sintering. *Geophysical Research: Planets*. doi:10.1029/2018JE005773

Morley, Q. (2019). *ARD3 Drive System*. Thingiverse. https://www.thingiverse.com/thing:3610134

Morley, Q. (2021). *Spherical Iris Core Catcher*. Thingiverse. https://www.thingiverse.com/thing:4864404

Mowlem, M., et al. (2016). Probe technologies for clean sampling and measurement of subglacial lakes. *Philosophical Transactions of the Royal Society A, 374*(20150267). http://dx.doi.org/10.1098/rsta.2015.0267

Mowlem, M. (2021). Personal Communication.

Morrison, C. (2021). Personal Communication.

NASA. (2008). *Spirit Digs a Trench*. https://www.nasa.gov/multimedia/imagegallery/image_feature_133.html

NASA Mars Exploration Rovers. (n.d.). *Instruments*. https://mars.nasa.gov/mer/mission/instruments/

NASA Mars 2020 Mission. (n.d. a). *MOXIE*. https://mars.nasa.gov/mars2020/spacecraft/instruments/moxie/

NASA Mars 2020 Mission. (n.d. b). *SuperCam for Scientists*. https://mars.nasa.gov/mars2020/spacecraft/instruments/supercam/for-scientists/

NASA Mars 2020 Mission. (n.d. c). *RIMFAX for Scientists.* https://mars.nasa.gov/mars2020/spacecraft/instruments/rimfax/for-scientists/

NASA SMD (2020). *Playing Lacrosse on Titan.* https://science.nasa.gov/technology/technology-highlights/playing-lacrosse-on-titan

National Academies. (2003). *Assessment of Mars Science and Mission Priorities*. National Academies Press. https://doi.org/10.17226/10715

Nerozzi, S., Ortiz, M. R., Holt, J. W. (2021). The north polar basal unit of Mars: An Amazonian record of surface processes and climate events. *Icarus, 373*. https://doi.org/10.1016/j.icarus.2021.114716

Novak, K. S., Kempenaar, J. G., Redmond, M., Daimaru, T., & Lee, C.-J. (2019). *Thermal Design of the Sample Handling Assembly in the Sampling and Caching Subsystem on the Mars 2020 Rover*. https://hdl.handle.net/2346/84712

Orosei, R., et al. (2018a). Radar evidence of subglacial liquid water on Mars. *Science*, *361*(6401). https://doi.org/10.1126/science.aar7268

Orosei, R., et al. (2018b). Radar evidence of subglacial liquid water on Mars (Supplement). *Science*, *361*(6401), 490–493. https://www.sciencemag.org/lookup/doi/10.1126/science.aar7268

Orosei, R., et al. (2018c). Radar evidence of subglacial liquid water on Mars (eLetters & responses). *Science*, *361*(6401), 490–493. https://www.sciencemag.org/lookup/doi/10.1126/science.aar7268

Orosei, R., & Mitri, G. (2021). Personal Communication.

Paulsen, G. et al., (2013). Wireline Deep Drill for the Exploration of Icy Bodies. *LPSC 2013, 1333*.

Plaut, J. J. et al. (2007). Subsurface Radar Sounding of the South Polar Layered Deposits of Mars. *Science 216*(5821). https://doi.org/10.1126/science.1139672

Phillips, R. J., et al. (2011). Massive CO2 ice deposits sequestered in the south polar layered deposits of Mars. *Science*, *332*(6031). https://doi.org/10.1126/science.1203091

Piqueux, S., Byrne, S., Richardson, M. I. (2003). Sublimation of Mars's southern seasonal CO_2 ice cap and the formation of spiders. *Geophysical Research, 108*(8). doi:10.1029/2002JE002007

Putzig, N. E. & Mellon, M. T. (2007). Apparent thermal inertia and the surface heterogeneity of Mars. *Icarus 191*. https://doi.org/10.1016/j.icarus.2007.05.013

Putzig, N. E., et al. (2011). SHARAD observations of recent geologic features on Mars. *ESPC-DPS 2011*. https://ui.adsabs.harvard.edu/abs/2011epsc.conf.1591P/abstract

Putzig, N. E. (2021). Personal Communication.

Quinn, R. et al. (2013). Perchlorate Radiolysis on Mars and the Origin of Martian Soil Reactivity. *Astrobiology 13*(6). doi:10.1089/ast.2013.0999

Rodriguez, E. (2021). Personal Communication.

Rutishauser, A. et al. (2018). Discovery of a hypersaline subglacial lake complex beneath Devon Ice Cap, Canadian Arctic. *Science Advances, 4*(4). doi:10.1126/sciadv.aar4353

Sanladerer, T., & Hermann, S. (2019). Silent Stepper Drivers & Topology Optimization. In *The Meltzone Podcast (46.49-56.59)*. https://www.youtube.com/watch?v=3oJBmRfcD8U

Scanlon, K. E., Head, J. W., Fastook, J. L. & Wordsworth, R. D. (2017). The Dorsa Argentea Formation and the Noachian-Hesperian climate transition. *Icarus, 299*. http://dx.doi.org/10.1016/j.icarus.2017.07.031

Schaler, E. W. (2021). Personal Communication.

Schaler, E. W. (2021). *SWIM -- Sensing with Independent Micro-swimmers*. NASA STMD. https://www.nasa.gov/directorates/spacetech/niac/2021_Phase_I/SWIM/

Schmidt, B., et al. (2021). Dive, Dive, Dive: Accessing the Subsurface of Ocean Worlds. *Bulletin of the AAS, 53*(4). https://doi.org/10.3847/25c2cfeb.ffef076e

Schumacher, C., et al. (2015). Microstructures to control elasticity in 3D printing. *ACM Transactions on Graphics*, *34*(4). https://doi.org/10.1145/2766926

Schwamb, M. E., et al. (2018). Planet Four: Terrains - Discovery of araneiforms outside of the South Polar layered deposits. *Icarus, 308.* https://doi.org/10.1016/j.icarus.2017.06.017

Sharpe, R. D., & Cork, G. G. (1995). Geology and Mining of the Miocene Fish Creek Gypsum in Imperial County, California. In M. Tabilio & D. L. Dupras (Eds.), *29th Forum on the Geology of Industrial Minerals: Proceedings. Special Publication 110* (pp. 169–180). California Department of Conservation, Division of Mines and Geology. https://ia800309.us.archive.org/34/items/29thforumongeolo110foru/29thforumongeolo110foru.pdf

Skelley, A. M. et al. (2007). Organic amine biomarker detection in the Yungay region of the Atacama Desert with the Urey instrument. *Geophysical Research: Biogeosciences, 112*:G4

Sleater, R. (n.d.). *NASA BRAILLE: Biologic and Resource Analog Investigations in Low Light Environments*. Retrieved October 30, 2021, from https://nasa-braille.org/caves-creatures-the-cosmos/

Smith, H. D., & McKay, C. P. (2005). Drilling in ancient permafrost on Mars for evidence of a second genesis of life. *Planetary and Space Science*, *53*(12), 1302–1308. https://doi.org/10.1016/j.pss.2005.07.006

Smith, I. B. (2017). Where Ice Flows on Mars; Where Ice Does not Seem to Flow; Why the Difference? *LSPC 2017*, *2489.* https://www.hou.usra.edu/meetings/lpsc2017/pdf/2489.pdf

Smith, I. B., et al. (2020). The Holy Grail: A road map for unlocking the climate record stored within Mars' polar layered deposits. *Planetary and Space Science, 184*. https://doi.org/10.1016/j.pss.2020.104841

Smith, I. B., et al. (2021a). A Solid Interpretation of Bright Radar Reflectors Under the Mars South Polar Ice. *Geophysical Research Letters*, *48*(15). https://doi.org/10.1029/2021gl093618

Smith, I. B., et al. (2021b). A Solid Interpretation of Bright Radar Reflectors Under the Mars South Polar Ice - Supporting Information. *Geophysical Research Letters*, *48*(15). https://doi.org/10.1029/2021GL093618

Smith, P. H. (2005). The Phoenix mission to Mars. *2004 IEEE Aerospace Conference Proceedings (IEEE Cat. No. 04TH8720)*, 337–342. https://doi.org/10.1109/AERO.2004.1367617

Sori, M. M., Byrne, S., Hamilton, C. W., & Landis, M. E. (2016). Viscous flow rates of icy topography on the north polar layered deposits of Mars. *Geophysical Research Letters.* doi:10.1002/2015GL067298

Sori, M. M., & Bramson, A. M. (2019). Water on Mars, With a Grain of Salt: Local Heat Anomalies Are Required for Basal Melting of Ice at the South Pole Today. *Geophysical Research Letters*, *46*(3), 1222–1231. https://doi.org/10.1029/2018GL080985

Stone W. et al. (2018) Project VALKYRIE: Laser-Powered Cryobots and Other Methods for Penetrating Deep Ice on Ocean Worlds. In: Badescu V., Zacny K. (eds) *Outer Solar System*. Springer. https://doi.org/10.1007/978-3-319-73845-1_4

Talalay, P.G. (2014). Drill heads of the deep ice electromechanical drills. In *Cold Regions Science and Technology* (Vol. 97, pp. 41–56). https://doi.org/10.1016/j.coldregions.2013.09.009

Talalay, P.G. (2016). *Mechanical Ice Drilling Technology*. Singapore: Springer Geophysics.

The Planetary Society. (n.d.). *Cost of Perseverance*. Retrieved August 17, 2021, from https://www.planetary.org/space-policy/cost-of-perseverance

The Planetary Society. (2016). *Planetary Deep Drill.* Retrieved from https://www.planetary.org/explore/projects/planetary-deep-drill/about-planetary-deep-drill.html

Ueda, H., & Kalafut, J. (1989). Experiments on the cutting process in ice. *CRREL Report*, *1989*(5). http://hdl.handle.net/11681/9067

Vasavada, A. R., et al. (2000). Surface properties of Mars' polar layered deposits and polar landing sites. *Journal of Geophysical Research: Planets*, *105*(3). https://doi.org/10.1029/1999JE001108

Voitkovskii, K.F. (1960). *Mechanical Properties of Ice.* Armed Services Technical Information Agency. http://dtic.mil/dtic/tr/fulltext/u2/284777.pdf

Walker, W.Q., et. al. (2017). *Statistical Characterization of 18650-format Lithium-Ion Cell Thermal Runaway Energy Distributions*. NASA Johnson Space Center.

Whitten, J. L., & Campbell, B. A. (2018). Lateral Continuity of Layering in the Mars South Polar Layered Deposits From SHARAD Sounding Data. *Journal of Geophysical Research: Planets*, *123*(6), 1541–1554. https://doi.org/10.1029/2018JE005578

Whitten, J. L., Campbell, B. A., & Plaut, J. J. (2020). The Ice Content of the Dorsa Argentea Formation From Radar Sounder Data. *Geophysical Research Letters*, *47*(23). https://doi.org/10.1029/2020GL090705

Zacny, K. (2018a). *Drilling: How do we access subsurface on Mars.* https://www.kiss.caltech.edu/workshops/marsX/presentations/Zacny.pdf

Zacny, K. (2021). Personal Communication.

Zacny, K., Bartlett, P., Davis, K., Glaser, D., and Gorevan, S. (2006) Test Results of Core Drilling in Simulated Ice-Bound Lunar Regolith for the Subsurface Access System of the Construction and Resource Utilization eXplorer (CRUX) Project. *Earth & Space 2006: Engineering, Construction, and Operations in Challenging Environments*. https://doi.org/10.1061/40830(188)64

Zacny, K., & Cooper, G. (2007). Methods for cuttings removal from holes drilled on Mars. *Mars 3*, 42-56. doi:10.1555/mars.2007.0004

Zacny, K., et al. (2019a). Application of Pneumatics in Delivering Samples to Instruments on Planetary Missions. *2019 IEEE Aerospace Conference*. https://doi.org/10.1109/AERO.2019.8741887

Zacny, K., et al. (2019b). Reaching Europa's Ocean with Nuclear-Powered Thermo-Mechanical Drill. *LPSC 2019*, 2048. https://www.hou.usra.edu/meetings/lpsc2019/pdf/2048.pdf

Zacny, K., et al. (2016). Development of a Planetary Deep Drill. *Earth and Space 2016*, 256–266. https://doi.org/10.1061/9780784479971.027

Zacny, K., et al. (2020). Drill for Acquisition of Complex Organics (DrACO) for Dragonfly – A New Frontiers Mission to Explore Titan. *LPSC 2020*, 1763.

Zacny, K., et al. (2018b). SLUSH: Europa hybrid deep drill. *2018 IEEE Aerospace Conference*. doi:10.1109/AERO.2018.8396596

Zacny, K., et al. (2013). Wireline Deep Drill for Exploration of Mars, Europa, and Enceladus. *Proceedings, IEEE Aerospace Conference*. doi:10.1109/AERO.2013.6497189

Zacny, K., Paulsen, G., & Szczesiak, M. (2011). Challenges and Methods of Drilling on the Moon and Mars. 2011 Aerospace Conference. doi:10.1109/AERO.2011.5747261

Zimmerman, W., et al. (2002) The Mars '07 North Polar Cap deep penetration cryo-scout mission. *Proceedings, IEEE Aerospace Conference.* doi:10.1109/AERO.2002.1036850

Zuber, M. (2007). Density of Mars' South Polar Layered Deposits. *Science 317*:5845. doi:10.1126/science.1146995

Appendix A – Power Model Equations

Term	Units	Symbol
General Symbols		
Temperature	K, °C	T
Voltage	V	V
Current	A	I
Power	W	P
Energy	kJ, Wh	E
Potential or stored energy	kJ, Wh	PE
Time	s, min, h	t
Speed	m/s	v
Diameter	m, mm	D
Length	m, mm	L
Mass	kg	m
Rotational speed	rpm	ω
Gravitational constant	m/s^2	g
Depth	m	H
Number of two-way trips	--	N_{trips}
Change in depth	m	ΔH
time duration of single trip	s, min, h	t_{trip}
time duration of science gathering actions outside of normal traveling and drilling actions	s, min, h	$t_{science}$
Electrical Symbols		
State of charge	%	SoC
Depth of discharge	%	DoD
Minimum state of charge	%	SoC_{min}
Maximum charge level	%	SoC_{max}
Charge cycles	--	CC
Number of strings	--	$N_{strings}$
Number of cells per string	--	N_{cells}
Battery string voltage	V	V_{string}
Battery string capacity	Wh	E_{string}
Power draw of drive train (nominal speed)	W	P_{drive}
Single battery voltage	V	V_{cell}
Single battery cell capacity	Wh	E_{cell}
Total battery capacity	Wh	E_{total}
Useable battery capacity	kJ	$E_{useable}$
Hotel loads (estimated)	W	P_{hotel}
Drive loads (estimated)	W	P_{drive}
Drilling motor load (estimated)	W	P_{drill}
Energy required for hotel loads (single trip)	kJ	E_{hotel}

Energy required for the drive (single trip)	kJ	E_{drive}
Energy required for the drill motor (single trip)	kJ	E_{drill}
Energy required for a single trip	kJ	E_{trip}
Efficiency of the drive motor	%	η_{drive}
Mechanical Symbols		
Bot outer diameter	mm	D_b
Bot body length	m	L_b
Core length	m	L_c
Bore travel speed	m/s	v_{drive}
Number of bots	--	N_{bots}
Energy consumed for a round trip	kJ	E_{rt}
Change in potential energy from top to bottom of hole	kJ	E_{down}
Change in potential energy from bottom to top of hole	kJ	E_{up}
Bot mass	kg	m_b
Core mass	kg	m_c
Total efficiency of the drive	%	η_{drive}
Efficiency of the drive treads	%	η_{tread}
Efficiency of the drive motor gearing	%	η_{gear}
Model Symbols		
Core drilling time	s	t_{drill}
Core drilling energy	kJ	$E_{coredrill}$

Term	**Symbol**
Particular two-way trip	k
Particular electrical load	i
Particular charge cycle	c

Battery Capacity and State of Charge (SOC)

Useable energy in the batteries is reduced to less than 100% to increase the cycle life and decrease the risk of catastrophic failures.

$$E_{string} = E_{cell} \cdot N_{cells}$$

$$E_{total} = E_{string} \cdot N_{strings} = E_{cell} \cdot N_{cells} \cdot N_{strings}$$

$$E_{useable} = E_{total}(SOC_{max} - SOC_{min})$$

The current battery state of charge is given generically as the fraction of total energy (fully charged) remaining in the battery.

$$SOC = \frac{(E_{total} - E_{drained})}{E_{total}}$$

Starting from SOC_{max}:

$$SOC = SOC_{max} - \frac{E_{drained}}{E_{total}}$$

Remaining capacity before SOC_{min}:

$$E_{remaining} = E_{total}(SOC - SOC_{min}) = E_{useable} - E_{drained}$$

As the battery is cycled (Discharged and Charged), the capacity decays gradually. The rate of this decay is dependent on several factors, the biggest of which tend to be temperature and the maximum and minimum SOC during the cycle. The graph below shows a typical Lithium battery capacity response as a function of recharge cycles. The different slopes are a result of changing the high and low ends of the cycle (in % full charge).

The initial capacity is less than 100% because the testing lab found most batteries underperforming their rated specification even when new.

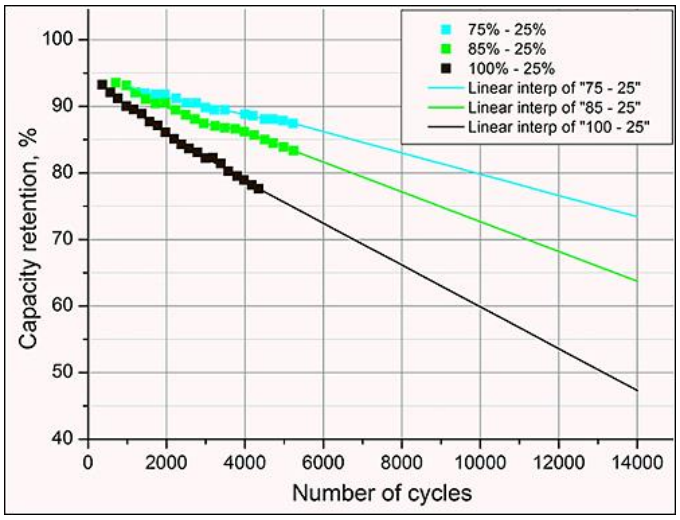

Figure A1: Figure 5 from Battery University, (2021).

The linear interpolation equation for 85%-25% follows:

$$Capacity\ in\ percent = m(N_{cycles}) + b$$

Cycle Limits	Slope	Intercept	80% Capacity Point
85%-25%	-.002%	93.5%	7000 cycles
100%-25%	-.0036%	93.2%	3800 cycles

Incorporating this capacity degradation in the equation for useable capacity provides us equations for useable capacity at a specific number of charge cycles. The intercept (b) is replaced with 1 in this case, because unlike the nominal battery capacity, we can use 100% of the initial useable capacity since it is calculated from the

$$E_{total(degrade)} = E_{total\ rated}(m(N_{cycles}) + b)$$

$$E_{useable(c)} = E_{total(degrade)}(SOC_{max} - SOC_{min})$$

$$E_{useable(c)} = E_{useable}(m(N_{cycles}) + b)$$

Early in the drilling, the minimum SOC may not have been reached after a single trip. If two full trips could be made prior to recharging the borebot, it may be desirable to do this to reduce the number of recharge cycles on the cells. However, the number of drilling trips that meet this criteria is likely to be small enough that the increased risk of reduced power availability early in the mission likely overwhelms any added benefit.

Achievable depth as a function of charge cycles and number of borebots follows. The two equations represent the decisions discussed above. If there is sufficient battery capacity for more than one trip, then the number of recharge cycles can be reduced early in the mission as shown in the upper equation. However, if it is desired to recharge after every cycle, the maximum depth achievable becomes simpler to estimate.

$$H = \begin{cases} \Delta H \cdot N_{bots} \cdot \sum_{c=1}^{N_{cycles}} E_{useable} \,/\, E_{trip} & recharge\ when\ necessary \\ \Delta H \cdot N_{bots} \cdot N_{cycles} & recharge\ every\ trip \end{cases}$$

Because the useable battery capacity is assumed to change linearly, the upper of the two equations can be solved piece-wise by finding the point at which two trips can no longer be made with the existing capacity on that trip.

Note: All this discussion assumes the electric loads are such that no more than two trips could be possible before a recharge. If somehow that two trips becomes three or more, the solution to the above equations would be found in a similar way.

$$2 \cdot E_{trip} = E_{useable} \cdot \left(m\left(N_{2-trip\ cycles}\right) + b\right)$$

$$N_{2-trip\ cycles} = \frac{2 \cdot \frac{E_{trip}}{E_{useable}} - b}{m}$$

Once this cycle count is known, the summation can be performed as follows:

$$\sum_{c=1}^{N_{cycles}} E_{useable} \,/\, E_{trip} = 2 \cdot N_{2-trip\ cycles} + \left(N_{cycles} - N_{2-trip\ cycles}\right)$$

If instead, we have a target depth and discover irregular battery performance, or varying electrical loads, we can determine the expected number of charge cycles necessary to achieve that target depth.

$$N_{trips} = \frac{H}{\Delta H}$$

Trip Duration

For simplicity, the time required to drill the core is assumed constant. During the first several meters of drilling though, the time required to drill dominates the total trip duration. Later in the drilling, the drive time dominates. The depth at which this switch occurs is dependent primarily on vehicle travel speed. The depth components in the following equations represent the down and return trip plus the additional depth drilled on this run.

$$t_{trip(k)} = t_{drill(k)} + \frac{2H + \Delta H_{(k)}}{v_{drive}}$$

$$t_{trip(k)} \approx t_{drill(k)} \quad Early\ in\ mission$$

$$t_{trip(k)} \approx t_{drill(k)} + \frac{2H}{v_{drive}} \quad Later\ in\ mission$$

Drive Energy Requirements

The following are the potential energy changes solely from travel down, and then back up from the bottom of the hole.

$$E_{down} = m_b g H$$

$$E_{up} = (m_b + m_c) g (H + \Delta H)$$

$$E_g = E_{up} + E_{down}$$

E_g is the amount of energy required to raise and lower the bot in the hole solely due to gravitational forces. Neglecting friction and other losses, this is the least amount of energy required to do this task and was used as a starting point for estimating battery loads until more information is gathered on actual drive performance. Actual energy used by the drive system must be greater and is shown below.

$$E_{drive} \geq E_g$$

$$E_{drive} = E_g * \frac{1}{\eta_{drive}}$$

$$E_{drive} = \frac{1}{\eta_{drive}} [(m_b + m_c) g (H + \Delta H) + m_b g H]$$

This is rearranged to make it easier to solve using a given depth.

$$E_{drive} = \frac{g}{\eta_{drive}} [H(2m_b + m_c) + \Delta H(m_b + m_c)]$$

Efficiency of the drive is made up of several components; e.g., battery chemical, motor speed control, electric motor, motor gearing, and drive mechanical component efficiencies.

Friction is expected to be nearly constant and very low due to the hard substrate and smooth borebot body. If frictional losses are to be accounted for, they can be added as follows as a constant force over the distance of travel down and back up again:

$$E_{drive} = \frac{g}{\eta_{drive}} [H(2m_b + m_c) + \Delta H(m_b + m_c)] + 2H \cdot F_{frict}$$

Primary Electrical Loads

Hotel, drive system, and drilling motor loads are assumed to be the largest drains on the power system for battery demand modeling.

$$E_{trip} = E_{drill} + E_{drive} + E_{hotel}$$

Total hotel loading may vary throughout the trip depending on what instruments and equipment is running at the time. The total energy used by these loads depends on their individual run times during a given trip.

$$E_{hotel(i)} = t_{hotel(i)} \cdot P_{hotel(i)}$$

The maximum time the hotel loads are active is just the maximum trip duration. Time spent out of the hole being manipulated on the lander is ignored for this analysis. The most effective way to reduce hotel loads aside from disabling them or using low-power modes is to decrease the driving duration by increasing drive speed.

$$t_{hotel_{max}} = t_{trip} = \frac{2H + \Delta H}{v_{drive}} + t_{drill}$$

$$E_{hotel} = \sum_{i=1}^{N} E_{hotel(i)}$$

Drilling energy load is a big unknown, but thanks to excellent research from Honeybee Robotics and other teams we have several experimental data sets to build order of magnitude estimates from (Magnani, 2004; Zacny et al., 2006). In gas concrete, with a 38 mm drill at 130 rpm, a 150 mm core required 45 kJ to complete (Magnani, 2004).

$$E_{drill} = t_{drill} \cdot P_{drill}$$

Appendix B – Power Model Script

```
   'Excel VBA script. Note: .xlsm files should be available from the github link at https://borebots.fyi/

Function CurrentCapacity(nomCapacity, m, b, cycles)
   'Returns the linear interpolation of capacity decay as a function of recharge cycles
   'Could be used for any linear slope adjustment.  m and b are % values

   CurrentCapacity = nomCapacity * (m * cycles + b)

End Function

Function UseableCapacity(currCap, maxSOC, minSOC)

   'Takes a Known current battery storage capacity and returns the limited
   'useable capacity based on the max and minimum state of charge allowed by
   'desired operating procedure.  max and min SOC must be fractional (0.0-1.0)

   If maxSOC < minSOC Then
      UseableCapacity = currCap 'Error Checking'
   Else
      UseableCapacity = currCap * (maxSOC - minSOC)
   End If

End Function

Function remainingCapacity(currCap, currSOC, minSOC)

   'Takes a known current capacity and based on the minimum SOC allowed,
   'returns the remaining capacity in mAh
   ' Allowed to return a negative.

   remainingCapacity = currCap * (currSOC - minSOC)

End Function

Function maxDepthbyCycles1(dH, maxCycles, bots)

   'Takes the change in depth (core length est.) each drill trip
   'maximum recharge cycles of the batteries and number of bore bots
   'Returns the maximum depth achievable assuming recharge after every drill trip.
   'Assumes inputs remain constant through the mission also.

   maxDepthbyCycles1 = dH * bots * maxCycles

End Function
```

```
Function maxDepthbyCycles2(dH, maxCycles, bots, Euseable, Etrip)

   'Takes the change in depth (core length est.) each drill trip, maximum recharge cycles of the batteries
   'and number of bore bots. Version 2 of this function takes the estimated electrical loads and nominal
   'battery capacity into account also. Returns the maximum depth achievable assuming recharge only
   'when necessary. Assumes inputs and battery capacity remain constant through the mission.

   Dim tripsPerCharge As Integer
      tripsPerCharge = (Euseable \ Etrip) 'backslash is the DIV operator. Used here to divide and always
   round down'
   If tripsPerCharge > 3 Then 'Just basic realism here, the batteries won't be magic'
      tripsPerCharge = 3
   End If

   maxDepthbyCycles2 = dH * bots * maxCycles * tripsPerCharge

End Function

Function maxDepthbyCycles3(dH, maxCycles As Integer, bots As Integer, Euseable, Etrip, m, b)

   'Like the other versions, but this accounts for the change in capacity over time.
   'This still only uses a constant trip energy use, so it has no limit unless Etrip is changed

   Nfail = (Etrip / Euseable - b) / m 'Point at which no trips can be made due to loss of capacity'
   If Nfail > maxCycles Then 'clip the number of cycles as limited by battery capacity if applicable'
      Nfail = maxCycles
   ElseIf Nfail < 0 Then 'No trips can be made with the existing load and batteries'
      Nfail = 0
   End If

   Nswitch = (2 * Etrip / Euseable - b) / m 'Point beyond which only one trip can be made before a
   recharge is required'
   Dim NswitchInt As Integer
   NswitchInt = Nswitch 'Round off the decimal from Nswitch'
   If NswitchInt > Nfail Then 'If the switch-over point is past the number of cycles, just set it to maxCycles'
      NswitchInt = Nfail
   ElseIf NswitchInt < 0 Then 'This happens if there are no 2-trip cycles possible'
      NswitchInt = 0
   End If

   Dim Nremain As Integer
   Nremain = Nfail - NswitchInt 'Number of charge cycles that yield only 1 trip'

   maxDepthbyCycles3 = dH * bots * (2 * NswitchInt + Nremain)

End Function
```

```
Function minCyclesForDepth3(dH, depth, bots As Integer, Euseable, Etrip, m, b) As Integer

   'This is working backwards from maxDepthByCycles3.  Finds the minimum cycle life required
   'To achieve a given depth. ****Returns a PER-BOT number of cycles.***

   'Both Ndouble and Nsingle are in units of Charge Cycles. [Cycles = trips for Nsingle] and [2*Cycles = trips for Ndouble]'
   Ndouble = tripCutoffCycles(Euseable, Etrip, m, b, 2) 'Point beyond which only one trip can be made before a recharge is required'
   Nsingle = tripCutoffCycles(Euseable, Etrip, m, b, 1) 'Point beyond which no trips can be made due to battery degradation'
   'MsgBox Ndouble
   Dim failure As Boolean
   failure = False

   If Nsingle = 0 Then
      failure = True 'Error, cannot make a single trip due to loads'
      MsgBox "minCyclesForDepth3 Nsingle=0"
   End If

   requiredTrips = depth / dH / bots 'Trips for each bot given the desired depth and core length'

   possibleDoubleTrips = 2 * Ndouble 'Number of trips possible with the double trip cycles'
   possibleSingleTrips = (Nsingle - Ndouble) 'Number of trips with single trip cycles (singles overlap the doubles)'
   possibleTotalTrips = possibleSingleTrips + possibleDoubleTrips

   If requiredTrips > possibleTotalTrips Then 'Too many trips for success'
      failure = True
      MsgBox "minCyclesForDepth3 required>possible trips"
   End If

   Dim reqCycles As Integer
   If requiredTrips > possibleDoubleTrips Then 'double trips can't cover all the required trips'
      reqCycles = Ndouble + (requiredTrips - 2 * Ndouble) 'all the double trips plus the remaining singles'
   Else
      reqCycles = requiredTrips \ 2 'This is integer division so it may drop a single cycle, but we'll assume its tolerable'
   End If

   If failure = False Then
      minCyclesForDepth3 = reqCycles
   Else
      minCyclesForDepth3 = -1
   End If
End Function
```

```
Function tripCutoffCycles(Euseable, Etrip, m, b, trips) As Integer

   'Find the number of recharge cycles available that will accomodate <trips> number of two-way trips
   'Returns a number of charge cycles
   cutoff = (trips * Etrip / Euseable - b) / m

   If cutoff < 0 Then 'negative means there are no charge cycles that will allow <trips> number of trips before a recharge'
      cutoff = 0
   End If

   tripCutoffCycles = cutoff

End Function

Function estimatedTripEnergy(depth, Edrill, tDrill, Pdrive, Photel, speed, Optional dH As Single = 0.15, Optional WOB As Boolean = True)

   'Estimates total energy for a given trip number based on drill energy, and duration, and drive speed
   'Assumes drive is used continuously during drilling to provide WoB. Returns in units of Joules
   'Currently using a constant for WOB power required 5% of normal drive power.  NEEDS REFINEMENT

   tTrip = estimatedTripDuration(depth, speed, tDrill, dH) 'total time duration of the trip'

   If WOB = True Then 'Drive is used to provide WOB
      estimatedTripEnergy = Edrill + (Photel) * tTrip + Pdrive * (tTrip - tDrill) + Pdrive * 0.05 * (tDrill)
   Else    'Drive is NOT used to provide WOB, so it only gets used during travel
      estimatedTripEnergy = Edrill + (Photel) * tTrip + Pdrive * (tTrip - tDrill)
   End If

End Function

Function estimatedTripDuration(depth, speed, tDrill, Optional dH As Single = 0.15)

   estimatedTripDuration = 2 * depth / speed + dH / speed + tDrill

End Function

Function drivePower(g, botMasskg, speedMS, friction, systemEff)

   'Returns the electric power required by the bot drive system. Takes into account total system
   'efficiency and speed (cm/s) along with a base level of internal friction/drag in Newtons

   drivePower = minimumDrivePower(g, botMasskg, speedMS) / systemEff + friction * speedMS

End Function
```

```
Function minimumDrivePower(g, botMasskg, speedMS)

   'Returns the minimum drive power possible due to speed (cm/s), mass (kg), and gravitation
   'Units in joules/Sec = Watts.  Assumes traveling vertically

   minimumDrivePower = g * botMasskg * (speedMS)

End Function

Function maxDepthToMinSOC(maxSOC, minSOC, m, b, nomCap, Edrill, tDrill, Pdrive, Photel, speed, bots,
Optional dH As Single = 0.15, Optional WOB As Boolean = True)

   Dim Ecurr As Double 'current battery capacity
   Dim Euse As Double 'current useable battery capacity
   Dim Emargin As Double
   Dim depth As Double
   Dim trips As Integer
   Ecurr = CurrentCapacity(nomCap, m, b, 0) 'Initialize the variables
   Euse = UseableCapacity(Ecurr, maxSOC, minSOC)

   'MsgBox "maxDepth m"
   'MsgBox m
   'MsgBox "maxDepth b"
   'MsgBox b

   Emargin = Euse
   trips = 0

   Do Until Emargin < 0

      cycles = trips / bots
      Ecurr = CurrentCapacity(nomCap, m, b, cycles) 'Initialize the variables
      Euse = UseableCapacity(Ecurr, maxSOC, minSOC)
      depth = trips * dH
      Etrip = estimatedTripEnergy(depth, Edrill, tDrill, Pdrive, Photel, speed, dH, WOB) / 1000 'Conv. to kJ
      trips = trips + 1
      Emargin = Euse - Etrip 'margin to minSOC is the useable less the trip energy
      'MsgBox Etrip
      'MsgBox Emargin
   Loop

   maxDepthToMinSOC = depth

End Function
```